

VESTIBULAR CONTRIBUTIONS TO VOLUNTARY REACHING MOVEMENTS AND  
POST-STROKE MOTOR IMPAIRMENT

by

Angelo Bartsch-Jiménez

A Dissertation Presented to the  
FACULTY OF THE USC GRADUATE SCHOOL  
UNIVERSITY OF SOUTHERN CALIFORNIA  
In Partial Fulfillment of the  
Requirements for the Degree  
DOCTOR OF PHILOSOPHY  
(BIOKINESIOLOGY)

May 2025

## **Dedication**

This work would not have been possible without the unwavering support of my beautiful wife, Priscilla (Pía), and our daughter, Allegra. They were the driving force that kept me going through every challenge. In moments of doubt and exhaustion, it was your laughter, encouragement, and late-night conversations that kept me grounded and hopeful.

I am deeply grateful to my entire family and friends who visited us and helped make our home abroad feel warm and familiar, despite the distance and time differences. A special thank you to my parents, Ivonne and Pepe, who never missed an important holiday, and to Moorene, Fernando, Constanza, Gerardo, Carlos and Rosa. Their love and presence helped us recharge and reminded us of what truly matters.

*Thank you for walking this path with me.*

*Though I was conferred the degree, it is you to whom I owe it!*

## Agradecimientos

Este trabajo no habría sido posible sin la ayuda incondicional y el apoyo de mi bella esposa, Pricilla (Pía) y nuestra hija Allegra. Fueron el motor que me permitió seguir luego de cada reto y obstáculo. En momentos de duda y cansancio, fueron las risas, el aliento y conversaciones nocturnas las que me mantuvieron con esperanza.

Estoy también profundamente agradecido de toda mi familia y amigos que visitaron e hicieron sentir mi hogar un lugar familiar y cálido, a pesar de la distancia y los cambios horarios. Un agradecimiento especial a mis padres, Ivonne y Pepe, que nunca se perdieron una festividad importante. A Moorene, Fernando, Constanza, Gerardo, Carlos y Rosa. Su amor y presencia nos ayudaron a recargarnos de energía y amor y nos recordaron lo que realmente importa.

*Gracias por acompañarme en este camino.*

*El título es mío, pero see lo debo a ustedes!*

## **Acknowledgements**

I would like to acknowledge the support I received—both academic and personal—from my fellow students in the ValeroLab. They walked this path with me and helped make it more bearable. A special mention to Hesam, Majid, Niyo, and Romina, as well as to those who graduated or had the courage to move on: Dario, Suraj, Miguel, and Lemma. I am especially grateful to Jackie and Oscar, with whom I could speak freely in Spanish—no language barriers, just true connection. We never missed a good laugh.

# Table of Contents

Dedication . . . . .	ii
Agradecimientos . . . . .	iii
Acknowledgements . . . . .	iv
List of Tables . . . . .	vii
List of Figures . . . . .	ix
Abstract . . . . .	xiii
Chapter 1: <i>Introduction</i> . . . . .	1
1.1    Background: Sensorimotor disruptions in stroke . . . . .	1
1.2    Motivation: How this work advances our understanding of sensorimotor disruptions in stroke . . . . .	2
1.2.1    What are pathological synergies? . . . . .	2
1.2.2    Where do pathological synergies come from? . . . . .	3
1.2.3    Characterization of synergies and pathological synergies . . . . .	6
1.2.3.1    The difference between <i>coarse</i> and <i>fine</i> synergies . . . . .	7
1.2.3.2    The difference between <i>descriptive</i> and <i>prescriptive</i> synergies . . . . .	8
1.2.3.3    Measuring shared neural drive to muscles . . . . .	9
1.3    Statement of the problem . . . . .	12
1.4    Precedent logic and overarching hypothesis . . . . .	13
1.5    Significance of testing the overarching hypothesis . . . . .	15
1.6    Thesis outline . . . . .	15
Chapter 2: Contributions of vestibular motor output to arm muscle during voluntary movement in young neurotypical . . . . .	18
2.1    Abstract . . . . .	18
2.2    Introduction . . . . .	19
2.3    Materials and Methods . . . . .	21
2.4    Results . . . . .	26
2.5    Discussion . . . . .	33
Chapter 3: Contributions of vestibular brainstem output to pathological synergies following stroke . . . . .	39
3.1    Abstract . . . . .	39
3.2    Introduction . . . . .	40
3.3    Materials and Methods . . . . .	42

3.4	Results . . . . .	49
3.5	Discussion . . . . .	55
3.6	Appendix . . . . .	62
Chapter 4: Discussion and Future work . . . . .		66
4.1	Main findings . . . . .	66
4.2	Future work . . . . .	69
4.2.1	Investigating the task-dependent suppression of Vestibular responses . . . . .	69
4.2.2	Investigating ipsilateral cortico-vestibular downregulation . . . . .	70
4.2.3	Neural Mechanisms Underlying Synergies . . . . .	71
Appendix 1: Introducing the distinction between ‘ <i>Fine synergies</i> ’ vs. ‘ <i>Coarse synergies</i> ’ to better describe sensorimotor disruptions . . . . .		73
4.3	Introduction . . . . .	74
4.4	Materials and Methods . . . . .	76
4.5	Results . . . . .	79
4.6	Discussion . . . . .	83
4.7	Supplemental Data . . . . .	90
Appendix 2: An open source package in R to help researchers estimate shared neural drive between physiological signals . . . . .		93
4.8	Signal Simulation and Magnitude-Squared Coherence Estimation . . . . .	93
4.8.1	Generating simulated signals . . . . .	94
4.8.2	Estimating Magnitude-Squared Coherence . . . . .	95
4.8.3	Transforming magnitude-squared coherence into <i>z</i> -scores . . . . .	96
Bibliography . . . . .		98

# List of Tables

2.1	Robust repeated measures ANOVAs: degrees of freedom, F ratio, p-value, and effect size ( $\eta^2$ ). Muscles: <i>Sternocleidomastoid</i> (SCM), <i>Upper Trapezius</i> (UTrap), <i>Biceps brachii</i> (Bic), <i>Triceps brachii</i> (Tric), and <i>Anterior, Middle, and Posterior Deltoid</i> (ADelt, MDelt, PDelt). Subscripts indicate Neck-Neck muscles: N-N, Neck-Arm muscles: N-A, and Arm-Arm muscles: A-A. . . . .	30
2.2	Adjusted p-values for <i>post-hoc</i> comparisons using Bonferroni corrections (adjusted for 2 comparisons). Red text indicates significant differences between stimulus types: No Stimulation ( <i>None</i> ), <i>Sham</i> and Galvanic Vestibular Stimulation ( <i>GVS</i> ). Muscles: <i>Sternocleidomastoid</i> (SCM), <i>Upper Trapezius</i> (UTrap), <i>Biceps brachii</i> (Bic), <i>Triceps brachii</i> (Tric) and <i>Anterior, Middle and Posterior Deltoid</i> (ADelt,MDelt,PDelt). Subscript indicates Neck-Neck muscles:N-N, Neck-Arm muscles:N-A, and Arm-Arm muscles: A-A. . . . .	31
3.1	Demographic and clinical characteristics of the study participants. Age and stroke onset is reported in years. . . . .	43
3.2	<b>Our results at Rest confirmed the known effect of GVS stimulation on neck muscles [Bartsch and Valero-Cuevas, 2025], but show a significant effect of body Side only in Stroke participants.</b> The Stroke group showed a significant <i>Side</i> effect (Paretic vs. Non-paretic) on Neck IMC <sub>z</sub> (SCM-UTrap) during <i>Rest</i> , which was confirmed by corrected pairwise comparisons. On the other hand, both groups showed a main effect for <i>Stimulus Type</i> , also in Neck muscles. Additionally, a <i>Stimulus Type</i> × <i>Side</i> interaction was identified in Neck muscles of the Stroke group. The table presents results from robust repeated measures ANOVAs, including degrees of freedom, F ratio, and p-value, for the following muscles: <i>Sternocleidomastoid</i> (SCM), <i>Upper Trapezius</i> (UTrap), <i>Biceps brachii</i> (Bic), and <i>Anterior, Middle, and Posterior Deltoid</i> (ADelt, MDelt, PDelt). Red text indicates significant differences at 0.05*, and 0.01** levels. . . . .	50
3.3	Comparison of the Right side of controls (n=14) with both, the <i>paretic</i> and <i>non-paretic</i> (n=13) side of Stroke participants during <i>Rest</i> . Unexpectedly, when GVS is applied, only the <i>non-paretic</i> side showed statistical differences in neural drive to neck muscles in the alpha band when compared to controls (right side). Red text indicates significant differences (groups and stimulus types). Muscles: <i>Sternocleidomastoid</i> (SCM), <i>Upper Trapezius</i> (UTrap), <i>Biceps brachii</i> (Bic), and <i>Anterior, Middle and Posterior Deltoid</i> (ADelt, MDelt, PDelt). . . . .	60

3.4	Compared to controls, the <i>paretic</i> side of stroke participants showed decreased neural drive to Biceps and Deltoid (Bic-ADelt, Bic-MDelt, Bic-PDelt, ADelt-MDelt) during reaching. The shoulder position (Neutral vs. Abducted) also showed decreased neural drive. . . . .	61
3.5	GVS increases $IMC_z$ (GVS vs. None, and GVS vs. Sham) in neck muscles across frequency bands for the Control group during Rest. Conversely, no Sham effect was found (None vs. Sham). The table summarizes adjusted p-values for <i>post-hoc</i> comparisons using Bonferroni corrections (adjusted for 2 comparisons) for Stimulus type in the Control group during Rest. Red text indicates significant differences between stimulus types: No Stimulation ( <i>None</i> ), <i>Sham</i> and Galvanic Vestibular Stimulation ( <i>GVS</i> ). Muscles: <i>Sternocleidomastoid</i> (SCM), <i>Upper Trapezius</i> (UTrap), <i>Biceps brachii</i> (Bic), and <i>Anterior, Middle and Posterior Deltoid</i> (ADelt,MDelt,PDelt). . . . .	62
3.6	When GVS is applied at <i>Rest</i> , only the paretic side of stroke shows increased coherence to neck muscles across frequency bands. No Sham effect was found on either side (None vs. Sham). The table summarizes adjusted p-values for <i>post-hoc</i> comparisons for each arm using Bonferroni corrections (adjusted for 2 comparisons) for Stimulus type in the stroke group during Rest. Red text indicates significant differences between stimulus types: No Stimulation ( <i>None</i> ), <i>Sham</i> and Galvanic Vestibular Stimulation ( <i>GVS</i> ). Muscles: <i>Sternocleidomastoid</i> (SCM), <i>Upper Trapezius</i> (UTrap), <i>Biceps brachii</i> (Bic), and <i>Anterior, Middle and Posterior Deltoid</i> (ADelt,MDelt,PDelt). . . . .	65
4.1	Spatiotemporal gait patterns mean ( $\pm$ standard deviation) in drop foot (DF) and Control (C) groups. . . . .	79
4.2	Cumulative variance accounted for extracted from NMF for each subject in the Control group, with the respective Mean and Standard Deviation across factors. . . . .	91
4.3	Cumulative variance accounted for extracted from NMF for each subject in the Drop Foot group, with the respective Mean and Standard Deviation across factors. . . . .	91
4.4	Cumulative variance accounted for extracted from PCA for each subject in the Control group, with the respective Mean and Standard Deviation across Principal Components. . . . .	92
4.5	Cumulative variance accounted for extracted from PCA for each subject in the Drop Foot, with the respective Mean and Standard Deviation across Principal Components. . . . .	92

## List of Figures

2.3 The *Sternocleidomastoid* (SCM) muscle shows a stereotypical response across all tasks, while the *Upper Trapezius* (UTrap), shows a smaller response restricted to *Rest*, emphasizing its suppression during *Isometric* and *Reaching* tasks. *Top:* Raw and Processed (GVS artifact removed, full-wave rectified and band-pass filtered) EMG activity from *Sternocleidomastoid* (SCM) and *Upper Trapezius* (UTrap) muscles during each task (when GVS was applied) for a typical participant. Each trace corresponds to one second of activity, which was extracted when the signal was stable (5s after the tasks started)

*Bottom:* Mean ( $\pm$ SD) Raw and Processed EMG activity (across stimuli) in response to Galvanic Vestibular Stimulation (GVS), from 50ms before to 110ms after the stimuli was delivered. For visualization purposes of the stereotypical response, all stimuli were aligned to their delivery time ( $t = 0$ ). It showcases the averaged EMG responses across all stimuli from a single participant (number of averaged stimuli highlighted inside each plot). The light trace shows the GVS artifact while the darker trace shows the EMG after this artifact was removed and the signal processed (full-wave rectified and band-pass filtered). The shaded gray area represents the 10 ms window (ranging from -2 ms to 8 ms) during which the GVS artifact was removed prior to signal processing (see Section 2.3). Following this window, suppression of the UTrap response is observed during voluntary action of the arm, as opposed to SCM responses, which are always visible. . . . .

28

2.4 During Rest, Galvanic vestibular stimulation (GVS) increases intermuscular coherence (IMC) across alpha, beta and gamma frequencies between neck muscles, but not arm, muscles. We compared  $z$ -transformed IMC coherence across frequency bands during Rest under three different stimulus types: No Stimulation (*None*), *Sham* and GVS. Neck muscles are *Sternocleidomastoid* (SCM) and *Upper Trapezius* (UTrap). Arm muscles are *Biceps brachii* (Bic) and *Anterior Deltoid* (ADelt). Red dotted line indicates the 95% upper confidence interval estimated from 1,000 randomizations of the original signals. The middle and lower panels include the mean  $IMC_z$  across stimulus types on top of their corresponding box for easy comparison while keeping the same scales across muscle pairs. . . . .

29

2.5 Galvanic Vestibular Stimulation (GVS, blue line) increases vestibular drive to neck muscles (SCM-UTrap) at Rest. However, it's suppressed during Reaching and Isometric tasks. GVS did not increase vestibular output to neck-arm and arm muscles (SCM-Bic and Bic-MDelt, respectively), neither at Rest nor during unperturbed voluntary action of the arm. No differences were found between Sham and No stimulation (which excludes a placebo effect). Mean ( $\pm$ SD)  $z$ -transformed  $IMC_z$  coherence across subjects during rest condition under three different Stimuli: No Stimulation (*None*), *Sham* and Galvanic Vestibular Stimulation (GVS). Each plot (except for SCM-UTrap at Rest) includes an inset where the signals are autoscaled. Neck muscles are SCM: *Sternocleidomastoid* and UTrap: *Upper Trapezius*. Arm muscles are Bic: *Biceps Brachii* and MDelt: *Middle Head of Deltoid*. Values above the dotted red line can be considered to have significant  $IMC_z$ , as per the 95% upper confidence interval estimated from 1,000 randomizations of the original signals. Alpha, beta and gamma frequency bands are identified by blue vertical dashed line on top of upper panel. . . . .

32

3.1	Tasks performed by each participant. Left: At the beginning of the experiment, each participant sat comfortably in a chair with their hands on their lap, while EMG was recorded at <i>Rest</i> . Middle: During the <i>Reaching</i> task, participants are asked to rotate an horizontal ergometer inwards (counterclockwise for the right arm, and clockwise for the left arm) to produce a cyclical movement. Right: In the <i>Reaching with abducted shoulder</i> condition, subjects were asked to perform the same reaching-like movement while keeping their shoulder abducted at 90°. Verbal encouragement was constantly provided to avoid shoulder drifting. . . . .	44
3.2	EMG signals and intermuscular coherence ( $IMC_z$ ) reveal lower responses to GVS in the <i>non-paretic</i> side (red trace) of stroke participants during <i>Rest</i> , compared to the right side of controls (black trace). The left panel shows the raw (light trace) and processed (dark trace) EMG signals for the Sternocleidomastoid (SCM) and Upper Trapezius (UTrap) muscles in a representative participant. Note the lower GVS-driven responses on the <i>non-paretic</i> side of both muscles. The middle panel shows a boxplot with individual $IMC_z$ means, highlighting the lower coherence levels on the <i>non-paretic</i> side, compared to the paretic side as well as control participants. The right panel shows the group mean $IMC_z$ ( $\pm SD$ ) for the SCM-UTrap muscle pair. Significant differences in the alpha band (8-16 Hz) were observed between the <i>non-paretic</i> side and controls ( $p=0.029$ ), but no significant differences were found between the paretic side (blue trace) and controls ( $p=0.385$ ). Values above the dotted dark red line can be considered to have significant $IMC_z$ , as per the 95% upper confidence interval estimated from 1,000 randomization of the original signals. . . . .	52
3.3	The paretic side of stroke survivors had lower intermuscular coherence values when compared to control participants. Left: mean $IMC_z$ for each participant during both reaching tasks. Right: group mean intermuscular coherence for control participants and each side of stroke. Values above the dotted dark red line can be considered to have significant $IMC_z$ , as per the 95% upper confidence interval estimated from 1,000 randomization of the original signals. SCM: <i>Sternocleidomastoid</i> , UTrap: <i>Upper Trapezius</i> , Bic: <i>Biceps brachii</i> ; ADelt, MDelt and PDelt <i>Anterior, Middle</i> and <i>Posterior Deltoid</i> respectively. . . . .	54
3.4	During Rest, stroke participants showed a statistically significant difference between both sides on intermuscular coherence ( $IMC_z$ ) in neck muscles (SCM-UTrap, Effect for Side, $p = 0.037$ ), which was not observed in Controls ( $p = 0.28$ ). Galvanic vestibular stimulation (GVS) changed $IMC_z$ in neck muscles for both groups (Control: $p = 0.01$ , Stroke: $p < 0.001$ ). Additionally, the Stroke group showed a significant interaction with decreased $IMC_z$ on the Non-paretic side during GVS. Post-hoc comparisons with Bonferroni corrections of the neck muscles (SCM-UTrap) showed that GVS increased IMC only in the Paretic (R) side across all frequency bands (alpha to gamma), as seen in the Control group. Unexpectedly, the Non-paretic side did not show differences when comparing GVS and No Stimulation. SCM: <i>Sternocleidomastoid</i> ; UTrap: <i>Upper Trapezius</i> ; Bic: <i>Biceps brachii</i> ; ADelt, MDelt and PDelt <i>Anterior, Middle</i> and <i>Posterior Deltoid</i> respectively. . . . .	63

3.5 During Rest, Neck muscles (SCM-UTrap) from the Non-paretic (Left) side of Stroke participants showed lower levels of $IMC_z$ in the alpha band when compared with Control participants (effect for <i>Side</i> in the alpha band, $p = 0.031$ , top panel). No differences were found between the Paretic (R) side of Stroke participants and the Control group when comparing the same muscle pair ( $p = 0.428$ ). The Stimulus type had a significant effect across frequency bands (Post hoc comparison, lower panel). GVS showed an overall effect of increased $IMC_z$ in the same neck muscles when comparing both sides of Stroke with the Control group. A Post hoc analysis (with bonferroni corrections) showed that GVS did not increase $IMC_z$ on the Non-paretic side of Stroke participants ( $p=0.029$ ). SCM: <i>Sternocleidomastoid</i> ; UTrap: <i>Upper Trapezius</i> . . . . .	64
4.1 Cumulative variance accounted for each Factor extracted by NMF in drop foot (DF) and Control (C). . . . .	80
4.2 A-B: Reconstructed muscle activity profiles based on weights extracted from first two <i>coarse synergies</i> for each group, accounting for > 86% of variance in each group. Shaded areas identify differences between groups based on SPM{t} results and their corresponding levels of significance. C-D: Coarse synergies muscle weights extracted from NMF for unimpaired control participants (C) and persons with drop foot (DF). *Significant at 5%; **Significant at 1% . . . . .	81
4.3 Cumulative variance accounted for each PC extracted from residuals by PCA in drop foot (DF) and control (C). . . . .	82
4.4 A-C: Reconstructed muscle activity profiles based on loadings extracted from first three ‘fine synergies’ for each group. D-F: Fine synergies loadings extracted from PCA for unimpaired control participants and persons with drop foot. Also note the loadings in DF are in general closer to +1 in the DF case, indicating greater synergistic correlation among muscle activations. . . . .	83
4.5 Mean Fine synergy loadings for each group extracted by PCA. . . . .	84
4.6 Kinematic and Kinetic data from lower extremity in the Drop Foot group. . . . .	90
4.7 Simulated signals (left): Both signals share a single frequency (8 Hz), with a noise level set at 0.5 (arbitrary units). The signal duration is set in seconds. Both signals overlap due to the shared frequency between them. Fast Fourier Transform (right): An FFT analysis is performed to confirm a shared frequency (8Hz) plus added noise. . . . .	95
4.8 Magnitude-squared coherence spectrum of the simulated signals. The coherence is highest at the shared frequency of 10 Hz. . . . .	96
4.9 Magnitude-squared and z-transformed coherence for simulated signals. The coherence is highest at the shared frequency of 10 Hz . . . . .	97

## **Abstract**

This dissertation investigates the role of vestibular motor output in modulating voluntary arm movements and its potential contribution to pathological synergies following stroke. The research is motivated by the unknown contribution of the vestibular system to arm movement and to motor impairment following stroke. Our work examines whether vestibular stimulation increases shared neural drive to arm muscles at rest and during voluntary movement in young neurotypical participants. Moreover, building upon these findings, we explore if the baseline neural drive found in young neurotypical participants is increased in stroke survivors.

In a series of experiments, we employed galvanic vestibular stimulation (GVS) to selectively increase vestibular drive and measure its impact on intermuscular coherence (IMC) —a measure of shared neural drive— between neck and arm muscles. We found that when GVS was applied during both rest and unperturbed voluntary movements, no IMC changes were observed in arm muscles. Consequently, we provide evidence to exclude a vestibular shared neural drive to arm muscles during voluntary movement in young neurotypical participants.

Unexpectedly, when GVS is applied at rest, we found a significant IMC increase in neck muscles, when compared to both No Stimulation and Sham conditions. However, when GVS was applied during voluntary isometric contractions and reaching movements, such GVS-driven responses were suppressed. Given that Sham stimulation did not change IMC neither at rest nor voluntary movement, the observed changes are most likely arising from vestibular stimulation. These findings suggest that, under normal conditions,

vestibular responses from neck muscles are suppressed during voluntary movements to avoid the conflicting effect between these responses and the ongoing movement.

Building upon this baseline characterization, the study extended the investigation to a clinical population by comparing stroke survivors with right hemiparesis to age-matched control subjects. By including GVS, we aimed to establish the contribution of vestibular brainstem output to motor impairment and pathological synergies. In stroke survivors, the *paretic* arm showed lower IMC in arm muscles during voluntary reaching tasks, particularly when the shoulder was abducted during the movement. However, when GVS was applied, no IMC changes were found in arm muscles from the same *paretic* side, neither with neutral nor abducted shoulder. This lack of changes indicates that an upregulated vestibular drive is unlikely to be a mechanism underlying the motor impairments observed in the *paretic* side of stroke survivors.

Interestingly, the *non-paretic* side of stroke survivors showed an IMC decrease in neck muscles when GVS was applied during rest, which may reflect disruptions in ipsilesional cortico-vestibular pathways. These differential responses across both sides underscore the complex interplay between descending cortical and subcortical pathways in mediating motor function after stroke. Specifically, the IMC decrease in arm muscles from the *paretic* side might reflect disruption in motor pathways, such as the corticospinal tract, while the *non-paretic* side likely reflects disruptions in brainstem pathways, such as those from the vestibular system.

The experimental design of our experiments involved a comprehensive set of conditions that included No Stimulation, Sham, and GVS during both resting and voluntary movement tasks, allowing for a detailed analysis of the contributions from vestibular and non-vestibular descending pathways. By measuring pairwise coherence between muscle groups involved in arm movement, the study provides quantitative evidence on how vestibular signals are integrated—or suppressed—within the broader context of voluntary motor control. The methodological approach, which combined stimulation protocols with signal analysis

techniques, represents a significant advance in our ability to disentangle the overlapping neural drive that contribute to movement execution.

There are several implications of these findings. First, the demonstration of vestibular suppression during voluntary arm movements—observed in young and control participants as well as on the paretic side in stroke patients—further supports a hierarchically organized motor system, with competing and collaborating signals driving voluntary movement. This selective suppression likely optimizes the execution of complex motor tasks by minimizing interference from lower-level neural signals. Second, in the context of stroke, the absence of increased vestibular drive in the paretic arm under GVS suggests that other mechanisms—such as disruptions in subcortical and reticulospinal pathways—may play a more prominent role in the development of pathological synergies, which needs to be further addressed.

Overall, this dissertation not only refines our understanding of the neural mechanisms underlying voluntary movement, but also provides supporting evidence to exclude the contribution of vestibular drive to post-stroke motor impairment. The work lays a critical foundation for future research aimed at developing targeted rehabilitation strategies that address both cortical and subcortical contributions to motor dysfunction.

In summary, this research advances the field by providing comprehensive evidence that vestibular contributions are dynamically regulated during voluntary arm movements; however, they are unlikely to underlie pathological synergies in the *paretic* side following stroke. Moreover, our results underscore a broader impact of stroke, as the *non-paretic* side showed decreased neural drive on neck muscles, when compared with control participants.

# **Chapter 1**

## ***Introduction***

### **1.1 Background: Sensorimotor disruptions in stroke**

Stroke ranks fifth among all causes of death in the US, it's one of the leading causes of severe long-term disability in stroke survivors and decreases functionality in more than half of those aged 65 and over [Tsao et al., 2022]. Stroke is clinically characterized by both positive and negative signs, arising not only from corticospinal tract (CST) damage but also from dysregulation of the uninjured subcortical pathways [Krakauer, 2005, Li et al., 2019]. Negative signs include weakness (paresis) and loss of dexterity (fractionated motor control). In contrast, positive signs involve hyperreflexia, increased muscle tone (spasticity), abnormal resting postures, and pathological synergies [Krakauer, 2005, Kamper et al., 2006, Hadjiosif et al., 2021, 2022]. In most stroke survivors, arm and hand movements are disrupted by exhibiting ‘pathological’ *flexion synergies* (abnormal coupling of shoulder abduction, elbow flexion and forearm supination) [Twitchell, 1951, Brunnstrom, 1970]. As a result of the movement disruptions, the expression of pathological synergies leads to impaired voluntary reaching and grasping movements, including reduced ability to control hand opening and grasping forces [Lan et al., 2017], reduced elbow and shoulder excursion angles [Beer et al., 2007], and decreased reaching velocity, distance, and working area [Sukal et al., 2007, McPherson et al., 2018, Ellis et al., 2018]. Novel interventions aiming to restore neural drive balance –particularly from

upregulated sources— are more likely to improve functionally relevant outcomes through neural —rather compensatory— mechanisms.

## 1.2 Motivation: How this work advances our understanding of sensorimotor disruptions in stroke

### 1.2.1 What are pathological synergies?

*Pathological flexion synergies* have been described as an abnormal muscle coupling involving elbow flexors, shoulder abductors, and retraction or elevation of the shoulder girdle in stroke survivors [Twitchell, 1951, Brunnstrom, 1970]. In the literature, pathological flexor synergies are also referred to as *loss of independent joint control*, *loss of joint individuation*, or simply *abnormal (motor) synergies* to refer to the dynamic and task-dependent reduction of joint individuation due to abnormal muscle coupling during proximal joint utilization [Ellis et al., 2016]. Dewald et al. hypothesized that this abnormal muscle coupling could result not only from the damage to corticospinal tract—as initially proposed by Twitchell—but also from an increased drive from residual subcortical (brainstem) pathways, such as the reticulospinal and vestibulospinal tracts (vestibular motor output) [Dewald et al., 1995]. Further research has found that increased shoulder abduction load—such as during reaching against gravity—exacerbates abnormal muscle coactivation patterns in the muscles involved in the pathological flexor synergy, as well as the ability to move outside of this flexion pattern. As a result, reaching movements are negatively affected by increased load levels, as the reaching area decreases due to higher muscle co-activation and limiting angle excursion in elbow and shoulder joints [Sukal et al., 2007, Ellis et al., 2008, 2016].

## 1.2.2 Where do pathological synergies come from?

Lawrence and Kuypers described the differences in motor impairment following surgical lesions to CST [Lawrence and Kuypers, 1968a], and brainstem descending pathways in non-human primates [Lawrence and Kuypers, 1968b]. Lesion to the CST caused permanent loss of independent movements of the digits, which only recovered if the CST lesion was incomplete. Following these focal lesions, no other deficit —such as weakness and spasticity— was found [Lawrence and Kuypers, 1968a, Krakauer, 2005]. Interestingly, macaques do not develop pathological flexion synergies after surgical CST lesions, likely because these controlled and focal lesions do not induce the widespread neural disruption. As opposed to these surgical lesions, stroke in humans typically involve both cortical and subcortical areas, resulting in a complex interplay of negative and positive motor signs, masking the individual contributions of the mechanisms underlying pathological synergies. These differences underscore a limitation of the macaque model in replicating the complex pathology of human stroke [Xu et al., 2024, Nogles and Galuska, 2023].

The primary mechanism underlying pathological synergies is stroke-related damage to motor pathways, which leads to the disruption of monosynaptic corticomotoneuronal connections to muscles [Brunnstrom, 1970, McMorland et al., 2015, Krakauer, 2005]. According to Krakauer's perspective, two additional key mechanisms —and likely their interaction— contribute to their emergence: (i) increased drive from descending subcortical (brainstem) pathways and (ii) maladaptive changes in segmental reflex circuits [Krakauer, 2005]. For example, it has been proposed that upregulated descending supraspinal pathways increase the motoneuron membrane potential, bringing them closer to the activation threshold and leading to an increase in stretch reflex excitability [Miller and Rymer, 2017]. Similarly, given the dexterity loss, motor commands to individual muscles may instead co-activate muscles that are closer to their activation threshold, resulting in the emergence of pathological synergies [McMorland et al., 2015]. Consequently, pathological synergies result from disrupted CST drive, which impairs the corticomotoneuronal connections essential for

fine motor control. Additionally, upregulated subcortical drive increases motoneuron excitability and reflex responses. Together, these changes reduce the threshold for muscle activation, causing motor commands to recruit and coactivate multiple muscles, which leads to the emergence of pathological synergies.

Increased drive from subcortical pathways –as a mechanism underlying pathological synergies— has been supported by neurophysiological and neuroimaging studies. Insufficient CST input, leads to progressive loss of inhibitory cortical control over brainstem circuitry, increasing subcortical drive and motor excitability [Shimizu et al., 2002, Niehaus et al., 2003, McMorland et al., 2015, Emos and Rosner, 2023]. Potential sources of subcortical (brainstem) drive are the reticulo (RST), vestibulo (VST), rubro (RuST), and tectospinal (TST) tracts. However, RuST and TST are unlikely to be involved in upper extremity motor impairment; the contribution of the RuST is questionable due to its underdeveloped nature in humans [Nathan and Smith, 1982, 1955]. Similarly, the TST is primarily involved in head and neck movement [Brown, 1994, Mukherjee and Chakravarty, 2010]. As such, the RST and vestibular motor output are most likely involved in motor impairment of the arm. Importantly, it has been shown that both, the resticulo (RST) and vestibular motor output become upregulated following stroke [Miller et al., 2014, Baker et al., 2015, Miller et al., 2016, Miller and Rymer, 2017, McPherson et al., 2018, Taga et al., 2021].

The possible contribution of the reticulospinal tract to pathological synergies is supported by its role in voluntary arm movement during the preparation and execution phases of reaching and grasping. Moreover, its stimulation, produces coordinated multi-joint flexion patterns in the ipsilateral upper limb [Buford, 2009, Brownstone and Chopek, 2018]. Its involvement in motor impairment is further evidenced by evidence from Choudhury et al., who observed increased forearm flexor activation during acoustic startle responses paired with visual stimuli (StartReact effect), a phenomenon thought to be mediated by the reticulospinal system. Similarly, McPherson et al. showed increased recruitment of reticulospinal projections to the paretic limb of stroke survivors which correlated with the level of shoulder abduction loading and pathological synergy expression [McPherson et al., 2018].

The vestibular system —through vestibular motor output signals— also plays a crucial role in movement control by modulating motor neuron excitability and muscle tone. Stimulation of the vestibular system increases the excitability of both alpha and gamma motoneurons, as well as the amplitude of stretch reflexes [Lance and McLeod, 1981, Molina-Negro et al., 1980]. Moreover, the tonic vibration reflex (TVR), disappears following surgical transection of the lateral vestibular nucleus and is restored through lateral vestibulospinal tract stimulation [Lance and McLeod, 1981]. In the upper extremity, muscle responses to vestibular stimulation —assessed by vestibular evoked myogenic potentials (VEMPs)— have been recorded in the *deltoid*, *biceps*, *triceps*, *brachioradialis*, *flexor carpi radialis* and *palmaris longus* [Papathanasiou et al., 2013, Valente et al., 2020, Cherchi et al., 2009]. After stroke, these responses have been found asymmetric in ocular, neck, and arm muscles, with higher responses on the paretic side when compared with the non paretic side of stroke survivors. Importantly, they are strongly correlated with spasticity [Miller et al., 2014, 2016, Miller and Rymer, 2017]. These findings provide evidence not only of increased vestibular motor output to neck and arm muscles after stroke, but also of maladaptive changes in reflex responses (third mechanism underlying pathological synergies) arising from the vestibular system.

In summary, most evidence supports increased reticulospinal drive as the origin of pathological synergies after stroke. However, based on the previous findings, the vestibular motor output may also contribute through two key mechanisms (as proposed by Krakauer):

- Increased drive from descending subcortical (brainstem) pathways: The vestibular motor output is an important contributor to voluntary movement control by regulating motoneuron excitability and muscle tone. Moreover, vestibulospinal drive is increased on the paretic side of stroke survivors [Miller and Rymer, 2017, Miller et al., 2016].
- Maladaptive changes in segmental reflex circuits: Stroke survivors exhibit increased muscle tone and exaggerated reflex responses (VEMPs), they show a strong correlation, and both are mediated by the VST [Miller et al., 2014].

The potential role of vestibular output as an underlying mechanism in pathological synergies underscores the need to further investigate its contribution to motor impairment.

### 1.2.3 Characterization of synergies and pathological synergies

*Muscle Synergies* in neurotypical animals and humans can be defined as a broad class of strategies to control multiple muscles. The muscle synergy hypothesis proposes that the central nervous system (CNS) selects and activates muscles by grouping them into functional units using a combination of a small number of patterns among all the available degrees of freedom [d'Avella and Tresch, 2001, d'Avella et al., 2003, Tresch and Jarc, 2009]. Muscle synergies are identified by applying dimensionality reduction techniques to electromyographic (EMG) data [Valero-Cuevas et al., 2009a, Clewley et al., 2008], which allows the researcher to capture the lower-dimensional structure of the neural control of movement [d'Avella et al., 2003, Tresch and Jarc, 2009, Kutch and Valero-Cuevas, 2012, Rabbi et al., 2020, Ting and McKay, 2007, Valero-Cuevas, 2016, Clewley et al., 2008]. Independently on whether or not these 'synergies' are of neural origin [Tresch and Jarc, 2009, Kutch and Valero-Cuevas, 2012], they are 'descriptive' of the basis functions that best explain a high percentage of the variance in the data [Valero-Cuevas, 2016, Brock and Valero-Cuevas, 2016]. The researcher must first determine *a priori* if linear or nonlinear basis functions are most appropriate, and what is the discrete number of basis functions (i.e., synergies) that explain a 'high enough' percentage of the variance [Clewley et al., 2008]. In practice, the most popular methods for dimensionality reduction are Non-Negative Matrix Factorization (NMF) [Lee and Seung, 1999, Rabbi et al., 2020], Principal Component Analysis (PCA) [Ting and Macpherson, 2005], Independent Component Analysis (ICA) [Hyvärinen and Oja, 2000], and Factor Analysis (FA) [Saito et al., 2015].

### 1.2.3.1 The difference between *coarse* and *fine* synergies

In the fields of biomechanics and neuromechanics, the number of synergies that together explain 80- 90% of the variance are considered sufficient to explain the dominant characteristics of the data and, therefore, most informative [Turpin et al., 2021, d'Avella et al., 2003, Tresch and Jarc, 2009, Kutch and Valero-Cuevas, 2012, Rabbi et al., 2020, Ting and McKay, 2007, Valero-Cuevas, 2016, Ó'Reilly and Federolf, 2021]. These are called '*coarse synergies*' [Bartsch-Jimenez et al., 2023] and their residuals (i.e., which represent the remaining 20–10% of the variance) are, by construction, data (i) in which the investigator is *a priori* not interested (because they explicitly set the cut-off for variance explained), (ii) which cannot be accounted for by the linear model (a by-product of the preferred method [Clewley et al., 2008]), or (iii) are considered noise (an assumption which must be proven) [Barradas et al., 2020, Valero-Cuevas et al., 2009b]. In either case, they are considered irrelevant or unimportant.

The interpretation and selection of *coarse synergies* –while discarding *fine synergies*—has been questioned, as *fine synergies* can reveal subtle yet functionally meaningful differences across populations [Bartsch-Jimenez et al., 2023]. While *coarse synergies* capture the dominant features of muscle coordination necessary to meet task constraints —often shared across participants— they may obscure group-specific differences, particularly in neurologically impaired populations. In contrast, *fine synergies*, derived from the residual variance, have been shown to uncover differences in the coordination structure of muscle activations that are not evident in *coarse synergies*. Specifically, compared to controls, the first two *fine synergies* extracted from gait data in participants with *drop foot* have significantly higher correlations at both the muscle level (individual muscle loadings) as well as at the synergy level (mean loadings within each synergy). These group differences were present even in weak muscles such as the *tibialis anterior*, highlighting that the observed changes reflect altered coordination strategies rather than mere differences in muscle strength [Bartsch-Jimenez et al., 2023]. Thus, analyzing *fine synergies* has shown a more effective

approach to detecting subtle differences in synergies (such as higher correlation among muscle activations) in neurologically impaired populations (see Appendix 1) [Bartsch-Jimenez et al., 2023].

### 1.2.3.2 The difference between *descriptive* and *prescriptive* synergies

The mechanical characteristics of a limb (such as joints and muscles involved, degrees of freedom at each joint) along with task constraints (such as force levels, movement direction, object compliance, etc.), define the range of feasible motor activation patterns within which voluntary movement must take place [Valero-Cuevas, 2016]. Successful task execution occurs within the lower-dimensional space that can be described by a limited set of basis functions (i.e., synergies) that spans the feasible muscle activation set [Brock and Valero-Cuevas, 2016]. Synergies identified through dimensionality reduction techniques are *descriptive* as they capture statistical correlations in muscle activation patterns. However, they do not necessarily reflect an underlying neural control strategy and cannot be used to identify the source of neural drive. In contrast, *prescriptive synergies* are imposed by the nervous system to optimize task execution while inhabiting the feasible muscle activation set. To define a synergy as *prescriptive*, researchers must provide evidence that the observed correlations in muscle activations arise from neural mechanisms rather than being artifacts of the chosen statistical analysis. Independent of the chosen method to identify *descriptive* and *prescriptive* synergies, current dimensionality reduction techniques do not establish a neural origin for the extracted synergies. Additional experimental validation is required to determine whether observed muscle activation patterns reflect a statistical artifact or a true neural origin [Kutch and Valero-Cuevas, 2012, Brock and Valero-Cuevas, 2016]. Importantly, it is essential to complement such experimental validation with statistical and mathematical methods capable of identifying shared drive to muscles and their common neural origin.

### 1.2.3.3 Measuring shared neural drive to muscles

#### What is intermuscular coherence?

Coherence analysis quantifies the degree of linear association (i.e. correlation) and synchronization between two time series in the frequency domain. As a measure of correlation, it's mathematically bounded between zero and one, where one indicates a perfect linear relationship (neural drive synchronization or shared neural drive) and zero indicates no linear relationship between both time series [Grosse and Brown, 2005, Farina et al., 2014]. Intermuscular coherence (IMC) assesses the degree of shared neural drive to two muscles on the basis of their EMG signals [Boonstra, 2013]. Similarly, corticomuscular coherence (CMC) assesses the degree of shared neural drive between the motor cortex and associated body muscles [Liu et al., 2019]. In general, coherence provides insights into the origin and coordination of muscle activity during specific movements or tasks [Boonstra, 2013], which is unfeasible with conventional synergy analysis (extracted with dimensionality reduction techniques, see subsection 1.2.3) [Laine and Valero-Cuevas, 2017, Laine et al., 2021]. As such, IMC has been proposed as the best current available tool to measure shared neural drive to muscles. For example, IMC is used to measure shared neural drive from the CST, as it reflects the synchronization of neural signals in the beta band (16–30 Hz). Although there is no direct physiological relationship between motor unit firing rates and corticospinal drive, evidence from (i) animal, (ii) clinical, and (iii) pharmacological studies supports its role as a marker of CST activity:

- i. In non-human primates, Murthy and Fetz observed beta-band synchronization in sensorimotor cortical areas of awake monkeys during food retrieval tasks. Similarly, Baker et al. investigated corticomuscular and intermuscular coherence in trained monkeys performing a precise holding task to obtain food rewards. Their findings revealed synchronized beta-band activity between the primary motor cortex and hand muscles (first dorsal interosseous and abductor digiti minimi), as well as increased IMC between these hand muscles [Baker et al., 1997].

ii. Clinical studies have shown that beta-band coherence is decreased when there's a lesion to the upper, but not lower motoneuron. Specifically, in primary lateral sclerosis (PLS) —a variant of upper motor neuron disease— there is selective damage to both, pyramidal neurons in cortical layer V and the CST, without anterior horn cells damage. Conversely, anterior horn cells are selectively degenerated in progressive muscular atrophy (MA), while no changes occur in the CST. When comparing upper and lower limb intermuscular coherence, significant beta-band coherence was observed in all control subjects and participants with progressive MA, but not in the participants with PLS. The results suggest that intermuscular coherence in the 15–30 Hz range depends on an intact corticospinal tract and is not affected during selective anterior horn cell destruction [Fisher et al., 2012]. Following stroke, it has been shown significantly lower coherence compared with healthy controls for arm muscles (anterior deltoid, biceps and triceps brachii) at both the beta and lower gamma (30-40 Hz) bands during a reaching task [Fang et al., 2009]. Similarly, it has also been shown to decrease coherence in hand muscles (first dorsal interosseous muscle, adductor pollicis, and abductor pollicis brevis) during a pinching task [Larsen et al., 2017].

iii. Further evidence for beta-band IMC arising from CST comes from pharmacological studies. Benzodiazepines —such as diazepam—are known to increase beta-band activity in the frontal cortex, an effect that can be reversed with the antagonist flumazenil. Their pharmacological effect was confirmed by an increase in beta-band coherence following diazepam administration in neurotypical participants, which was reversed after the antagonist was administered [Baker and Baker, 2003].

Regarding the representation of subcortical pathways in a specific band of IMC or CMC, evidence suggests that the rubrospinal tract is primarily reflected in the alpha band (8–16 Hz). This activity likely originates in the reticular formation and is transmitted via the rubrospinal tract and corticoreticular loops [Grosse and Brown, 2003, Thevathasan et al., 2012, Tattersall et al., 2014, Lau et al., 2015, McPherson et al., 2018, He et al., 2021]. Grosse and Brown recorded EMG signals from upper limb muscles in healthy

subjects exposed to unexpected acoustic stimulation —which is thought to be mediated by the reticular formation. Alpha band IMC coherence increased in the deltoid and biceps muscles during the startle response but remained unchanged during sham stimulation or voluntary contraction [Grosse and Brown, 2003]. Additional evidence comes from clinical studies using deep brain stimulation (DBS). In individuals with Parkinson’s disease, DBS led to increased alpha band coherence between the cortex and the reticular formation during gait [Thevathasan et al., 2012, Tattersall et al., 2014, Lau et al., 2015, He et al., 2021].

While the rubrospinal tract primarily contributes to coherence in the alpha band, the vestibular motor output exhibits a broader frequency range of synchronized neural drive, spanning from the alpha to gamma bands, with intermuscular coherence observed from 0 up to 70 Hz. This finding suggests that alpha band IMC contributions from the vestibular motor output may overlap with both the CST and RST, highlighting its involvement across multiple descending pathways [Blouin et al., 2011, Forbes et al., 2015]. In particular, vestibular reflexes exhibit distinct task-dependent and frequency-specific properties in axial versus appendicular muscles. Vestibular reflexes are evoked in appendicular muscles when they are involved in postural control, with coherence in leg muscles (soleus and gastrocnemius) spanning from 0 to 70Hz during quiet standing [Blouin et al., 2011], and between 2-20 Hz during locomotion [Forbes et al., 2015]. On the other hand, neck muscle reflexes are evoked regardless of the requirement to maintain balance, showing responses in the 0–20 Hz frequency range [Forbes et al., 2015].

Alternative sources of alpha band drive include the cerebello-thalamo-cortical loop, spinal interneuron networks, and monosynaptic stretch reflex loops [Groß et al., 2002, Christakos et al., 2006]. However, intermuscular coherence requires neural drive synchronization across multiple muscles and limbs, which argues against a spinal origin or a non-descending subcortical pathway. Thus, the corticospinal (CST), vestibulospinal (VST), and rubrospinal (RST) pathways remain the most likely and well-supported contributors to alpha and beta band coherence [Grosse and Brown, 2003, Blouin et al., 2011, Fisher et al., 2012]. Interpreting changes in these frequency bands requires caution, as multiple pathways contribute to

overlapping frequency ranges. Specifically, VST and RST contribute to alpha band coherence, while both VST and CST can be involved in beta band activity. As such, changes in these bands must be interpreted with caution, as there is overlap between pathways. Specifically, VST and RST are shown in the alpha frequency band, while VST and CST are reflected in the beta band, potentially masking the source for such changes. Despite these limitations, intermuscular coherence has been shown to reveal the neural origin for coactivated muscles in a synergy, outperforming correlation analysis of EMG signals [[Laine and Valero-Cuevas, 2017](#)].

### 1.3 Statement of the problem

Stroke is a leading cause of long-term disability worldwide, resulting in severe sensorimotor impairments. *Pathological synergies*—defined as abnormal muscle coupling patterns that disrupt voluntary arm movement—are a major contributor to motor dysfunction. In most stroke survivors, these synergies manifest as pathological flexion synergies (involving abnormal coupling of shoulder abduction, elbow flexion, and forearm supination). These intrusive movement patterns severely limit the ability to perform reaching and grasping movements, and are further exacerbated during voluntary shoulder abduction. Current approaches to studying pathological synergies rely on methods—such as dimensionality reduction techniques for synergy extraction—that describe patterns of muscle co-activation without providing insights into their neural origins. Intermuscular coherence (IMC), on the other hand, offers a powerful tool for assessing shared neural drive to muscles, allowing researchers to identify synchronized neural drive across different frequency bands. The mechanism underlying such pathological synergies is thought to result from a combination of damage to the corticospinal tract (CST) and increased drive from subcortical pathways, such as the reticulospinal tract (RST) and vestibular motor output. While the role of the RST in pathological synergies has been relatively well-studied, the contribution of the vestibular output remains poorly understood. The vestibular motor output is known for its critical role in modulating motor neuron

excitability, muscle tone, and postural control. Moreover, its upregulation after stroke has been linked to increased spasticity and maladaptive reflex responses. However, its specific contribution to pathological synergies during voluntary reaching movements has not been systematically addressed nor excluded.

This work aims to establish whether vestibular brainstem output contributes to pathological synergies by measuring shared neural drive to muscles (as measured by intermuscular coherence) during voluntary reaching movements. A better understanding of the mechanisms underlying pathological synergies will offer new insights for developing targeted rehabilitation strategies that aim to reduce motor impairment following stroke.

## 1.4 Precedent logic and overarching hypothesis

**Scientific Premise 1:** Pathological synergies in stroke survivors arise from increased drive in descending subcortical (brainstem) pathways and maladaptive reflex responses [Krakauer, 2005]. Importantly, both vestibular motor output and reticulospinal drive have been shown to increase following stroke, potentially contributing to abnormal muscle co-activation patterns [McPherson et al., 2018, Miller et al., 2016].

**Scientific Premise 2:** During voluntary reaching movements, increased shoulder abduction loads exacerbate pathological synergies and muscle co-activation patterns in stroke survivors [Sukal et al., 2007, Ellis et al., 2008, 2016].

We hypothesize that shared neural drive –as measured by IMC— increases during shoulder abduction, and is further increased by vestibular stimulation, providing support for a vestibular mechanism underlying pathological synergies (see Figure 1.1). Conversely, if vestibular stimulation during shoulder abduction does not increase shared neural drive beyond abduction alone (i.e., without stimulation), our findings would argue against a vestibular contribution to pathological synergies in stroke.

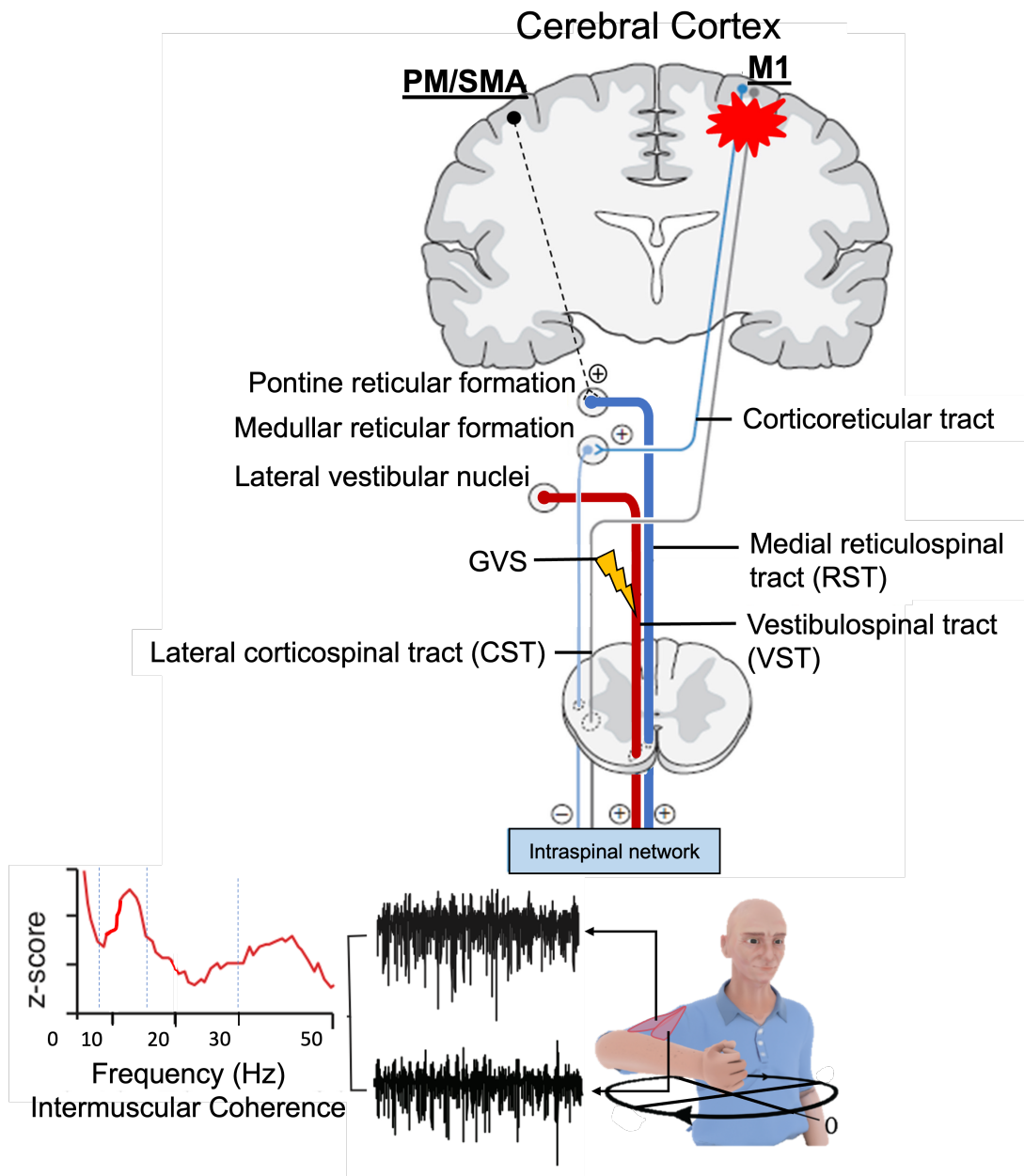


Figure 1.1: Proposed mechanism underlying pathological synergies: Disruption of the corticospinal tract leads to increased subcortical drive (RST and vestibular motor output), as well as maladaptive changes in reflex activity. Shoulder abduction is expected to increase neural drive and exacerbate pathological synergies. Neural drive can be measured through Intermuscular Coherence, which in the alpha frequency band (8- 16 Hz) suggests preferential subcortical drive, such as reticulo- and vestibulo-spinal tracts, while the beta (16- 30 Hz) and gamma (30- 60 Hz) frequency bands suggest preferential cortical and vestibular drive. Galvanic Vestibular Stimulation (+): Excitatory; (-): Inhibitory. Thicker lines indicate increased drive, while thinner lines indicate pathway disruption. Adapted from Li, Chen, Francisco, Zhou, and Rymer [2019].

## 1.5 Significance of testing the overarching hypothesis

The mechanisms underlying pathological synergies have predominantly focused on the role of increased neural drive from the reticulospinal tract. However, the specific contribution of vestibular motor output remains poorly understood. This work will provide a much-needed characterization of the vestibular system's role in voluntary movement, both in young neurotypicals and following stroke. By establishing a baseline shared neural drive in healthy individuals, our study will offer critical insights into how these mechanisms are affected following stroke, while controlling for physiological factors such as age and dominance. This baseline will also serve as a reference against which to compare other neurological conditions to which the vestibular motor output might also contribute. Importantly, our findings will have significant implications for developing targeted therapeutic interventions aimed at improving motor function and rehabilitation outcomes for stroke survivors. By understanding the vestibular contribution to motor dysfunction, we could inform novel treatment strategies that target both the vestibular system and motor recovery pathways, leading to better rehabilitation outcomes.

## 1.6 Thesis outline

Chapter 2 presents a characterization of vestibular drive to neck and arm muscles during Rest and Voluntary movements (Reaching and Isometric contractions) in young neurotypical participants. To investigate the contribution of vestibular drive to arm muscle, we apply Galvanic Vestibular Stimulation (GVS) to compare with Sham and No Stimulation stimuli types. These results serve as a critical baseline against which to compare changes in shared neural drive to neck and arm muscles following stroke as well as other neurological conditions where vestibular drive might be dysregulated. This work was published in the Journal of Physiology [[Bartsch and Valero-Cuevas, 2025](#)].

Chapter 3 builds upon the findings from the previous chapter to investigate if and how stroke alters vestibular contributions to voluntary arm movement by comparing stroke survivors to age-matched controls. To test our hypothesis, we include both shoulder abduction and Galvanic Vestibular Stimulation (GVS) as experimental conditions. We hypothesize that intermuscular coherence increases during shoulder abduction, but not during vestibular stimulation, excluding a common vestibular mechanism underlying pathological synergies. This work will be published shortly.

Chapter 4 summarizes the research presented from Chapter 2 and 3 and discusses future work.

Appendix 1: Presents our work on the ability of conventional dimensionality reduction techniques to identify differences between neurotypical participants and individuals with neurological conditions. We applied principal component analysis (PCA) and non-negative matrix factorization (NMF) to identify muscle synergies by reducing the complexity of high-dimensional electromyographic (EMG) data. In this context, we introduced the concepts of *Coarse* and *Fine* synergies, where *Coarse* synergies represent dominant features of muscle co-activation, while *Fine* synergies capture more subtle adaptations in participants with motor impairment. Our findings contribute to the discussion on the limitations of standard synergy extraction techniques and provide insights into whether alternative approaches may be needed to better characterize the neural basis of pathological synergies. This work was published in the Frontiers in sports and active living journal [[Bartsch-Jimenez et al., 2023](#)]

Appendix 2: Describes the R-based package designed for analyzing shared neural drive using electromyographic (EMG) signals. R is an open-source statistical computing environment, ensuring unrestricted access and promoting the democratization of knowledge. The package offers a documented and integrated workflow, enabling users to perform the entire analysis –from signal processing to statistical hypothesis testing— within the same computational environment. By providing an accessible and standardized approach on a widely used open-source platform, this package aims to familiarize users with the analyses

commonly employed in coherence studies. This is especially beneficial in contexts where access to commercial software is limited, supporting global research initiatives in motor control, neurophysiology, and rehabilitation.

# **Chapter 2**

## **Contributions of vestibular motor output to arm muscle during voluntary movement in young neurotypical**

**Vestibular contribution to motor output is also suppressed by voluntary action of the arm** by Bartsch-Jiménez A and Valero-Cuevas FJ. *Journal of Physiology*, 2025.

### **2.1 Abstract**

The vestibular sensory system is among the oldest and most fundamental contributors to motor behavior as it is critical to maintaining posture and balance. However, such low-level motor responses could interfere with cortically-mediated voluntary behavior that naturally involves posture and balance. Consequently, it has been proposed that—much like the inhibition of reflex responses—vestibular contributions to motor output is ‘gated’ (dubbed *vestibular suppression*) to avoid undesirable self-perturbations during voluntary head movements. Here we demonstrate such suppression also occurs for unperturbed voluntary arm function. Our evidence comes from comparing coherence at baseline (No Stimulation) and after Sham and Galvanic Vestibular Stimulation (GVS). Specifically, neck muscles showed shared neural drive (intermuscular coherence), which increased with GVS—but not Sham—at Rest. This GVS-mediated increased coherence in

neck muscles, however, was suppressed during voluntary isometric contractions and reaching movements of the arm on the same side as the GVS was applied. No changes were found in pairwise intermuscular coherence during Sham (compared with No stimulation) or in arm muscles at either rest or during voluntary movement during GVS in neurotypical adults. In addition to extending vestibular suppression to unperturbed voluntary arm function, these results provide support for the common (yet unproven to our knowledge) notion that arm muscles do not receive vestibular neural drive during unperturbed voluntary movement. Moreover, these results shed light on the mechanisms that mediate competing descending outputs for voluntary function, and serve as a baseline against which to compare potential task-dependent dysregulation of vestibular-mediated output to the neck and arms in stroke and neurological conditions.

## 2.2 Introduction

The otoliths and semicircular canals are constantly sensing expected and unexpected head orientation and movement relative to space [Cullen, 2023b,a]. These inputs are integrated with somatosensory and predictive self-motion signals from the brainstem, cerebellum and cortex [Cullen and Zobeiri, 2021]. Such integration is essential for reflexive stabilization of gaze and posture, and accurate control of voluntary movements [Cullen, 2023a,b].

While vestibular reflexes are essential for providing robust responses to unexpected external stimuli, they could be counter-productive when they interfere or compete with motor signals for voluntary movements [Lopez and Cullen, 2024, Niyo et al., 2024]. Consider how vestibular reflexes can be in competition with voluntary function when, for example, voluntary head rotations need to be ignored during reaching movements. Experimental evidence shows that these reflexes —observed as electromyographic responses to perturbations— are largely suppressed during active head movements. [Kwan et al., 2019, Cullen, 2023b,a]. Notably, responses in the vestibular nuclei are suppressed (*vestibular suppression*), and occur in neck muscles during voluntary and self-initiated head movements [Cullen and Zobeiri, 2021]. Importantly, vestibular

suppression in leg muscles is also seen and modulated during voluntary leg movements for locomotion [Dakin et al., 2013] —presumably to avoid motor interference. On the other hand, the contribution of vestibular drive to upper extremity voluntary movement is critical for sensing our self-initiated movements relative to the environment [Cullen, 2023a]. Moreover, allows us to estimate additional physical forces (e.g., coriolis and centrifugal forces) needed to plan and execute an accurate movement, such as during reaching. Accordingly, the motor pathways controlling reaching movements demonstrate feedback-mediated responses at a minimal latency of 50ms. These responses compensate for displacements of the body and limb —relative to a reaching target— produced by externally applied perturbations as well as during self-motion [Adamovich et al., 2001, Azadjou et al., 2023]. Moreover, they are reduced after unilateral vestibular lesions, excluding their emergence from the proprioceptive system [Raptis et al., 2007]. In fact, the vestibular system contributes to the high-level planning of reaching movements, which is crucial for achieving accurate movement performance [Schlack et al., 2002, Klam and Graf, 2006, Azadjou et al., 2023]. For example, neurons in the macaque parietal cortex show increased firing responses to vestibular signals, which are integrated with other somatosensory inputs, including proprioception, vision, and touch [Cullen, 2023b]. Furthermore, the Corticospinal tract and brainstem output—from the Medial Longitudinal Fasciculus (MLF) which contains reticulo-, vestibulo- and tecto-spinal tracts—send converging and overlapping signals to the spinal cord during reaching and grasping tasks [Riddle and Baker, 2010].

The contribution of the vestibular system to voluntary movement is determined by measuring vestibulospinal drive while applying GVS. Vestibular afferents are stimulated through current applied via transmastoid surface electrodes, increasing vestibulospinal drive, without affecting proprioception and tactile sensory information [Forbes et al., 2015, Kwan et al., 2019, Cullen, 2023b]. The GVS-mediated increase in vestibular drive evokes both ocular and postural responses with electromyographic responses in axial and appendicular muscles with a latency of 8 to 50ms [Forbes et al., 2015, Cullen, 2023a].

Given that upper limb movement also depends on accurate suppression of reflexes and accurate estimation of position and velocity of the body, we investigated the vestibular contribution to arm movements and whether suppression is also a mechanism to enable voluntary arm movements in humans. We hypothesize that, as in voluntary neck and leg movements, vestibular contributions to the activation of neck and arm muscles should differ between rest and voluntary movement of the arm. To test our hypothesis, we compared shared neural drive –as measured by IMC– to neck and arm muscles during rest and voluntary arm movement when No stimulation and GVS was applied. Moreover, we also compared No stimulation and GVS to Sham stimulation to exclude a placebo effect or an alternative mechanism –such as tactile or proprioception– that could explain changes in neural drive. Understanding the role of the brainstem vestibular output in arm movements could then provide valuable insights into its contribution to motor impairments following neurological conditions such as stroke.

## 2.3 Materials and Methods

### Ethical Approval

The study conformed to the standards set by the Declaration of Helsinki, except for registration in a database. All participants gave their informed written consent to participate in this study, which was approved by the University of Southern California Internal Review Board (USC IRB: HS-17-00304).

### Study participants

Seventeen right-handed individuals participated in the study (n=17; 7 males; 10 females), with a mean age of 21.5 years (ranging from 18 to 27 years), all free from pain, injury or any conditions affecting upper limb movement. Importantly, all participants were free from any neurological condition affecting control of the upper extremity (neurotypical).

## Tasks

Participants performed the following tasks while sitting. *Rest*: Participants were seated with their hands resting on their lap or armrest. They were encouraged to stay relaxed and silent for 90 seconds at the beginning of the experimental procedures to collect baseline muscle activity (Fig. 2.1, left panel). *Voluntary reaching*: Participants were seated in front of a hand-powered ergometer mounted to be rotated in the horizontal plane with their right arm (Fig. 2.1, middle panel). The protocol for this task is thoroughly described in a previous article [Laine et al., 2021]. *Isometric contraction*: Participants were seated with the backrest inclined 15° backwards (Fig. 2.1, right panel). They were encouraged to keep their heads as close as possible to the headrest, without supporting any weight on it. This position was enforced to have a bilateral isometric contraction of the Sternocleidomastoid muscles, and Upper Trapezius for head stabilization. Simultaneously, they held a 2.26 Kg dumbbell with their hands, while their forearm is kept parallel to the ground and the arm parallel to the inclined backrest, but without any support on it. This position induced an isometric co-contraction of the Biceps Brachii, Anterior and Middle Deltoid muscles. Participants were encouraged to hold this position for 90 seconds, while verbal feedback was provided to correct or return to the instructed position if they departed from it. They were allowed to rest or to support their heads/extremities if they felt fatigued, however, it was not needed by any participant.

## Stimulus Types

For each task, participants were subjected to three Stimulus Types; No stimulation GVS, and Sham stimulation. Based on previous protocols on human participants, GVS consisted of a binaural galvanic stimulation where the positive electrode was placed on the right mastoid process (negative electrode on the left mastoid process) [Forbes et al., 2015]. The position of the electrodes was chosen to induce a vestibular response on the right-side of the body, which was confirmed by visual inspection of the EMG signal from the SCM muscle

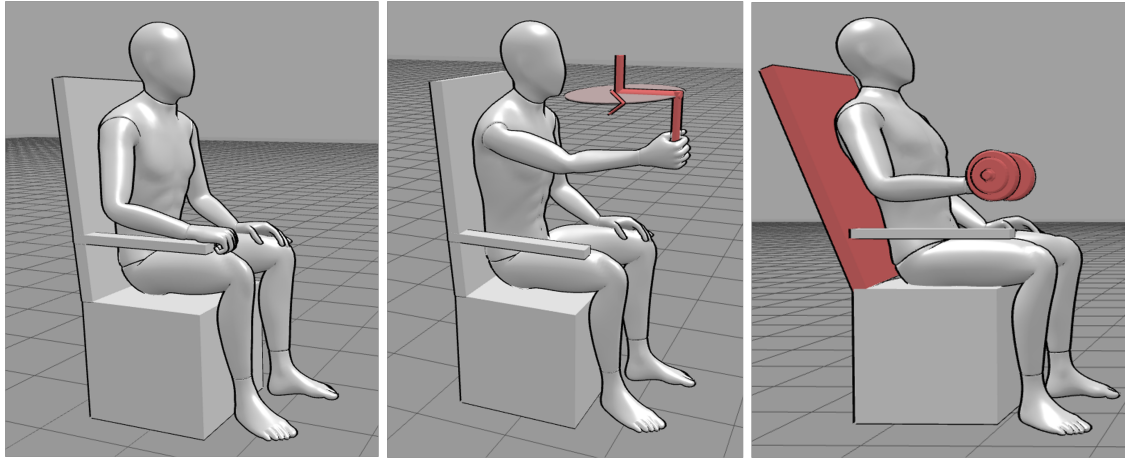


Figure 2.1: Tasks performed by each participant. Left: At the beginning of the experiment, each participant sat comfortably in a chair with their hands on their lap, while EMG was recorded at *Rest*. Middle: During the *Reaching* task, participants are asked to rotate an horizontal ergometer in a counterclockwise rotation with their right arm to produce a cyclical movement. Right: In the *Isometric* condition, subjects were positioned with a 15° inclined backrest, while raising their head from the headrest to activate the sternocleidomastoid muscles. Meanwhile, their right upper extremity remained unsupported as they held a 2.26kg dumbbell, with their forearm parallel to the ground and their arm aligned with the backrest.

(see Fig. 2.3, lower left panel). The stimulation frequency was set at 4 Hz, with an amplitude ranging between 0.8 and 1.2mA. The amplitude was modulated to avoid EMG signal saturation from the SCM muscle or if the participant felt uncomfortable. Independent of the stimulation amplitude, the Sternocleidomastoid response to GVS was always clearly visible and greater than the EMG signal at rest. For the Sham stimulation, a mechanical vibration (400 Hz) was delivered on the right mastoid (same location as the positive GVS's electrode). Each participant completed nine randomized conditions: three Tasks (Reaching, Isometric and Rest) and three Stimulus Types (GVS, None and Sham). To mitigate potential carryover effects of GVS and Sham, the *Rest + No stimulation* condition was always completed first. Moreover, to assess the potential carryover effects of GVS, the resting condition was repeated at the end of the experiment. Subsequently, the *Rest + No stimulation* conditions at the beginning and end of the experimental procedures were compared, to determine if the vestibular drive remains increased over time, even after GVS has ceased.

## Data acquisition and processing

A custom game was designed in c# to collect the angle data from the ergometer and provide live real time feedback about the user's rotation velocity (Unity3D, San Francisco, CA, USA). Custom hardware provided a pulse via an Arduino MEGA (Arduino, Somerville, MA, USA) to synchronize EMG data, angle measurements, and GVS stimuli delivery time. We collected EMG signals at 2.5 kHz from seven muscles of the right upper extremity using a DataLINK system and associated software (Biometrics Ltd, Newport, UK). Surface EMG sensors (Biometrics Ltd SX230: bipolar, gain: 1,000, bandwidth: 20–460 Hz) were placed over the right arm: Biceps Brachii (Bic), lateral head of the Triceps Brachii (Tric), Anterior, Middle and Posterior Deltoid (ADelt, MDelt, PDelt, respectively), upper Trapezius (UTrap) and Sternocleidomastoid muscles (SCM), following standard recommendations from SENIAM. Electrode placement and signal quality were confirmed using palpation of each muscle and observation of the EMG during voluntary activation. This set of muscles is sufficient for a general analysis of coupling among the shoulder/elbow muscles relevant to our task [Laine et al., 2021]. All EMG signals were processed offline using R/Rstudio [R Core Team, 2021]. To remove GVS artifacts, a 10ms window surrounding each stimulus (from 2ms before to 8ms after the electrical pulse) was replaced with empty or missing values from the SCM, Deltoid (ADelt, MDelt, PDelt), and UTrap EMG signals (see Fig. 2.3, bottom panel). The missing data points were then interpolated to prevent aliasing and preserve the signal's frequency characteristics. Since vestibular responses have a latency of 8 to 50ms, we prevented their removal from the signals during the replacing and interpolation process. [Forbes et al., 2015]. Signal processing was done according to our previous published paper (for a detailed description see Laine et al. 2021). In summary, all EMG signals were downsampled to 1,000 Hz, band-pass filtered between 8 to 250 Hz, and then full wave rectified. The filter's purpose was to remove any remaining artifacts arising from GVS, as well as from those frequencies irrelevant for intermuscular

coherence analysis. EMG rectification was done to enhance intermuscular coherence and avoid distortion of motor synchronization [Boonstra and Breakspear, 2012].

## Statistical analysis

Coherence analysis measures the shared neural drive between two signals in the frequency domain (correlation in the frequency domain). As such, intermuscular coherence (IMC) assesses the degree of synchronization between the neural drive to two muscles on the basis of their EMG signals [Boonstra, 2013]. Consequently, we calculated magnitude squared coherence between each muscle pair using 300 ms windows and a 50% overlap [Laine et al., 2021].

A threshold to determine significant pairwise coherence was built for easy visual inspection (see red dotted line in Fig. 2.4 and 2.5). To estimate the coherence expected by chance, we generated 1,000 phase-randomized surrogate series for each muscle pair and participant following the methods described by Ebisuzaki [1997]. Coherence was calculated for each surrogate pair. A 95% confidence interval (95% CI) was constructed for each muscle pair based on the *z-transformed* coherence values obtained from the surrogates. This interval was built across all frequency bands to provide a stringent and robust criterion for assessing statistical significance during visual inspection. Importantly, this 95% CI was not used in hypothesis testing but rather as a visual reference to highlight when individual pairwise coherence exceeds the highest values expected by chance. In other words, individual pairwise coherence above the 95% CI is likely to be significant, revealing true shared drive between the two muscles.

For unbiased statistical estimation during hypotheses testing, all raw –magnitude-squared– coherence values were transformed to *z-scores* ( $\text{IMC}_z$ ) using Fisher's Z transform ( $\text{IMC}_z = \text{atanh}(\rho)$ ) before performing statistical comparisons [Laine et al., 2021]. We compared  $\text{IMC}_z$  across the three Stimulus Types and Tasks. The values of  $\text{IMC}_z$  across the frequency spectrum were gathered into three bands: alpha (8-16 Hz), beta (16-30 Hz) and gamma (30-50 Hz) frequency bands. This approach allowed us to minimize statistical error

by decreasing the number of *post-hoc* comparisons to make if the null hypothesis was rejected. Given the lack of a non-parametric alternative to test our hypotheses, a Robust Mixed Effect ANOVA model (i.e. robust repeated Measures ANOVA model) was used to test if GVS increased neural drive. The assumptions of the classical ANOVA statistical tests are not required to be met when performing these robust statistical methods. Then, if a GVS effect was found across frequency bands, we compared  $\text{IMC}_z$  using Statistical Parametrical Mapping (SPM) across the three Stimulus Types for each task separately (*Rest*, *Reaching* and *Isometric*) to identify the specific frequencies at which the differences were significant. Finally, to test for a carryover effect (i.e. long-lasting GVS effect), we compared coherence at the beginning and end of the experimental protocol when the participant was at rest and without any stimulus. Post-hoc comparisons were made using Dunnett test with Bonferroni corrections (adjusted for two comparisons: GVS vs. No Stimulation and GVS vs. Sham).

## 2.4 Results

As expected, the shared neural drive between neck muscles at *Rest* (as per  $\text{IMC}_z$ ) increased during GVS (Fig. 2.4). This was confirmed by a repeated measures ANOVA model with *post-hoc* comparisons and Bonferroni corrections at each frequency band (i.e., alpha to gamma, see Fig. 2.4 and Table 2.2). Importantly, no significant differences were found in  $\text{IMC}_z$  for neck muscles between None and Sham stimulus types (p-values: alpha=0.76, beta=0.7, gamma=0.55, see Table 2.2). This supports the notion that GVS increases vestibular output only to neck muscles (see upper panel in Fig. 2.4 and upper left panel in Fig. 2.5).

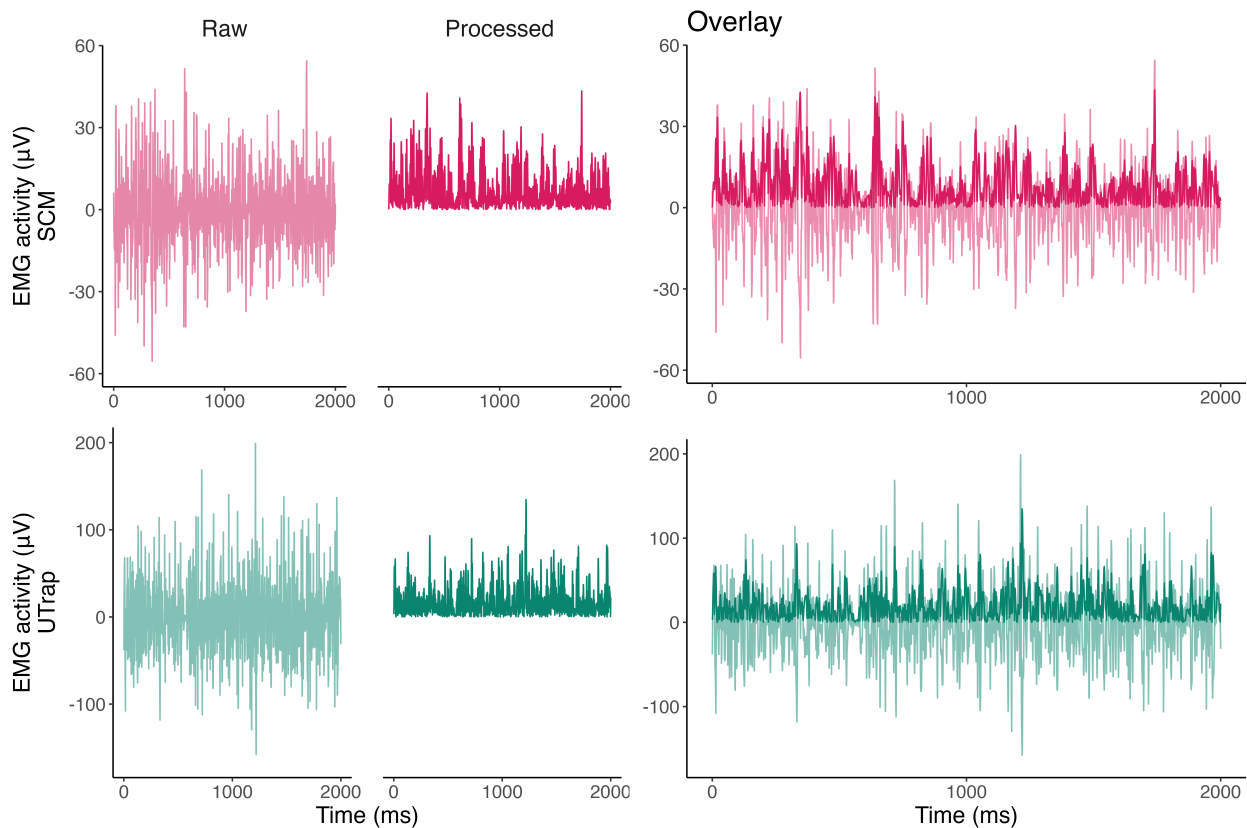


Figure 2.2: Raw, and processed (full-wave rectification and band-pass filtered) EMG signals from a typical participant without stimulation, recorded during the *Isometric* task, five seconds after the task started. Each trace represents 2 seconds of data. The left panel displays the *Raw* and *Processed* EMG signals for the *Sternocleidomastoid* (SCM) and *Upper Trapezius* (UTrap) muscles. The right panel overlays the signals with the sequential processing steps: the light trace corresponds to the Raw signal (see positive and negative values) and the darkest trace represents the final processed signal.

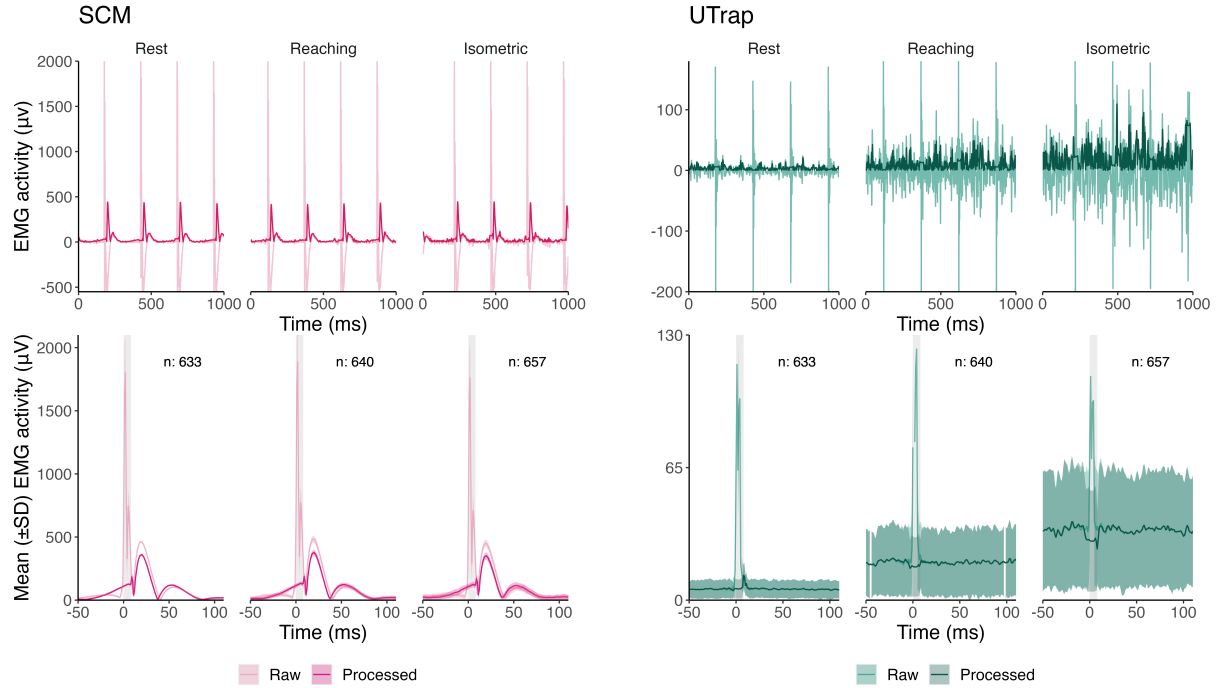


Figure 2.3: The *Sternoclidomastoid* (SCM) muscle shows a stereotypical response across all tasks, while the *Upper Trapezius* (UTrap), shows a smaller response restricted to *Rest*, emphasizing its suppression during *Isometric* and *Reaching* tasks. *Top:* Raw and Processed (GVS artifact removed, full-wave rectified and band-pass filtered) EMG activity from *Sternoclidomastoid* (SCM) and *Upper Trapezius* (UTrap) muscles during each task (when GVS was applied) for a typical participant. Each trace corresponds to one second of activity, which was extracted when the signal was stable (5s after the tasks started)

*Bottom:* Mean ( $\pm$ SD) Raw and Processed EMG activity (across stimuli) in response to Galvanic Vestibular Stimulation (GVS), from 50ms before to 110ms after the stimuli was delivered. For visualization purposes of the stereotypical response, all stimuli were aligned to their delivery time ( $t = 0$ ). It showcases the averaged EMG responses across all stimuli from a single participant (number of averaged stimuli highlighted inside each plot). The light trace shows the GVS artifact while the darker trace shows the EMG after this artifact was removed and the signal processed (full-wave rectified and band-pass filtered). The shaded gray area represents the 10 ms window (ranging from -2 ms to 8 ms) during which the GVS artifact was removed prior to signal processing (see Section 2.3). Following this window, suppression of the UTrap response is observed during voluntary action of the arm, as opposed to SCM responses, which are always visible.

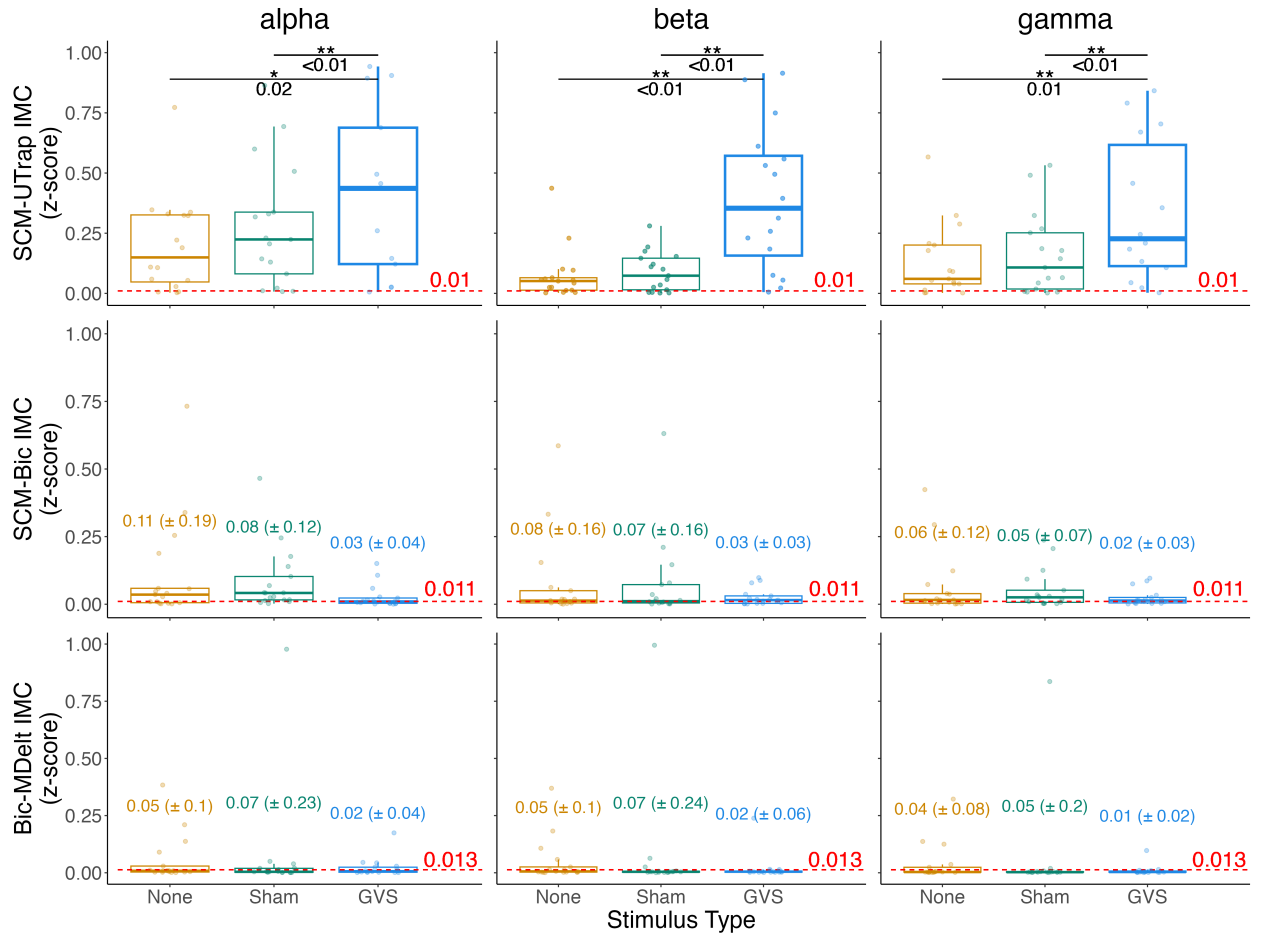


Figure 2.4: During Rest, Galvanic vestibular stimulation (GVS) increases intermuscular coherence (IMC) across alpha, beta and gamma frequencies between neck muscles, but not arm, muscles. We compared *z*-transformed IMC coherence across frequency bands during Rest under three different stimulus types: No Stimulation (None), Sham and GVS. Neck muscles are *Sternocleidomastoid* (SCM) and *Upper Trapezius* (UTrap). Arm muscles are *Biceps brachii* (Bic) and *Anterior Deltoid* (ADelt). Red dotted line indicates the 95% upper confidence interval estimated from 1,000 randomizations of the original signals. The middle and lower panels include the mean  $IMC_z$  across stimulus types on top of their corresponding box for easy comparison while keeping the same scales across muscle pairs.

Table 2.1: Robust repeated measures ANOVAs: degrees of freedom, F ratio, p-value, and effect size ( $\eta^2$ ). Muscles: Sternocleidomastoid (SCM), Upper Trapezius (UTrap), Biceps brachii (Bic), Triceps brachii (Tric), and Anterior, Middle, and Posterior Deltoid (ADelt, MDelt, PDelt). Subscripts indicate Neck-Neck muscles: N-N, Neck-Arm muscles: N-A, and Arm-Arm muscles: A-A.

Muscle	alpha			beta			gamma		
	F-value (DF <sub>1</sub> , DF <sub>2</sub> )	p-value	$\eta^2$	F-value (DF <sub>1</sub> , DF <sub>2</sub> )	p-value	$\eta^2$	F-value (DF <sub>1</sub> , DF <sub>2</sub> )	p-value	$\eta^2$
SCM-UTrap <sub>(N-N)</sub>	7.35 (1.5,24.6)	0.01	0.31	17.16 (1.2,19.8)	<0.001	0.52	9.35 (1.2,19.3)	<0.001	0.37
SCM-Bic <sub>(N-A)</sub>	1.62 (1.6,25.7)	0.22	0.09	0.79 (1.8,29.4)	0.45	0.05	0.95 (1.6,26.3)	0.38	0.06
UTrap-Bic <sub>(N-A)</sub>	1.04 (1.2,19.8)	0.34	0.06	1.07 (1.2,19)	0.33	0.06	1.09 (1.1,17.9)	0.32	0.06
UTrap-Tric <sub>(N-A)</sub>	1.34 (1.6,25.7)	0.27	0.08	0.88 (1.2,19.5)	0.38	0.05	1.54 (2,32)	0.23	0.09
UTrap-MDelt <sub>(N-A)</sub>	0.63 (1,16.6)	0.45	0.04	0.89 (1,16.2)	0.36	0.05	0.98 (1,16.7)	0.34	0.06
Bic-ADelt <sub>(A-A)</sub>	1 (1.7,27.1)	0.37	0.06	1.46 (1.3,21.6)	0.25	0.08	1.43 (1.3,20.9)	0.25	0.08
Bic-MDelt <sub>(A-A)</sub>	0.48 (1.4,23.1)	0.57	0.03	0.47 (1.4,23.1)	0.57	0.03	0.57 (1.4,22.1)	0.51	0.03
Bic-PDelt <sub>(A-A)</sub>	0.08 (1.8,28.3)	0.90	0.00	0.01 (1.7,27.5)	0.99	0.00	0.02 (1.5,24.1)	0.95	0.00
ADelt-MDelt <sub>(A-A)</sub>	1.09 (1.4,22.6)	0.33	0.06	0.29 (2,32)	0.75	0.02	0.66 (2,32)	0.52	0.04
ADelt-PDelt <sub>(A-A)</sub>	0.39 (1.2,19)	0.58	0.02	0.11 (1.6,25.9)	0.85	0.01	0.28 (1.6,26)	0.71	0.02
MDelt-PDelt <sub>(A-A)</sub>	0.1 (1.2,18.6)	0.79	0.01	0.38 (1.1,17.9)	0.57	0.02	1.14 (1.2,19.2)	0.31	0.07

Table 2.2: Adjusted p-values for *post-hoc* comparisons using Bonferroni corrections (adjusted for 2 comparisons). Red text indicates significant differences between stimulus types: No Stimulation (*None*), *Sham* and Galvanic Vestibular Stimulation (*GVS*). Muscles: *Sternocleidomastoid* (*SCM*), *Upper Trapezius* (*UTrap*), *Biceps brachii* (*Bic*), *Triceps brachii* (*Tric*) and *Anterior, Middle and Posterior Deltoid* (*ADelt,MDelt,PDelt*). Subscript indicates Neck-Neck muscles:*N-N*, Neck-Arm muscles:*N-A*, and Arm-Arm muscles: *A-A*.

Muscle	alpha			beta			gamma		
	None/ GVS	None/ Sham	GVS/ Sham	None/ GVS	None/ Sham	GVS/ Sham	None/ GVS	None/ Sham	GVS/ Sham
SCM- UTrap <sub>(N-N)</sub>	<.001	0.76	0.02	<.001	0.70	<.001	<.001	0.55	0.01
SCM- Bic <sub>(N-A)</sub>	0.12	0.69	0.08	0.22	0.96	0.24	0.22	0.75	0.18
UTrap- Bic <sub>(N-A)</sub>	0.60	0.31	0.30	0.43	0.34	0.29	0.52	0.32	0.29
UTrap- Tric <sub>(N-A)</sub>	0.11	0.67	0.17	0.28	0.49	0.28	0.10	0.79	0.19
UTrap-MDelt <sub>(N-A)</sub>	0.38	0.52	0.15	0.37	0.35	0.85	0.31	0.37	0.37
Bic- ADelt <sub>(A-A)</sub>	0.25	0.76	0.35	0.09	0.64	0.23	0.18	0.50	0.23
Bic- MDelt <sub>(A-A)</sub>	0.27	0.80	0.45	0.34	0.72	0.44	0.19	0.79	0.40
Bic- PDelt <sub>(A-A)</sub>	0.72	0.82	0.86	0.94	0.99	0.91	0.93	0.85	0.86
ADelt- MDelt <sub>(A-A)</sub>	0.36	0.57	0.25	0.87	0.45	0.57	0.77	0.25	0.45
ADelt- PDelt <sub>(A-A)</sub>	0.52	0.67	0.56	0.70	0.78	0.80	0.54	0.88	0.61
MDelt- PDelt <sub>(A-A)</sub>	0.85	0.85	0.22	0.62	0.46	0.64	0.26	0.33	0.63

A more detailed analysis of these GVS-driven increases in  $IMC_z$  between SCM-UTrap suggests such vestibular output spans a broad frequency spectrum. This was quantified by SPM analysis in 0.5 Hz bins across frequencies, which showed consistently increased  $IMC_z$  during GVS when compared to None and Sham stimulus types. Specifically,  $IMC_z$  was higher in the range from 12 and 50 Hz (high alpha to gamma bands,  $SPM\{F\}_{2,32}$ , Random Field Theory threshold=6.6,  $p < 0.001$ , Fig. 2.5).

A secondary analysis confirmed that our block-randomized application of the three Stimulus Types did not produce measurable carry-over effects. This was confirmed by comparing the baseline coherence of Neck muscles during *Rest + No stimulation* conditions at the beginning and the end of the experimental protocol ( $p = 0.3$ ). This finding supports the feasibility of complete task randomization in future studies.

Interestingly, GVS did not increase  $IMC_z$  between neck muscles (SCM-UTrap) during unperturbed voluntary *Reaching* or *Isometric Contraction*. This is supported by the results of both repeated measures

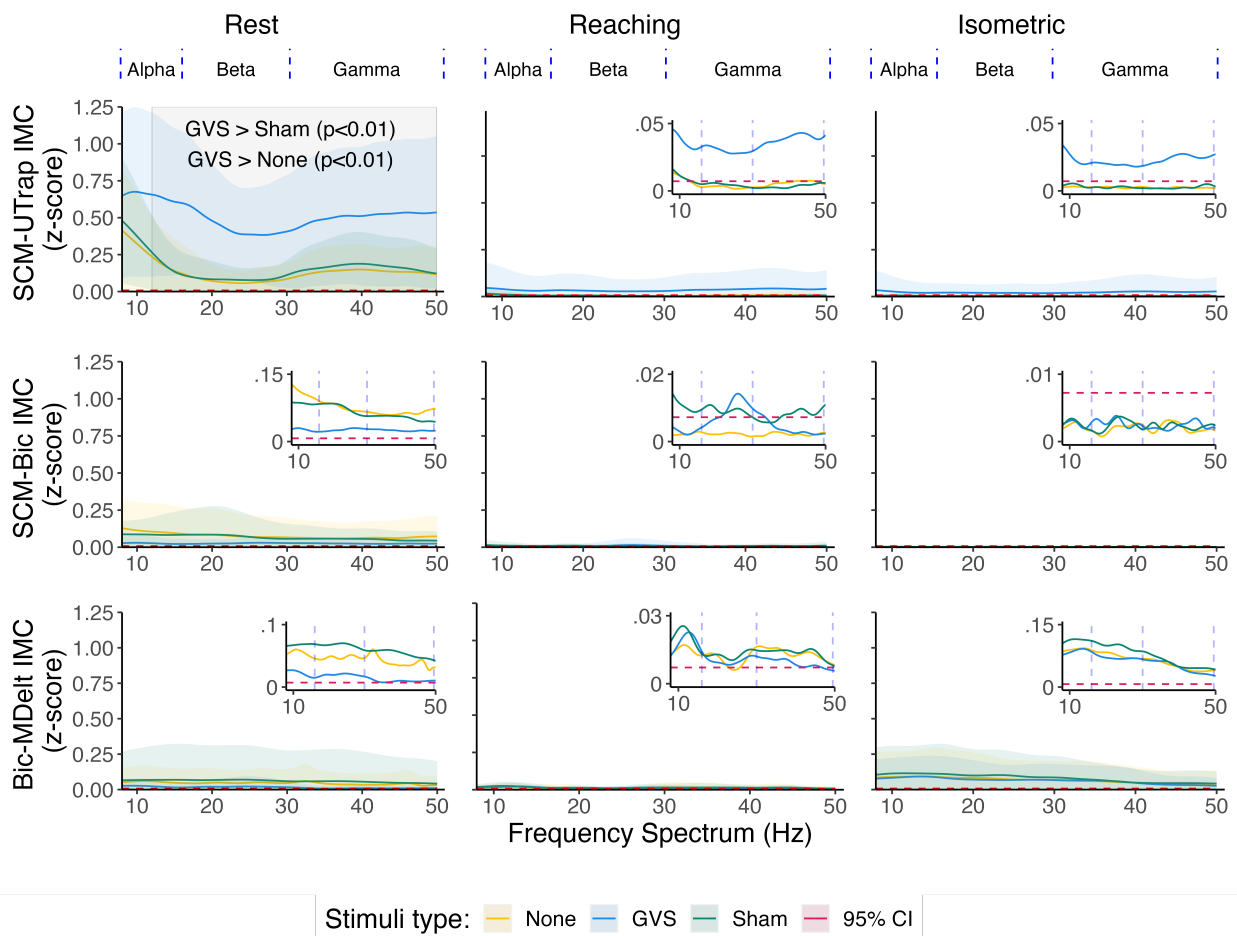


Figure 2.5: Galvanic Vestibular Stimulation (GVS, blue line) increases vestibular drive to neck muscles (SCM-UTrap) at Rest. However, it's suppressed during Reaching and Isometric tasks. GVS did not increase vestibular output to neck-arm and arm muscles (SCM-Bic and Bic-MDelt, respectively), neither at Rest nor during unperturbed voluntary action of the arm. No differences were found between Sham and No stimulation (which excludes a placebo effect). Mean ( $\pm$ SD)  $z$ -transformed IMC <sub>$z$</sub>  coherence across subjects during rest condition under three different Stimuli: No Stimulation (None), Sham and Galvanic Vestibular Stimulation (GVS). Each plot (except for SCM-UTrap at Rest) includes an inset where the signals are autoscaled. Neck muscles are SCM: *Sternocleidomastoid* and UTrap: *Upper Trapezius*. Arm muscles are Bic: *Biceps Brachii* and MDelt: *Middle Head of Deltoid*. Values above the dotted red line can be considered to have significant IMC <sub>$z$</sub> , as per the 95% upper confidence interval estimated from 1,000 randomizations of the original signals. Alpha, beta and gamma frequency bands are identified by blue vertical dashed line on top of upper panel.

ANOVA and SPM analysis, which did not reveal significant differences when comparing GVS with either Sham or No stimulation (see middle and right upper panel in Fig. 2.5). This is an example of vestibular suppression that, to our knowledge, has not been reported during voluntary function in human or non-human primates. Finally, vestibular output is neither present nor suppressed in arm muscles in any condition (*Rest, Reaching* and *Isometric*), demonstrated by no significant differences in  $\text{IMC}_z$  from muscle pairs in the active arm. This was supported by the results of both repeated measures ANOVA and SPM analysis (see middle and lower panels in Figs. 2.4 and 2.5).

## 2.5 Discussion

Our intermuscular coherence results —as per  $\text{IMC}_z$ —indicate that neck, but not arm muscles, receive shared neural drive from the vestibular system (brainstem vestibular output) in neurotypical participants. Importantly, this vestibular output to neck muscles is increased at *Rest* during GVS (see upper panels in Fig. 2.4 and left upper panel in Fig. 2.5), but suppressed during voluntary action of the arm (*Reaching* and *Isometric* contraction, see middle and right upper panel in Fig. 2.5), without reaching statistical significance during voluntary movement of the arm. In support of this central result, we did not see increases in  $\text{IMC}_z$  during the Sham condition when compared with No stimulation. Consequently, we can exclude a tactile or proprioceptive mechanism for the changes seen during GVS, as well as a placebo effect. We propose that this is a previously unreported form of *vestibular suppression* due to voluntary action of the arm —which was known to exist in neck muscles during head movements [Cullen and Zobeiri, 2021]. Moreover, the lack of increase in  $\text{IMC}_z$  with GVS between neck and arm muscles (SCM-Bic), and between arm muscles (Bic-MDelt) provides evidence that these arm muscles are unlikely to receive vestibular output at *Rest* or during unperturbed *Reaching* and *Isometric* tasks (see Figs. 2.4 and 2.5). We conclude that this previously unknown distribution and task-dependent suppression of brainstem vestibular output in neck vs. arm muscles during Rest and voluntary function sets a critical baseline in neurotypical adults. Given the

clinically practical nature of GVS and EMG recordings of the arm, this baseline can be used to quantitatively assess disruptions of cortical, vestibular and brainstem output in stroke survivors.

While there are limitations in our study, we believe these do not detract from our main results or conclusions. A potential limitation of our approach is the phase-randomization method used to estimate the confidence interval for the coherence expected by chance. While this method preserves the amplitude spectrum, it may not fully account for the temporal and frequency-dependent physiological characteristics of the original signals. This could result in a null distribution for coherence that does not perfectly capture the complexities of physiological signals. We used this methods for visualization purposes only, and thus –even if we had underestimated this threshold– it does not change the interpretation of our results. Another potential limitation is that the suppression of responses during voluntary arm movements could be attributed to a lower signal-to-noise ratio (SNR). However, we believe this is unlikely, as the UTrap response is only visible during Rest, and the EMG signal drops during voluntary arm movement (see Fig. 2.3). Second, the noise in our signal is relatively low. For example, we observe that during Rest, the baseline activity is minimal when compared with voluntary action (see Fig. 2.3). Therefore, any activity above the levels of the resting condition, must be attributed to signal arising from neural drive rather than noise. This implies that vestibular drive is not clearly identified or was suppressed by neural drive originating from other cortical and subcortical sources involved in voluntary movement. Consequently, we believe the suppression of vestibular responses during voluntary action is likely due to task-related neural modulation rather than an artifact of signal-to-noise ratio. We also acknowledge that our results might be explained as a direct stimulation of neck muscles, or stimulation of the XI (or *Accessory*) cranial nerve (innervating SCM and UTrap muscles), which might be feasible due to the proximity between the GVS electrode and the neck muscles. However, it has been found that current density decreases to 10% at a distance of 10mm from stimulating surface electrodes [Enoka et al., 2020], which is a small fraction of the distance between the stimulating electrode (behind the ear) and the SCM's innervation point by the XI cranial nerve, which is 4

to 9 centimeters below the mastoid process [Bordoni et al., 2018]. Moreover, we would not have seen any vestibular suppression had such spillover stimulation short-circuited brainstem vestibular output to neck muscles. Lastly, our removal of stimulation artifacts up to 8ms. after each stimulation pulse removes, by design, the effect of such direct stimulation as well [Pinto and De Carvalho, 2008]. However, this removal of the stimulation artifact every 250ms may explain the higher (and potentially artifactual) coherence below 8 Hz in Fig. 2.5.

## **Vestibular suppression during voluntary function is limited to neck muscles**

Vestibular suppression in neck muscles has been previously described during active head movements across several species, including human and non-human primates [Cullen, 2023b]. The purported utility is to suppress potentially counterproductive (involuntary) responses that could act as internal perturbations during voluntary movement [Cullen and Zobeiri, 2021, Cullen, 2023a]. It has been proposed that vestibular suppression in neck muscles occurs when the consequences of head movement (informed by efference copy and predicted by the cerebellum) are analogous to the expected sensory information received from proprioceptors [Cullen and Zobeiri, 2021, Cullen, 2023a]. Accordingly, we interpret the suppression of coherence between neck muscles (during GVS but also during no stimulation, Figure 2.5) as a mechanism to prevent the disruptive effect of vestibular output on head and neck kinematics during voluntary action of the arm. Case in point, our experimental design required participants to visually track a dolphin on a screen to maintain the cadence of the crank during *Reaching*, or maintain neck posture during *Isometric Contraction*. These natural tasks required active control of head and neck kinematics which could be perturbed by vestibular responses.

## **Vestibular output to arm muscles is absent across tasks**

Vestibular output is known to affect the involuntary or reactive activation of arm muscles during perturbations of the trunk [Adamovich et al., 2001]. However, our findings suggest that such vestibular-mediated adjustments are not involved or necessary during the self-initiated voluntary tasks we tested which provided stable and static trunk support. Acoustic startle studies suggest that stroke survivors exhibit greater responses on their *more-affected* (i.e. spastic-paretic) arm, presumably due to increased vestibular output [Miller and Rymer, 2017]. That is, the evoked latencies were shorter and strongly lateralized in stroke survivors, which was interpreted as being triggered from vestibular instead of acoustic pathways [Miller and Rymer, 2017]. Presumably, these increased vestibular-mediated responses result from the disruption of the inhibitory cortical pathways to brainstem and spine, such as those mediating vestibular projections [Miller et al., 2014, Miller and Rymer, 2017]. This lack of vestibular output to arm muscles in our neurotypical participants serves as a baseline for future studies to understand the disruption of pathways affecting arm control in hemiparetic stroke.

## **Our results support prior reports that intermuscular coherence of vestibular origin is broadly distributed across the frequency spectrum**

Intermuscular coherence in the beta band has been proposed as a biomarker that primarily reflects CST integrity, [Fisher et al., 2012, Larsen et al., 2017, Mima et al., 2001, Fang et al., 2009, Ko et al., 2023]. On the other hand, the alpha band is thought to do the same for RST and propriospinal pathways [Grosse and Brown, 2003, Thevathasan et al., 2012, Tattersall et al., 2014]. Our results during GVS, however, do not show a particular dominance of alpha, beta or gamma frequency bands. This supports prior work making the same inference. For example, during postural tasks, the SCM muscle has been shown to respond to stimulation with increased IMC in frequencies spanning up to 70 Hz, while lower limb muscles were

coherent under 25 Hz [Forbes et al., 2015]. Blouin et al. [2011] showed that during GVS, ankle muscles—such as gastrocnemius and soleus— are coherent during the stance phase of locomotion at frequencies of around 20 Hz. Moreover, during physical activity such as running, and jumping, the frequency range of vestibular-mediated responses can increase to 70 Hz (from alpha to gamma bands)[Carriot et al., 2014, Forbes et al., 2015]. In agreement with these previous findings, we found increased coherence from alpha to gamma frequency bands at Rest during GVS. Importantly, neural pathways might be reflected and overlapping across these frequency bands. For example VST and CST drive are both reflected on beta band, while RST and VST are both reflected on the alpha band. Therefore, changes in coherence on any given frequency should be interpreted carefully, specially under neurological conditions. This underscores the need to carefully interpret  $\text{IMC}_z$  in specific frequencies, particularly in stroke. That is, if the disruptions in descending pathways to the more affected arm has contributions from vestibular output, these changes in  $\text{IMC}_z$  may be reflected across a broad spectrum of frequency bands, masking decreased drive from such disrupted pathways.

In summary, our study demonstrated an increased neural drive to neck, but not arm muscles as a result of vestibular stimulation. The increased vestibular drive at rest was suppressed during isometric contraction and unperturbed voluntary reaching. These findings suggest that vestibular suppression—which has been described in head and neck muscles— also applies to voluntary arm movements. Furthermore, the absence of changes in neural drive to arm muscles during GVS provides evidence to exclude a vestibular contribution to unperturbed voluntary arm movement. Our results establish a baseline for the expected neural drive to arm and neck muscles, which could be valuable in clinical practice for quantitatively assessing disruptions of cortical, vestibular, and brainstem output in stroke survivors.

## **Conflict of Interest Statement**

The authors declare that the research was conducted in the absence of any commercial or financial relationships that could be construed as a potential conflict of interest.

## **Author Contributions**

AB and FVC contributed to conception and design of the study. AB performed the experiments, pre-processed the data and performed the statistical analysis. AB and FVC interpreted the results and wrote the manuscript. Both authors contributed to manuscript revision, read, and approved the submitted version.

## **Funding**

NSF CRCNS Japan-US 2113096, DARPA L2M Program W911NF1820264, and NIH R21-NS113613 to FVC; Division of Biokinesiology and Physical Therapy Graduate Teaching Assistantships to AB.

## **Acknowledgments**

We thank Sean Cheng and Yusuf Alvi for their help during the recruiting and testing stages of our research.

## **Additional information: Data availability statement**

The data that support the findings of this study are available from the corresponding author upon reasonable request.

# **Chapter 3**

## **Contributions of vestibular brainstem output to pathological synergies following stroke**

### **3.1 Abstract**

The spatiotemporal structure of muscle coordination emerges from the interaction of descending cortical, spinal, and brainstem pathways. Thus, disruptions in brainstem drive following stroke is thought to contribute to pathological synergies.

We use galvanic vestibular stimulation (GVS) to investigate the extent to which brainstem vestibular output may be disrupted in stroke survivors ( $n=14$ ) with right hemiparesis, as compared with age-matched controls ( $n=14$ ). We measured pairwise coherence between neck and arm muscles during *Rest* and two *Reaching* tasks. For each task, we applied three stimulus types: No stimulation, Sham, and GVS.

Compared to voluntary *Reaching* in control subjects, and as expected, stroke survivors showed disruptions in the *paretic* arm—in the form of lower coherence between arm muscles during No stimulation; especially with abducted shoulder. To our surprise, however, that same *paretic* side *did not* show disruptions to coherence between arm or neck muscles, compared to controls, when GVS was applied—neither at Rest nor during Reaching movements. This absence of IMC changes when GVS is applied on the *paretic* arm provides evidence to exclude increased vestibular drive as an underlying mechanism to motor impairment following stroke.

Interestingly, when compared with Control participants, the *non-paretic* side showed *decreased* coherence in neck muscles when GVS was applied at *Rest*, and remained low during *Reaching*. This decreased coherence on the *non-paretic* side, may result in additional movement disruptions arising from the non-paretic rather than the paretic side following stroke.

Further research is needed to, in particular, explore how these changes relate to reticulo-spinal, cortico-reticulo and cortico-spinal disruptions in the ipsi- and contra-lesional brain and brainstem in stroke.

## 3.2 Introduction

Motor impairment following stroke includes disruptions to arm and hand movements by exhibiting ‘pathological’ *flexion synergies*, which reflects loss of independent joint control. As such, flexion synergies are characterized by abnormal coupling of shoulder abduction, elbow flexion and forearm supination [Twitchell, 1951, Brunnstrom, 1970, Dewald et al., 1995]. Importantly, this abnormal muscle coupling is exacerbated during shoulder abduction [Dewald et al., 1995, McPherson et al., 2018]. As a result, the expression of pathological synergies leads to impaired voluntary reaching and grasping movements, including reduced ability to control hand opening and grasping forces [Lan et al., 2017], reduced elbow and shoulder excursion angles [Beer et al., 2007], as well as decreased reaching velocity, distance, and working area [Sukal et al., 2007, McPherson et al., 2018, Ellis et al., 2018]. The primary mechanism underlying pathological synergies is the disruption of corticospinal tract (CST) drive —compromising monosynaptic corticomotoneuronal projections to muscles. Two additional key mechanisms likely contribute to their emergence: (i) increased drive from descending subcortical (brainstem) pathways and (ii) maladaptive changes in segmental reflex circuits [Krakauer, 2005]. The reticulospinal tract (RST) has been proposed as one contributor to motor impairment and pathological synergies, either by increased drive or maladaptive reflex changes. For example, the StartReact effect —a response mediated by the reticulospinal system— is increased in arm muscles following stroke [Choudhury et al., 2019]. Similarly, the paretic limb of stroke survivors shows

increased RST recruitment, which correlates with both, shoulder abduction loading and synergy expression [McPherson et al., 2018]. The vestibular system is another likely contributor to motor impairment following stroke. The vestibular system not only regulates the excitability of alpha and gamma motoneurons and modulates stretch reflex amplitudes [Molina-Negro et al., 1980, Lance and McLeod, 1981], while regulated by voluntary motor commands. For example, vestibular neural drive to neck muscles is suppressed during voluntary arm movement [Bartsch and Valero-Cuevas, 2025]. Similarly, vestibular-evoked myogenic potentials (VEMPs) recorded in arm muscles [Papathanasiou et al., 2013, Valente et al., 2020, Cherchi et al., 2009], show asymmetric responses following stroke, with larger amplitudes on the paretic side compared to the non-paretic side. Importantly, these asymmetric responses are strongly correlated with spasticity [Miller et al., 2014, 2016, Miller and Rymer, 2017]. These findings provide evidence not only of altered vestibular brainstem output to neck and arm muscles after stroke, but also of maladaptive changes in reflex responses arising from upregulated vestibular drive. While the role of the RST in pathological synergies has been relatively well studied, the vestibular contribution to pathological synergies has not been addressed. In particular, the asymmetric responses to vestibular stimulation observed in stroke survivors may reflect an upregulation of vestibular drive on the paretic side, potentially contributing to motor impairment. Since pathological synergies are exacerbated during reaching tasks that involve shoulder abduction, it is critical to determine whether vestibular-evoked muscle responses are similarly increased during reaching with abducted shoulder. Consequently, this study aims to establish the contribution of vestibular brainstem output to pathological synergies by measuring shared neural drive to muscles –as measured by intermuscular coherence— during voluntary reaching movement. We hypothesize that intermuscular coherence increases during shoulder abduction in stroke, and further increases during vestibular stimulation, providing evidence for a common vestibular mechanism underlying pathological synergies. Ultimately, our findings will refine our understanding of the interplay between cortical and subcortical mechanisms in post-stroke motor

control, offering new insights into the neural origins of pathological synergies, which will be useful for developing targeted arm rehabilitation strategies.

### 3.3 Materials and Methods

#### Ethical Approval

The study conformed to the standards set by the Declaration of Helsinki, except for registration in a database. All participants gave their informed written consent to participate in this study, which was approved by the University of Southern California Internal Review Board (USC IRB: HS-19-00062).

#### Study participants

Fourteen chronic stroke survivors who were right-handed prior to stroke participated in the study (n=14; 9 males; 5 females), with a mean age of 58.5 years ( $\pm 8$ ). Stroke onset was 4.6 years (56 months) on average, ranging from 1.2 to 14 years. Inclusion criteria included a single unilateral cortical or subcortical brain lesion resulting in right hemiparesis. A trained physical therapist assessed upper extremity function using the 66-point upper extremity motor domain of the Fugl-Meyer Assessment [Fugl-Meyer et al., 1975]. The Fugl-Meyer score ranges from 0 to 66, where a maximal score indicates normal motor function. On average, participants scored 40.9 ( $\pm 19.6$ ) points. Additionally, all participants self-reported no history of vestibular, neurological, or auditory deficits. An age-matched group (Control) was also composed of fourteen right-handed participants (n=14; 10 males; 4 females), with a mean age of 58.3 years ( $\pm 8.6$ ). Importantly, all participants in the Control group were free from any neurological condition affecting control of the upper extremity (neurotypical).

Stroke participants had a left-side stroke, resulting in right-side hemiparesis. We use the paretic side as the frame of reference to refer and distinguish both sides of the body in stroke. The *paretic* side refers to

<b>Group</b>	<b>n</b>	<b>Age (<math>\pm</math> SD)</b>	<b>Sex (M/F)</b>	<b>Fugl-Meyer Score (<math>\pm</math> SD)</b>	<b>Stroke Onset (range)</b>
Stroke	14	58.5 ( $\pm$ 8.0)	9/5	40.9 ( $\pm$ 19.6)	4.6yrs (1.2 - 14)
Control	14	58.3 ( $\pm$ 8.6)	10/4	—	—

Table 3.1: Demographic and clinical characteristics of the study participants. Age and stroke onset is reported in years.

the right side muscles and structures, while the *non-paretic* side refers to muscles and structures of their left side of the body. Galvanic Vestibular Stimulation (GVS) increases Vestibular drive ipsilateral to the positive electrode location, and the results are always described ipsilateral to the paretic-centered frame of reference (see subsection 'Stimulus Types' for protocol description). For example, when describing the effect of GVS on the *paretic* side, the positive electrode of GVS is located on the right mastoid process and we measure muscle activity from the same (paretic) right side. Finally, to avoid confusion we refer to sides as *lesional*, *contralesional* and *contralateral* only if necessary. We did our best to avoid using 'affected' or 'less-affected' sides as it might be misleading or confusing terminology.

## Tasks

Participants performed the following tasks while sitting. *Rest*: Participants were seated with their hands resting on their lap or armrest. They were encouraged to stay relaxed and silent for 90 seconds at the beginning of the experimental procedures to collect baseline muscle activity (Fig. 3.1, left panel). *Reaching with neutral shoulder*: Participants were seated in front of a hand-powered ergometer mounted to be rotated in the horizontal plane with each arm separately (Fig. 3.1, middle panel). The ergometer provides a stable and standardized cyclical reaching-like movement pattern, while also ensuring a mirrored movement between arms. The protocol for this task is thoroughly described in previous articles [Laine et al., 2021, Bartsch and Valero-Cuevas, 2025]. In summary, the movement direction was mirrored between arms, with a counterclockwise rotation when it was performed with the right or *paretic* arm, and clockwise when performed with the left or *non-paretic* arm (for control and stroke participants respectively). *Reaching*

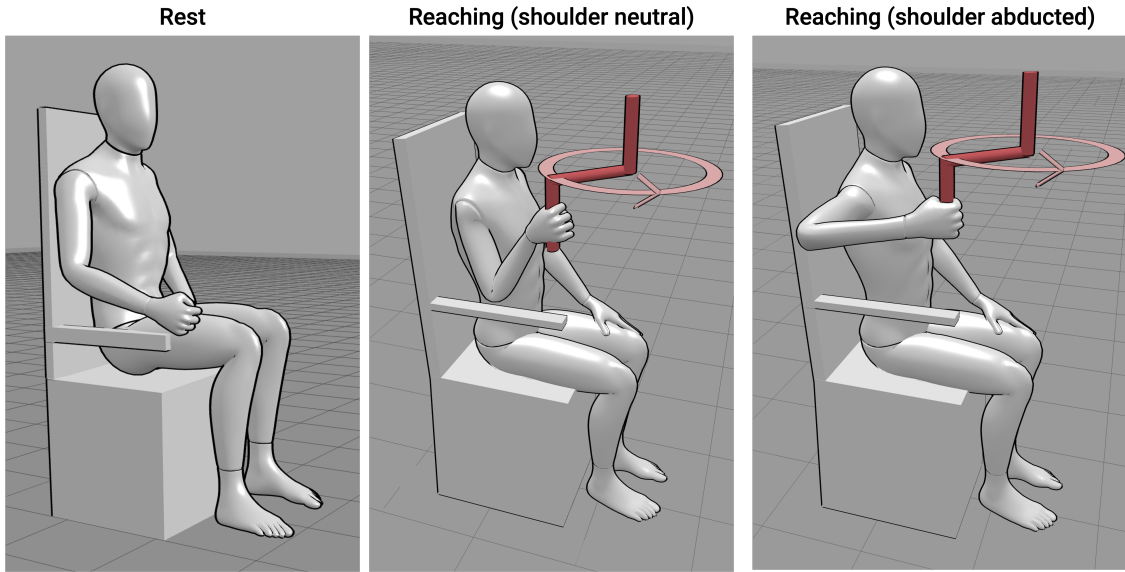


Figure 3.1: Tasks performed by each participant. Left: At the beginning of the experiment, each participant sat comfortably in a chair with their hands on their lap, while EMG was recorded at *Rest*. Middle: During the *Reaching* task, participants are asked to rotate an horizontal ergometer inwards (counterclockwise for the right arm, and clockwise for the left arm) to produce a cyclical movement. Right: In the *Reaching with abducted shoulder* condition, subjects were asked to perform the same reaching-like movement while keeping their shoulder abducted at 90°. Verbal encouragement was constantly provided to avoid shoulder drifting.

*with shoulder abduction:* Participants were seated and performed the same movement as in the previously described task, but with a constant shoulder abduction of 90° (Fig. 3.1, right panel). Verbal encouragement and feedback were given to help them maintain the instructed position if they deviated. Rest breaks were allowed in case of fatigue, but no participant requested them. During the reaching task with the abducted shoulder, eleven participants from the stroke group were able to successfully finish the task with their paretic arm. All participants from both groups were able to finish all the other tasks with both arms successfully.

## Stimulus Types

As in the previous chapter (for a detailed description see [Bartsch and Valero-Cuevas, 2025](#)), we applied three Stimulus Types; No stimulation GVS, and Sham stimulation. GVS consisted of a binaural galvanic

stimulation where the positive electrode was placed to induce a vestibular response on the tested side, which was verified by visual inspection of the SCM muscle (see Figure 3.2, left Panel) [Forbes et al., 2015]. The stimulation frequency was set at 4 Hz, with an amplitude ranging between 0.8 and 1.2mA and a pulse duration of 2ms. The amplitude was modulated to avoid EMG signal saturation from the Sternocleidomastoid muscle (SCM) or if the participant felt uncomfortable. Each participant received the same amplitude across all conditions to ensure comparable responses between sides. Independent of the stimulation amplitude, the SCM response to GVS was always clearly visible and greater than the EMG signal at rest (see Figure 3.2, left Panel). For the Sham stimulation, a mechanical vibration (400 Hz) was also delivered on the tested side (same location as the positive GVS's electrode). This approach provides a cutaneous sensation produced by the vibration that mimics the tactile input associated with GVS without delivering a stimulating current. As a result, participants are exposed to a similar sensory experience while ensuring that vestibular pathways are not stimulated.

Participants from the Stroke group completed nine randomized conditions with each arm: three Tasks (*Rest*, *Reaching with Neutral* and *Abducted* shoulder) and three Stimulus Types (GVS, None and Sham). All participants in the Control group performed these tasks using their Right arm. To assess the effect of limb dominance, a subset of participants (n=7) also completed the tasks with their Left arm. No carryover effects from GVS or Sham stimulation have been previously observed [Bartsch and Valero-Cuevas, 2025], however, the *Rest + No stimulation* condition was always completed first, while all the other conditions were randomized within each arm.

## Data acquisition and processing

A custom game was designed in c# to collect the angle data from the ergometer and provide live real time feedback about the user's rotation velocity (Unity3D, San Francisco, CA, USA). The game featured a dolphin that moved vertically on the screen in real time, with its position directly linked to the participant's rotation

speed. When the participant maintained the target speed, the dolphin aligned with a horizontal reference line centered on the display. If the rotation speed decreased, the dolphin sank below the line; if the speed increased beyond the target, the dolphin rose above it. Custom hardware provided a pulse via an Arduino MEGA (Arduino, Somerville, MA, USA) to synchronize EMG data, ergometer angle measurements, and GVS stimuli delivery time. We collected EMG signals at 2.5 kHz from seven muscles of each arm separately using a DataLINK system and associated software (Biometrics Ltd, Newport, UK). Surface EMG sensors (Biometrics Ltd SX230: bipolar, gain: 1,000, bandwidth: 20–460 Hz) were placed over the arm: Biceps Brachii (Bic), lateral head of the Triceps Brachii (Tric), Anterior, Middle and Posterior Deltoid (ADelt, MDelt, PDelt, respectively), upper Trapezius (UTrap) and Sternocleidomastoid muscles (SCM), following standard recommendations from SENIAM. Electrode placement and signal quality were confirmed using palpation of each muscle and observation of the EMG during voluntary activation. The selected set of muscles is sufficient for a general analysis of coupling among the shoulder/elbow muscles relevant to our task [Laine et al., 2021, Bartsch and Valero-Cuevas, 2025]. All EMG signals were processed offline using R/Rstudio [R Core Team, 2021].

To remove GVS artifacts, we visually inspected the spike-triggered average of each participant's trial to identify the duration of the stimulation artifact. On average, the artifact began 4.8 ms before and ended 8.4 ms after the electrical pulse was triggered. To prevent aliasing and preserve the signal's frequency characteristics, the artifacts were replaced with interpolated data from the corresponding SCM, Deltoid (ADelt, MDelt, PDelt), and UTrap EMG signals (see Figure 3.2, left panel). Since vestibular responses have a latency of 8 to 50ms, we prevented their removal from the signals during the replacing and interpolation process. [Forbes et al., 2015]. Signal processing was done according to our previous published papers (for a detailed description see Laine et al. 2021, Bartsch and Valero-Cuevas 2025). In summary, all EMG signals were downsampled to 1,000 Hz, band-pass filtered between 8 to 250 Hz, and then full wave rectified. The filter's purpose was to remove any remaining artifacts arising from GVS, as well as from those frequencies

irrelevant for intermuscular coherence analysis. EMG signals were full-wave rectified to improve the detection of synchronized oscillatory neural inputs shared across muscles, while preserving the signal characteristics required for reliable coherence analysis [Boonstra and Breakspear, 2012].

## Statistical analysis

Intermuscular coherence (IMC) assesses shared neural drive between two muscles on the basis of their EMG signals [Boonstra, 2013]. We calculated magnitude squared coherence between each muscle pair using 300 ms windows and a 50% overlap [Laine et al., 2021, Bartsch and Valero-Cuevas, 2025]. A significant pairwise coherence threshold was built for visual inspection. We generated 1,000 phase-randomized surrogate series for each participant's muscle pair following the methods described by [Ebisuzaki, 1997]. Individual pairwise coherence above the 95% CI is likely to be significant, revealing true shared drive between the two muscles. Averaging correlation coefficients ( $\rho$ ) leads to biased parameter estimates. Consequently, we applied Fisher's z-transformation ( $IMC_z = \text{atanh}(\rho)$ ) to all intermuscular coherence values to ensure unbiased statistical testing. This transformation was done on an individual basis (for each trial) before performing statistical comparisons [Laine et al., 2021, Bartsch and Valero-Cuevas, 2025]. We compared  $IMC_z$  across Stimulus Types, Tasks, and Sides (left and right in controls or paretic and non-paretic in stroke). The values of  $IMC_z$  across the frequency spectrum were gathered into three bands: alpha (8-16 Hz), beta (16-30 Hz) and gamma (30-50 Hz) frequency bands. This approach was adopted for two reasons. First, these bands are thought to reflect the origin of shared neural drive: beta-band coherence has been associated with corticospinal tract (CST) activity and is considered a marker of CST dysfunction [Fisher et al., 2012]; while alpha and alpha-to-gamma bands are thought to reflect reticulospinal (RST) [Grosse and Brown, 2003] and vestibulospinal (VST) pathways respectively. Second, aggregating coherence values into broader frequency bands helps reduce the number of post-hoc comparisons, thereby lowering the risk of type I error and increasing the robustness of statistical inferences when evaluating group or task-related

differences. Given the lack of a non-parametric alternative for testing our hypotheses, we employed a Robust ANOVA model (i.e., robust repeated measures ANOVA when testing for within subjects effects) to assess whether Stroke and GVS increases shared neural drive (as per  $\text{IMC}_z$ ). The advantage of these robust methods is that they provide unbiased parametric estimates, even when data depart from normality or when statistical assumptions are not fully met. Post-hoc comparisons were conducted with Bonferroni corrections when more than two conditions were compared (e.g., *Stimulus type*). For comparisons involving only two conditions (e.g., *Side* comparisons), no further analysis was performed, as it was deemed unnecessary.

### 3.4 Results

#### GVS increases neural drive in neck muscles from both *Sides* in the Control group

First, we compared shared neural drive —as measured by  $\text{IMC}_z$ — on both *Sides* of the Control group (neurotypical participants) to exclude the confounding effect of arm use or dominance on shared neural drive. To achieve this, we compared the overall mean  $\text{IMC}_z$  (across all frequencies) between both *Sides* (right vs. left) during *Rest* in a subset of participants ( $n = 7$ ). No significant differences in shared neural drive were found between *Sides* in any muscle pair (SCM-UTrap:  $p\text{-value}=0.28$ ; Bic-ADelt:  $p\text{-value}=0.49$ ; Bic-MDel:  $p\text{-value}=0.66$ ; Bic-PDel:  $p\text{-value}=0.39$ , see Table 3.2). Conversely, we found statistical differences on shared neural drive to neck muscles due to *Stimulus type* (SCM-UTrap:  $p\text{-value}=0.01$ , see Table 3.2). After confirming that the type of stimulation had a significant overall effect on  $\text{IMC}_z$ , we conducted additional analyses to identify which type of stimulus (i.e., GVS or Sham) and which frequency bands (alpha, beta, or gamma; see Table 3.5 in the Appendix) had statistically significant  $\text{IMC}_z$  changes. Consequently, we performed a Robust repeated measures ANOVA with post-hoc comparisons and Bonferroni corrections to account for the number of comparisons. The results confirmed two of our previous published findings: (i) shared neural drive between neck muscles at *Rest* increased only during GVS (alpha:  $p\text{-value}=0.002$ ; beta:  $p\text{-value}<0.001$ ; gamma:  $p\text{-value}<0.001$ ), and (ii) no significant differences were found in  $\text{IMC}_z$  for neck muscles between No Stimulation and Sham stimulus types ( $p\text{-value}=1$  across frequency bands due to Bonferroni corrections). These results further support the notion that GVS increases brainstem vestibular output only to neck muscles in our Control group, as previously described in young neurotypical participants [Bartsch and Valero-Cuevas, 2025].

Group	Muscle Pair	Effect (Factors)	F ratio	DF <sub>1</sub>	DF <sub>2</sub>	p-value
Control (n=7)	SCM-UTrap	Side (L/R)	1.26	1.00	11.90	0.28
		Stim type (None, Sham, GVS)	7.72	2.00	10.00	<b>0.01**</b>
		Stim type × Side	0.27	2.00	10.00	0.77
	Bic-ADelt	Side	0.52	1.00	12.00	0.49
		Stim type	4.36	2.00	8.60	0.05
		Stim type × Side	1.08	2.00	8.60	0.38
	Bic-MDelt	Side	0.21	1.00	9.00	0.66
		Stim type	1.25	2.00	9.30	0.33
		Stim type × Side	0.77	2.00	9.30	0.49
Stroke (n=14)	Bic-PDelt	Side	0.83	1.00	6.90	0.39
		Stim type	0.52	2.00	8.40	0.61
		Stim type × Side	0.89	2.00	8.40	0.45
	SCM-UTrap	Side (paretic/non-paretic)	4.97	1.00	20.10	<b>0.037*</b>
		Stim type	15.72	1.00	22.40	<b>0.001**</b>
		Stim type × Side	5.29	1.00	22.40	<b>0.031*</b>
	Bic-ADelt	Side	2.18	1.00	19.10	0.16
		Stim type	0.54	1.00	16.70	0.47
		Stim type × Side	0.15	1.00	16.70	0.70
	Bic-MDelt	Side	1.19	1.00	18.70	0.29
		Stim type	1.72	1.00	18.00	0.21
		Stim type × Side	0.03	1.00	18.00	0.86
	Bic-PDelt	Side	0.91	1.00	23.90	0.35
		Stim type	2.05	1.00	20.90	0.17
		Stim type × Side	0.82	1.00	20.90	0.38

Table 3.2: Our results at *Rest* confirmed the known effect of GVS stimulation on neck muscles [Bartsch and Valero-Cuevas, 2025], but show a significant effect of body *Side* only in Stroke participants. The Stroke group showed a significant *Side* effect (Paretic vs. Non-paretic) on Neck IMC<sub>z</sub> (SCM-UTrap) during *Rest*, which was confirmed by corrected pairwise comparisons. On the other hand, both groups showed a main effect for *Stimulus Type*, also in Neck muscles. Additionally, a *Stimulus Type* × *Side* interaction was identified in Neck muscles of the Stroke group. The table presents results from robust repeated measures ANOVAs, including degrees of freedom, F ratio, and p-value, for the following muscles: *Sternocleidomastoid* (SCM), *Upper Trapezius* (UTrap), *Biceps brachii* (Bic), and *Anterior, Middle, and Posterior Deltoid* (ADelt, MDelt, PDelt). Red text indicates significant differences at 0.05\*, and 0.01\*\* levels.

## GVS does not increase neural drive to neck muscles at *Rest* in the non-paretic side after Stroke

The same analysis was performed in the Stroke group to identify IMC<sub>z</sub> changes due to the *Side* and *Stimulus Type*. Similar to the Control group during *Rest*, Stroke participants showed statistical differences between

*Stimulus types* ( $p$ -value=0.001). As opposed to Controls, however, we found statistical differences between *Sides* (paretic vs. non-paretic) in Neck muscles (SCM-UTrap:  $p$ -value=0.037, see Table 3.2), as well as an interaction (Stimulus type  $\times$  Side,  $p$ -value=0.031, see Table 3.2). Consequently, only the Stroke group had differences between both Sides, excluding dominance as a confound for such differences.

As shared neural drive did not change between the left and right sides in Control participants, we selected the *right* side as the reference for comparisons with the *paretic* and *non-paretic* sides of the Stroke group. Similarly, we excluded the Sham stimulus from further analysis, as both groups showed no significant differences between No Stimulation and Sham (see Tables 3.5 and 3.6 for detailed posthoc comparisons). Consequently, we conducted a robust ANOVA analysis on each side of stroke to determine the effects of *Stimulus type* (GVS vs. None) and *Group* (control vs. stroke side). The purpose of this analysis was to determine which side of Stroke participants was affected relative to the reference side in Controls,

Unexpectedly, an overall significant *Group* difference was found when comparing the SCM-UTrap muscle pair between *control* participants and the *non-paretic* ( $p$  = 0.031), but not with the paretic side of stroke ( $p$  = 0.428; see Table 3.3).

Besides this *Group* effect, GVS also showed an overall significant effect when comparing *controls* with the *non-paretic* side of stroke participants (alpha:  $p$  = 0.018; beta:  $p$  = 0.002; gamma:  $p$  = 0.025, see Table 3.3). Post hoc analyses with Bonferroni corrections further revealed that  $IMC_z$  in neck muscles from the *non-paretic* side of stroke participants was significantly lower in the alpha band during GVS compared to control participants ( $p$  = 0.029; see Figure 3.2). In contrast, no differences during GVS were found —on shared neural drive to neck muscles— when comparing the *paretic* side of stroke participants and controls ( $p$  = 0.38, see Figure 3.2). Consequently, the differences in shared neural drive to neck muscles between stroke sides (*paretic* vs *non-paretic*) were further supported when comparing each side of stroke participants with Controls. Importantly, these differences were primarily driven by a reduction in neural drive on the *non-paretic* side —rather than by upregulated drive on the *paretic side*— when GVS was applied at Rest.

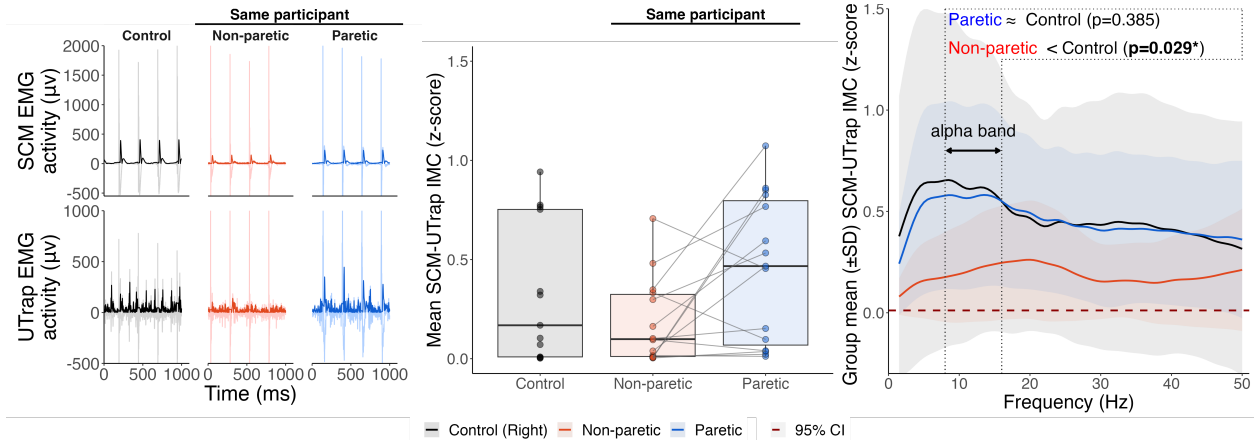


Figure 3.2: EMG signals and intermuscular coherence ( $IMC_z$ ) reveal lower responses to GVS in the *non-paretic* side (red trace) of stroke participants during *Rest*, compared to the right side of controls (black trace). The left panel shows the raw (light trace) and processed (dark trace) EMG signals for the Sternocleidomastoid (SCM) and Upper Trapezius (UTrap) muscles in a representative participant. Note the lower GVS-driven responses on the *non-paretic* side of both muscles. The middle panel shows a boxplot with individual  $IMC_z$  means, highlighting the lower coherence levels on the *non-paretic* side, compared to the *paretic* side as well as control participants. The right panel shows the group mean  $IMC_z$  ( $\pm SD$ ) for the SCM-UTrap muscle pair. Significant differences in the alpha band (8-16 Hz) were observed between the *non-paretic* side and controls ( $p=0.029$ ), but no significant differences were found between the *paretic* side (blue trace) and controls ( $p=0.385$ ). Values above the dotted dark red line can be considered to have significant  $IMC_z$ , as per the 95% upper confidence interval estimated from 1,000 randomization of the original signals.

## Decreased neural drive to arm muscles during shoulder abduction

We first compared the angular velocity of reaching-like movements as a metric of motor performance to exclude it as a potential confounding factor for subsequent findings related to changes in shared neural drive following stroke. The Right arm of Control and the Paretic arm of Stroke participants showed average velocities of 0.593 and 0.574 cycles per second, respectively. A Robust ANOVA model (repeated measures) to compare differences between *Group* (Control vs Stroke) and *Task* (Reaching with Neutral vs. Abducted shoulder) revealed no significant differences in angular velocity between the Right arm of Control and the Paretic arm of Stroke participants, nor between Reaching tasks (*Task*:  $p = 0.42$ ; *Group*:  $p = 0.09$ ; *Task*  $\times$  *Group*:  $p = 0.30$ ). Then, we assessed the effect of Stimulus type on shared neural drive during *Reaching* in Stroke participants. The results revealed that GVS did not increase  $IMC_z$  to neck muscles

(SCM-UTrap) from the *Paretic* side of stroke participants. This finding is supported by the results of robust repeated-measures ANOVA under both *Neutral* ( $p\text{-value}=0.142$ ) and *Abducted* shoulder positions ( $p\text{-value}=0.857$ ). These results confirm previous findings of gated vestibular output to neck muscles during voluntary movement. Similarly, GVS did not increase neural drive to any arm muscle on the *paretic* side (Bic-ADelt:  $p\text{-values}_{\text{Neutral}/\text{Abducted}}=0.31/0.73$ ; Bic-MDelt:  $p\text{-value}_{N/A}=0.71/0.9$ ; Bic-PDelt:  $p\text{-value}_{N/A}=0.45/0.97$ ). Importantly, these results provide evidence that excludes a vestibular contribution to upper arm neural drive during unperturbed voluntary reaching movements.

After we confirmed that GVS does not change intermuscular coherence during the reaching tasks, we removed these conditions from further analysis. We found that the *paretic* side of stroke participants showed significant differences when compared to control participants during the reaching tasks in the form of lower coherence. This is evidenced by the overall *Group* differences between Biceps and Deltoid (Bic-ADelt:  $p\text{-value}=0.005$ ; Bic-MDelt:  $p\text{-value}=0.004$ ; Bic-PDelt:  $p\text{-value}=0.048$ ; ADelt-MDelt:  $p\text{-value}<0.001$ , see Table 3.4). Similarly, the *Shoulder* position also showed lower IMC between neutral and abducted positions during the reaching tasks (Bic-ADelt:  $p\text{-value}=0.007$ ; Bic-MDelt:  $p\text{-value}=0.005$ ; Bic-PDelt=0.003; ADelt-MDelt:  $p\text{-value}=0.963$ , see Table 3.4). Finally, a detailed analysis found that the Bic-ADelt and Bic-MDelt muscles from the *paretic* side had lower coherence in both reaching tasks when compared to control participants (Bic-ADelt:  $p\text{-values}_{\text{Neutral}/\text{Abducted}}=p=0.023/0.001$ ; Bic-MDelt:  $p\text{-values}_{\text{Neutral}/\text{Abducted}}=0.001/0.001$ , see Figure 3.3). The Bic-PDelt muscle pair in the *paretic* side had lower coherence when reaching with shoulder abduction only ( $p<0.026$ ), when compared to control participants.

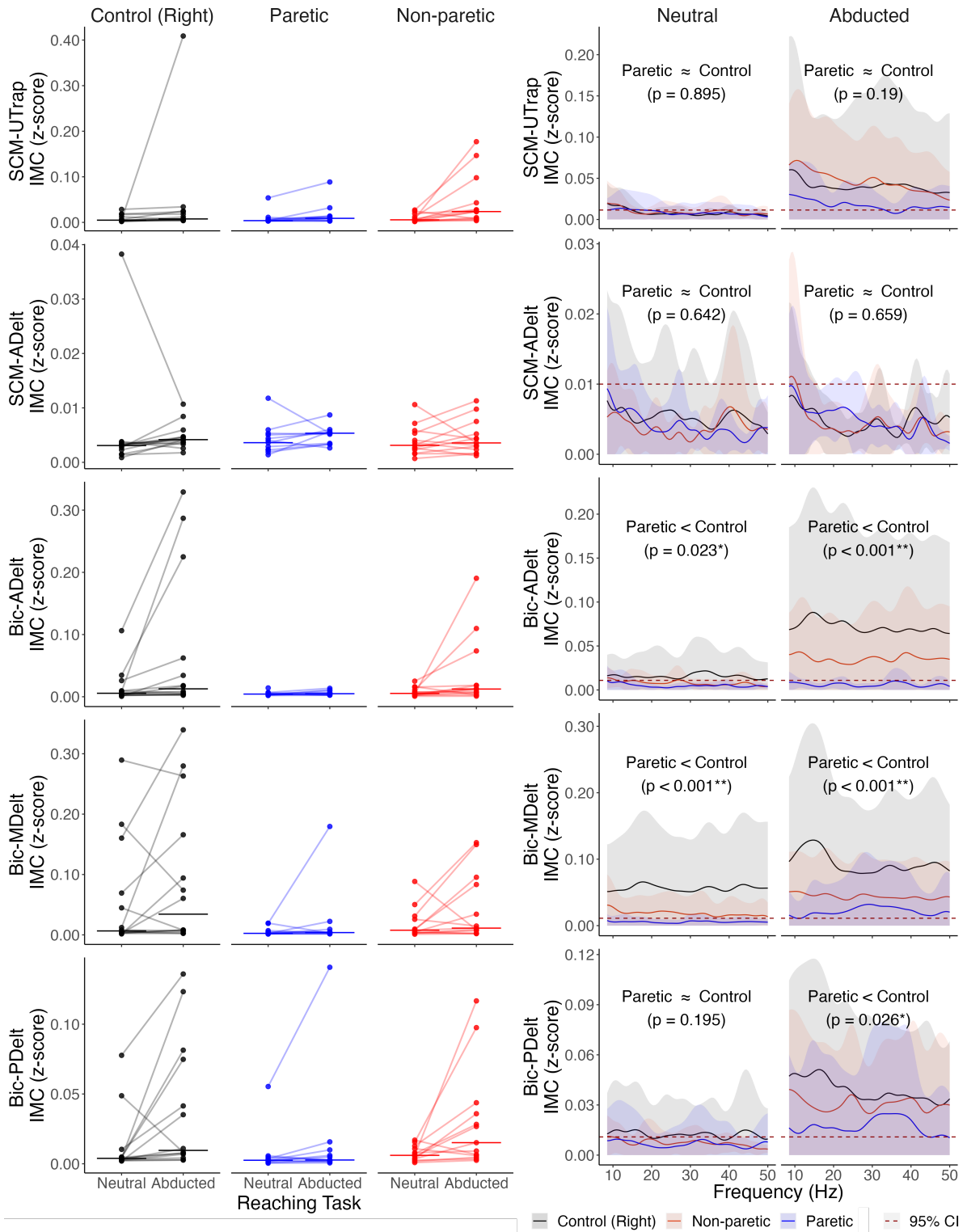


Figure 3.3: The paretic side of stroke survivors had lower intermuscular coherence values when compared to control participants. Left: mean IMC<sub>z</sub> for each participant during both reaching tasks. Right: group mean intermuscular coherence for control participants and each side of stroke. Values above the dotted dark red line can be considered to have significant IMC<sub>z</sub>, as per the 95% upper confidence interval estimated from 1,000 randomization of the original signals. SCM: Sternocleidomastoid, UTrap: Upper Trapezius, Bic: Biceps brachii; ADelt, MDelt and PDelt Anterior, Middle and Posterior Deltoid respectively.

### 3.5 Discussion

Our results indicate that in neurotypical participants (control group), neck muscles receive a shared neural drive —as measured by  $\text{IMC}_z$ — from the vestibular system (i.e., brainstem vestibular output). Specifically, when GVS is applied at *Rest*, neural drive increases similarly on both sides, indicating no lateral dominance. Supporting these results, we observed no increase in  $\text{IMC}_z$  during *Sham* when compared to *No* stimulation, excluding a proprioceptive or placebo effect as a likely mechanism for the GVS-driven changes. Moreover, the absence of changes in  $\text{IMC}_z$  between arm muscles (Bic-ADelt, Bic-MDelt, Bic-PDelt) suggests that arm muscles are unlikely to receive vestibular output during *Rest* or unperturbed *Reaching*. These findings are in agreement with previous results from young neurotypical participants [Bartsch and Valero-Cuevas, 2025].

When GVS is applied at *Rest*, there's no increased neural drive to neck muscles in the non-paretic side of stroke. As opposed to control participants, stroke survivors exhibited an asymmetric vestibular drive to neck muscles when GVS was applied during *Rest* (see Figure 3.2 and Table 3.2). Significant differences were found between GVS and *No* stimulation, as well as between the paretic and non-paretic sides. This asymmetry is consistent with previous reports of vestibular-evoked myogenic potentials (VEMPs) in the SCM muscle following stroke. Specifically, the ratio of the muscle peak amplitude responses between the paretic to non-paretic sides favored the amplitudes of the paretic side [Miller et al., 2014]. However, our detailed comparison between controls and both sides of stroke participants revealed that these asymmetries arise from suppressed GVS responses on the non-paretic side rather than increased responses on the paretic side. In fact, muscle responses on the SCM and the UTrap muscles reveal a lower amplitudes on the *non-paretic* side compared to both the *paretic* side and controls (see Figure 3.2). This finding suggests that the reduced coherence may result from disrupted ipsilesional neural drive to the neck muscles. Furthermore, since the vestibular nuclei project bilaterally to cortical areas [Fukushima, 1997] and vestibular stimulation preferentially activates the ipsilateral hemisphere [Schlindwein et al., 2008, Lopez et al., 2012, Indovina

et al., 2020], the selective suppression of coherence between neck muscles on the *non-paretic* side likely reflects disruptions or downregulation of ipsilesional cortico-vestibular pathways.

Neural drive to arm muscles from the *paretic* side is reduced during voluntary reaching. Following upper motor neuron damage, decreased shared neural drive has been described during voluntary movements —such as reaching, precision grip and pinching tasks. Such reductions in intermuscular coherence has been observed across frequency bands [Fang et al., 2009, Fisher et al., 2012, Larsen et al., 2017]. For example, intermuscular coherence in the beta band (16–30 Hz) was found to be decreased in patients with corticospinal tract degeneration (as seen in primary lateral sclerosis) while remaining intact in patients with lower motor neuron disease (as seen in progressive muscular atrophy) [Fisher et al., 2012]. Similarly, stroke participants have shown lower alpha and beta band coherence in hand muscles (first dorsal interosseous muscle, adductor pollicis, and abductor pollicis brevis), during pinching tasks [Larsen et al., 2017], as well as gamma band corticomuscular coherence in arm muscles (anterior deltoid, biceps, and triceps brachii) during reaching tasks [Fang et al., 2009]. In agreement with these findings, during voluntary reaching tasks, the paretic side of stroke participants showed a decreased shared neural drive to Biceps and Deltoid Muscle in both reaching tasks when compared to controls (see Table 3.4 and Figure 3.3). Given that lack of changes when GVS was applied during the reaching movements, it is likely that this decreased arises from disruptions to CST drive.

Although our study has limitations, we believe they do not undermine our primary findings. For instance, increased coherence in neck muscles might be attributed to direct electrical stimulation of the muscles or activation of the Accessory (XI) cranial nerve —given the close proximity of the GVS and sensing electrodes. However, such responses have been consistently observed in both our control group and neurotypical participants [Bartsch and Valero-Cuevas, 2025]. Notably, these responses occur with a higher latency than would be expected from direct stimulation alone. Furthermore, the selective vestibular suppression observed in stroke survivors and during voluntary movement would not occur if direct stimulation were solely

responsible. Lastly, our artifact removal process, applied after each stimulation pulse (every 250 ms), further minimizes the influence of direct stimulation [Pinto and De Carvalho, 2008], although it may also lead to an artifactual increase in coherence below 8 Hz and its 4 Hz harmonics. When considering the decreased drive to neck muscles on the non-paretic side, one alternative explanation is an abnormal reliance on ipsilateral, rather than the widely accepted contralateral innervation to muscles [Porter and Lemon, 1995, Natali et al., 2018]. For instance, it is known that ipsilateral axial muscles receive input from 5–15% of undecussated corticospinal fibers [Porter and Lemon, 1995, Natali et al., 2018]. Similarly, the SCM muscle is known to exhibit ipsilateral innervation [Balagura and Katz, 1980, Mazzini and Schieppati, 1992, DeToledo and David, 2001], and clinical studies have reported SCM weakness on the non-paretic side following stroke. The upper trapezius, however, shows weakness on the paretic side [Manon-Espaillat and Ruff, 1988, Anagnostou et al., 2011]. Despite these observations, we consider this alternative explanation unlikely because (i) at most 15% of the corticospinal tract remains undecussated; (ii) ipsilateral innervation has been documented for the SCM only; and (iii) our results clearly showed lower responses in both, the sternocleidomastoid and upper trapezius muscle, of which only the latter is likely innervated by the non-lesioned hemisphere. Given these inconsistencies, we propose that disruptions in ipsilateral cortico-vestibular pathways are the most plausible explanation for the suppression of shared neural drive to neck muscle of the non-paretic side in stroke. Finally, since we did not perform a topographic analysis of stroke-related neural damage –particularly within the corticospinal tract— it remains possible that some of the decreased neural drive on the paretic side could reflect dysregulation of uninjured pathways. Nonetheless, our findings agree with previous reports on stroke and upper motor neuron injuries, which strongly suggest that decreased neural drive primarily results from damage to motor pathways following stroke.

In summary, our study further supports a reliable increase in the shared neural drive ( $IMC_z$ ) to neck muscles of neurotypical individuals when galvanic vestibular stimulation (GVS) is applied at Rest. In contrast, stroke survivors exhibit an asymmetric response: while the paretic side shows GVS-induced

neural drive to neck muscles comparable to controls, the non-paretic side is unexpectedly suppressed. This selective suppression suggests a disruption of ipsilesional cortico-vestibular and brainstem pathways. Furthermore, our data reveal that neural drive in arm muscles is particularly decreased during reaching with an abducted shoulder. However, because GVS did not increase neural drive during reaching movements, our findings exclude a significant vestibular contribution –highlighting instead the likely role of the remaining motor pathways— to the disruption of voluntary arm movements following stroke.

## **Conflict of Interest Statement**

The authors declare that the research was conducted in the absence of any commercial or financial relationships that could be construed as a potential conflict of interest.

## **Author Contributions**

AB and FVC contributed to conception and design of the study. AB performed the experiments, pre-processed the data and performed the statistical analysis. AB and FVC interpreted the results and wrote the manuscript. Both authors contributed to manuscript revision, read, and approved the submitted version.

## **Funding**

NSF CRCNS Japan-US 2113096, DARPA L2M Program W911NF1820264, and NIH R21-NS113613 to FVC; Division of Biokinesiology and Physical Therapy Graduate Teaching Assistantships to AB.

## **Acknowledgments**

### **Additional information: Data availability statement**

The data that support the findings of this study are available from the corresponding author upon reasonable request.

Group	Band	Muscle	Effect	Statistic		p-value	
				Paretic	Non-paretic	Paretic	Non-paretic
Control vs Stroke	alpha	SCM-UTrap	Group	0.65	5.38	0.428	<b>0.031*</b>
			Stim type	16.52	6.62	<b>0.001*</b>	<b>0.018*</b>
			Group × Stim type	0.05	2.63	0.82	0.121
	beta	Bic-ADelt	Group	0.07	2.41	0.802	0.137
			Stim type	21.01	12.28	<b>0.001*</b>	<b>0.002*</b>
			Group × Stim type	0.01	1.72	0.914	0.205
	gamma	Bic-ADelt	Group	0.17	2.59	0.688	0.126
			Stim type	12.85	6.00	<b>0.002*</b>	<b>0.025*</b>
			Group × Stim type	0.01	1.91	0.942	0.185
Control vs Stroke	alpha	Bic-MDelt	Group	0.76	0.04	0.396	0.846
			Stim type	2.43	1.03	0.136	0.319
			Group × Stim type	0.61	0.72	0.446	0.402
	beta	Bic-MDelt	Group	0.27	0.11	0.61	0.745
			Stim type	5.96	3.98	<b>0.022*</b>	0.057
			Group × Stim type	0.14	0.03	0.716	0.875
	gamma	Bic-MDelt	Group	0.44	0.43	0.516	0.516
			Stim type	3.56	0.89	0.076	0.354
			Group × Stim type	0.48	1.26	0.499	0.27
Control vs Stroke	alpha	Bic-PDelt	Group	1.09	0.01	0.31	0.913
			Stim type	2.23	1.08	0.152	0.307
			Group × Stim type	0.08	0.12	0.786	0.729
	beta	Bic-PDelt	Group	0.56	0.01	0.46	0.942
			Stim type	4.34	2.94	<b>0.046*</b>	0.098
			Group × Stim type	0.01	0.04	0.906	0.844
	gamma	Bic-PDelt	Group	0.45	0.15	0.509	0.702
			Stim type	3.09	1.29	0.094	0.265
			Group × Stim type	0.09	0.26	0.772	0.616
Control vs Stroke	alpha	Bic-PDelt	Group	0.61	0.09	0.445	0.767
			Stim type	2.73	0.80	0.117	0.381
			Group × Stim type	0.22	1.27	0.647	0.274
	beta	Bic-PDelt	Group	0.09	0.04	0.77	0.852
			Stim type	6.46	4.12	<b>0.018*</b>	0.053
			Group × Stim type	0.00	0.13	0.994	0.718
	gamma	Bic-PDelt	Group	0.28	0.04	0.601	0.839
			Stim type	3.66	1.59	0.073	0.219
			Group × Stim type	0.23	0.77	0.638	0.39

Table 3.3: Comparison of the Right side of controls (n=14) with both, the *paretic* and *non-paretic* (n=13) side of Stroke participants during Rest. Unexpectedly, when GVS is applied, only the *non-paretic* side showed statistical differences in neural drive to neck muscles in the alpha band when compared to controls (right side). Red text indicates significant differences (groups and stimulus types). Muscles: *Sternocleidomastoid* (SCM), *Upper Trapezius* (UTrap), *Biceps brachii* (Bic), and *Anterior, Middle and Posterior Deltoid* (ADelt, MDelt, PDelt).

Group	Muscle	Effect	Statistic	p-value
Control vs Paretic side	Bic-ADelt	Shoulder	8.23	<b>0.007*</b>
		Group	8.82	<b>0.005*</b>
		Shoulder × Group	7.36	<b>0.01*</b>
	Bic-MDelt	Shoulder	8.93	<b>0.005*</b>
		Group	9.11	<b>0.004*</b>
		Shoulder × Group	3.38	0.073
	Bic-PDelt	Shoulder	9.70	<b>0.003*</b>
		Group	4.12	<b>0.048*</b>
		Shoulder × Group	2.11	0.153
	ADelt-MDelt	Shoulder	0.00	0.963
		Group	14.09	<0.001*
		Shoulder × Group	1.03	0.315

Table 3.4: Compared to controls, the *paretic* side of stroke participants showed decreased neural drive to Biceps and Deltoid (Bic-ADelt, Bic-MDelt, Bic-PDelt, ADelt-MDelt) during reaching. The shoulder position (Neutral vs. Abducted) also showed decreased neural drive.

### 3.6 Appendix

Group	Muscle Pair	Stim type	Frequency band		
			alpha	beta	gamma
Control (n=14)	SCM-UTrap	GVS vs. None	<b>0.002**</b>	<b>&lt;0.001**</b>	<b>&lt;0.001**</b>
		GVS vs. Sham	<b>0.001**</b>	<b>&lt;0.001**</b>	<b>&lt;0.001**</b>
		None vs. Sham	1.00	1.00	1.00
	Bic-ADelt	GVS vs. None	0.24	0.09	1.00
		GVS vs. Sham	0.15	0.09	0.89
		None vs. Sham	0.64	1.00	1.00
	Bic-MDelt	GVS vs. None	0.67	0.31	0.98
		GVS vs. Sham	0.67	0.31	0.98
		None vs. Sham	1.00	1.00	1.00
	Bic-PDelt	GVS vs. None	0.48	0.27	1.00
		GVS vs. Sham	0.44	0.27	1.00
		None vs. Sham	1.00	1.00	1.00

Table 3.5: GVS increases  $IMC_z$  (GVS vs. None, and GVS vs. Sham) in neck muscles across frequency bands for the Control group during Rest. Conversely, no Sham effect was found (None vs. Sham). The table summarizes adjusted p-values for *post-hoc* comparisons using Bonferroni corrections (adjusted for 2 comparisons) for Stimulus type in the Control group during Rest. Red text indicates significant differences between stimulus types: No Stimulation (*None*), *Sham* and Galvanic Vestibular Stimulation (*GVS*). Muscles: *Sternocleidomastoid* (SCM), *Upper Trapezius* (UTrap), *Biceps brachii* (Bic), and *Anterior, Middle and Posterior Deltoid* (ADelt,MDelt,PDelt).

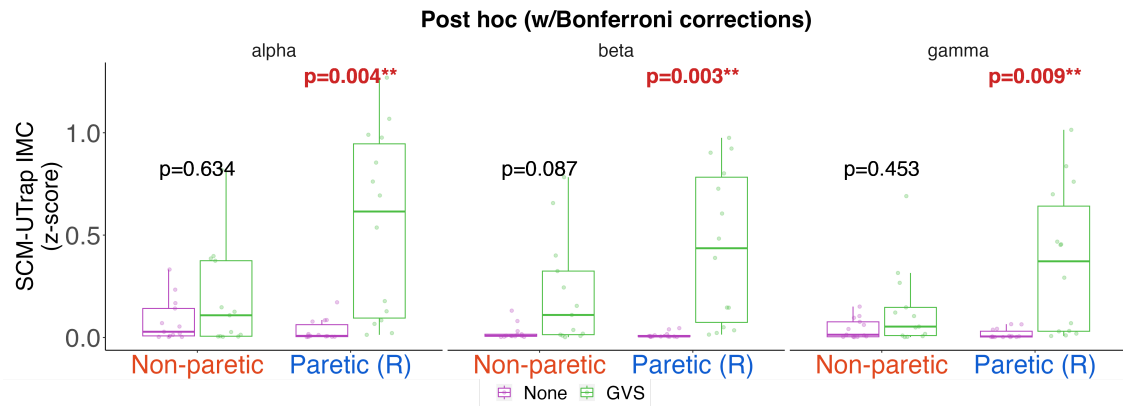
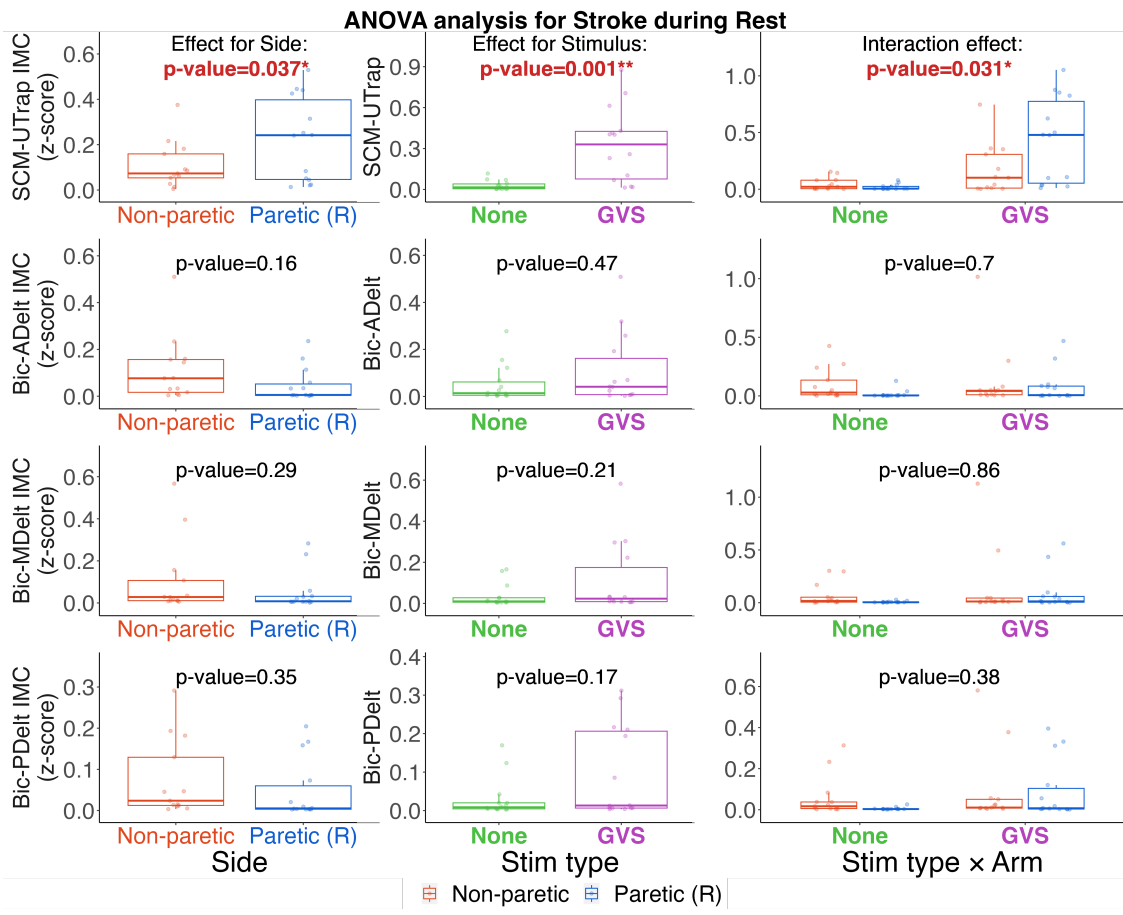


Figure 3.4: During Rest, stroke participants showed a statistically significant difference between both sides on intermuscular coherence ( $IMC_z$ ) in neck muscles (SCM-UTrap, Effect for Side,  $p = 0.037$ ), which was not observed in Controls ( $p = 0.28$ ). Galvanic vestibular stimulation (GVS) changed  $IMC_z$  in neck muscles for both groups (Control:  $p = 0.01$ , Stroke:  $p < 0.001$ ). Additionally, the Stroke group showed a significant interaction with decreased  $IMC_z$  on the Non-paretic side during GVS. Post-hoc comparisons with Bonferroni corrections of the neck muscles (SCM-UTrap) showed that GVS increased  $IMC_z$  only in the Paretic (R) side across all frequency bands (alpha to gamma), as seen in the Control group. Unexpectedly, the Non-paretic side did not show differences when comparing GVS and No Stimulation. SCM: Sternocleidomastoid; UTrap: Upper Trapezius; Bic: Biceps brachii; ADelt, MDelt and PDelt Anterior, Middle and Posterior Deltoid respectively.

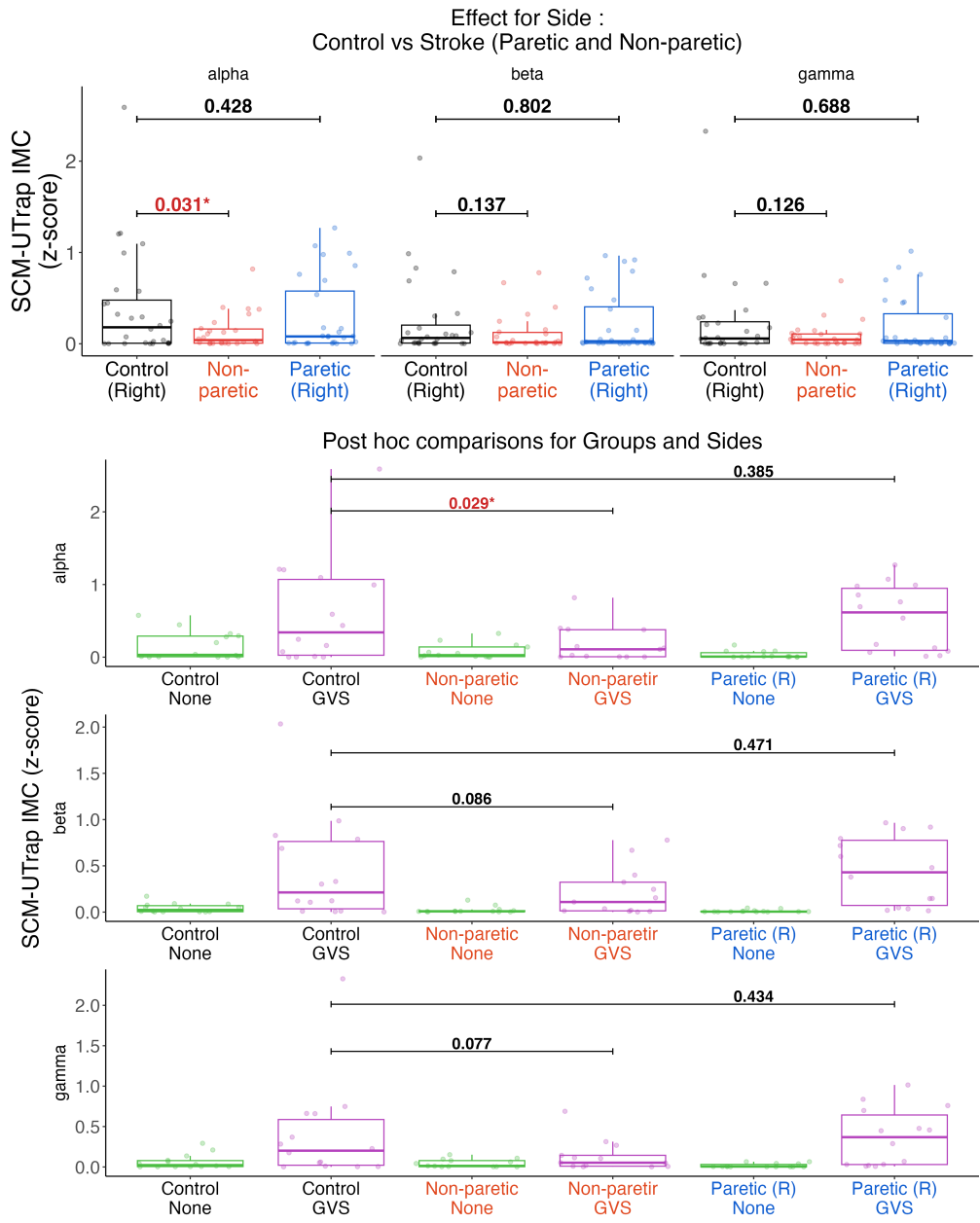


Figure 3.5: During Rest, Neck muscles (SCM-UTrap) from the Non-paretic (Left) side of Stroke participants showed lower levels of  $IMC_z$  in the alpha band when compared with Control participants (effect for *Side* in the alpha band,  $p = 0.031$ , top panel). No differences were found between the Paretic (R) side of Stroke participants and the Control group when comparing the same muscle pair ( $p = 0.428$ ). The Stimulus type had a significant effect across frequency bands (Post hoc comparison, lower panel). GVS showed an overall effect of increased  $IMC_z$  in the same neck muscles when comparing both sides of Stroke with the Control group. A Post hoc analysis (with bonferroni corrections) showed that GVS did not increase  $IMC_z$  on the Non-paretic side of Stroke participants ( $p=0.029$ ). SCM: Sternocleidomastoid; UTrap: Upper Trapezius.

Group	Muscle	Band	Stim type	$\hat{\psi}$ Right/Left	Lower CI Right/Left	Upper CI Right/Left	p-adjusted Right/Left
Stroke (n=14)	SCM- UTrap	alpha	GVS vs. None	0.51/0.12	0.17/-0.13	0.85/0.37	<b>0.004**</b> /0.634
			GVS vs. Sham	0.45/0.05	0.09/-0.23	0.81/0.33	<b>0.013*</b> /1
			None vs. Sham	-0.06/-0.07	-0.16/-0.18	0.04/0.04	0.388/0.307
	Bic- ADelt	beta	GVS vs. None	0.43/0.2	0.16/-0.03	0.71/0.43	<b>0.003**</b> /0.087
			GVS vs. Sham	0.41/0.19	0.12/-0.05	0.69/0.43	<b>0.005**</b> /0.147
			None vs. Sham	-0.03/-0.02	-0.07/-0.05	0.01/0.02	0.258/0.59
	Bic- MDelt	gamma	GVS vs. None	0.35/0.1	0.08/-0.08	0.62/0.29	<b>0.009**</b> /0.453
			GVS vs. Sham	0.3/0.06	0.01/-0.15	0.59/0.27	<b>0.042*</b> /1
			None vs. Sham	-0.05/-0.04	-0.11/-0.12	0.01/0.04	0.152/0.552
	Bic- PDelt	alpha	GVS vs. None	0.05/-0.1	-0.05/-0.25	0.16/0.06	0.567/0.324
			GVS vs. Sham	0.07/-0.08	-0.03/-0.23	0.17/0.06	0.234/0.408
			None vs. Sham	0.02/0.01	-0.04/-0.06	0.07/0.09	1/1
	Stroke (n=14)	beta	GVS vs. None	0.08/0.02	-0.04/-0.08	0.19/0.12	0.259/1
			GVS vs. Sham	0.07/0.02	-0.05/-0.08	0.19/0.12	0.414/1
			None vs. Sham	-0.01/0	-0.04/-0.03	0.02/0.03	1/1
	Stroke (n=14)	gamma	GVS vs. None	0.06/-0.09	-0.04/-0.26	0.16/0.08	0.329/0.489
			GVS vs. Sham	0.05/-0.05	-0.07/-0.19	0.16/0.08	0.809/0.923
			None vs. Sham	-0.01/0.04	-0.06/-0.04	0.03/0.12	1/0.622
	Stroke (n=14)	alpha	GVS vs. None	0.09/-0.05	-0.04/-0.15	0.21/0.05	0.225/0.506
			GVS vs. Sham	0.09/-0.06	-0.03/-0.14	0.21/0.01	0.184/0.088
			None vs. Sham	0/-0.01	0/-0.08	0.01/0.05	0.287/1
	Stroke (n=14)	beta	GVS vs. None	0.09/0.02	-0.04/-0.05	0.21/0.1	0.234/1
			GVS vs. Sham	0.09/0.01	-0.04/-0.05	0.22/0.08	0.225/1
			None vs. Sham	0/-0.01	0/-0.03	0/0.02	0.624/0.946
	Stroke (n=14)	gamma	GVS vs. None	0.08/-0.04	-0.05/-0.16	0.21/0.08	0.311/1
			GVS vs. Sham	0.09/-0.03	-0.05/-0.11	0.22/0.06	0.302/1
			None vs. Sham	0/0.02	0/-0.04	0.01/0.07	0.589/1
	Stroke (n=14)	alpha	GVS vs. None	0.08/-0.06	-0.02/-0.19	0.18/0.08	0.135/0.774
			GVS vs. Sham	0.08/-0.09	-0.02/-0.23	0.19/0.06	0.155/0.364
			None vs. Sham	0/-0.03	-0.01/-0.09	0.01/0.03	1/0.498
	Stroke (n=14)	beta	GVS vs. None	0.1/0.03	-0.02/-0.08	0.22/0.13	0.131/1
			GVS vs. Sham	0.1/0.02	-0.02/-0.09	0.22/0.12	0.13/1
			None vs. Sham	0/-0.01	0/-0.02	0/0.01	0.512/0.896
	Stroke (n=14)	gamma	GVS vs. None	0.08/-0.03	-0.02/-0.17	0.17/0.12	0.137/1
			GVS vs. Sham	0.08/-0.04	-0.02/-0.19	0.17/0.1	0.155/1
			None vs. Sham	0/-0.01	0/-0.06	0/0.03	0.869/1

Table 3.6: When GVS is applied at *Rest*, only the paretic side of stroke shows increased coherence to neck muscles across frequency bands. No Sham effect was found on either side (None vs. Sham). The table summarizes adjusted p-values for *post-hoc* comparisons for each arm using Bonferroni corrections (adjusted for 2 comparisons) for Stimulus type in the stroke group during Rest. Red text indicates significant differences between stimulus types: No Stimulation (*None*), *Sham* and Galvanic Vestibular Stimulation (*GVS*). Muscles: *Sternocleidomastoid* (SCM), *Upper Trapezius* (UTrap), *Biceps brachii* (Bic), and *Anterior, Middle and Posterior Deltoid* (ADelt,MDelt,PDelt).

# **Chapter 4**

## **Discussion and Future work**

### **4.1 Main findings**

The main mechanism underlying pathological synergies following stroke is the disruption to CST drive [Brunnstrom, 1970, McMorland et al., 2015], which leads to loss of inhibitory cortical control over brainstem circuitry [Shimizu et al., 2002, Niehaus et al., 2003, McMorland et al., 2015, Emos and Rosner, 2023]. As such, it has been proposed that increased drive from descending subcortical pathways—as well as maladaptive changes in segmental reflex circuits—also contribute to the emergence of such pathological synergies [Krakauer, 2005].

Evidence exploring these mechanisms focused their attention on the role of increased neural drive from the reticulospinal tract [Baker et al., 2015, Choudhury et al., 2019, McPherson et al., 2018, Taga et al., 2021]. While there's evidence supporting such contribution, other mechanisms such as increased drive arising from the remaining subcortical pathways have not been systematically studied during voluntary reaching movements. For example, it has been shown that just as the RST, vestibular brainstem output also becomes upregulated following stroke [Miller et al., 2014, 2016, Miller and Rymer, 2017]. This has been shown during isolated muscle contraction in neck and arm muscles, but not during voluntary reaching movements or when combined with shoulder abduction, which is known to exacerbate pathological synergies [Sukal et al., 2007, Ellis et al., 2008, 2016]. Our results provide a much-needed characterization of the vestibular

system's role in voluntary movement, both in neurotypical participants and following stroke. Importantly, it provides evidence to exclude a vestibular contribution to pathological synergies in stroke survivors.

First, we determined that during rest and voluntary arm movement (including reaching and isometric contractions), arm muscles from young neurotypical participants did not show shared vestibular drive when applying vestibular stimulation (see Chapter 2, and [Bartsch and Valero-Cuevas, 2025](#)). Consequently, our results excluded a vestibular contribution to voluntary arm movement in neurotypical participants. Unexpectedly, we found shared neural drive to neck muscles at rest, which was suppressed during both voluntary reaching and isometric contractions of neck and arm muscles. This is a form of task-dependent *vestibular suppression* due to voluntary arm movement –a phenomenon previously observed only in neck muscles during head movements [[Cullen and Zobeiri, 2021](#)]. As opposed to vestibular stimulation, sham did not increase intermuscular coherence to neck muscles, therefore, it is unlikely that another mechanism is involved in the increased coherence –and its suppression– to neck muscles when vestibular suppression was applied.

In Chapter 3 we compared the shared neural drive to arm muscles of stroke survivors (from both the paretic and non-paretic sides) with an age-matched control group. Our findings showed that the shared neural drive to arm muscles was not increased when vestibular stimulation was applied –neither at rest nor during voluntary arm movement— regardless of whether the shoulder was in a neutral or abducted position. Consequently, our findings exclude not only a vestibular contribution to voluntary arm movement in neurotypical participants (Chapter 2), but also an upregulation of vestibular output arising from progressive loss of inhibitory cortical control following stroke (Chapter 3). Moreover, during voluntary reaching with abducted shoulder, the paretic side of stroke survivors showed decreased coherence in arm muscles when compared to controls, which agrees with previous findings in stroke [[Fang et al., 2009](#), [Fisher et al., 2012](#), [Larsen et al., 2017](#), [Fisher et al., 2012](#)]. We interpret this reduction in shared neural drive as most likely emerging from disruptions in corticospinal pathways following stroke.

On the other hand, stroke survivors showed an unexpected asymmetric neural drive to neck muscles when vestibular stimulation was applied at rest. This asymmetry is also consistent with previous findings, where the ratio of the muscle responses from the paretic side where favored over the to non-paretic side when vestibular stimulation was applied [Miller et al., 2014]. When comparing the non-paretic side of stroke with the control group, we were able to show that the asymmetries arise from suppressed or reduced responses on the non-paretic side instead of increased responses on the paretic side. These results may reflect disruptions of ipsilesional cortico-vestibular and brainstem pathways.

Our characterization of vestibular contributions —or the lack thereof— to voluntary arm movement provides valuable insights for rehabilitation. Since our results exclude an upregulation of vestibular output to voluntary arm movements in both neurotypical and stroke populations, therapeutic strategies should primarily target the disrupted corticospinal pathways and the compensatory role of the remaining subcortical pathways such as the reticulospinal tract. Our results suggest that the non-paretic side also undergoes neurophysiological changes following stroke. The asymmetries in neck muscle responses and the decreased shared neural drive to the non-paretic side highlight the importance of its inclusion in both assessments and rehabilitation protocols to improve recovery outcomes. In summary, our results showed that vestibular stimulation does not increase shared neural drive to arm muscles in either neurotypical participants or stroke survivors, excluding a vestibular contribution to voluntary arm movement and as a mechanism underlying pathological synergies. In contrast, neck muscles showed shared neural drive at rest in neurotypical participants —young and control—, however, this drive is suppressed during voluntary reaching and isometric contractions, suggesting a task-dependent gating mechanism. Moreover, in stroke survivors, the decreased shared neural drive in arm muscles—particularly on the paretic side as well as the observed asymmetries in neck muscle responses point to disrupted corticospinal pathways and altered brainstem circuitry. These findings imply that rehabilitation efforts should prioritize interventions targeting

corticospinal recovery and the compensatory role of other subcortical pathways. Additionally, addressing both the paretic and non-paretic sides will likely improve recovery and postural control.

## 4.2 Future work

While this dissertation advances our understanding of vestibular contributions to voluntary reaching movement and stroke-related motor impairments, several questions remain open.

### 4.2.1 Investigating the task-dependent suppression of Vestibular responses

The results from Chapter 2 showed that vestibular drive to neck muscles –seen at rest— is suppressed during unperturbed voluntary arm movement. Our interpretation is that vestibular-mediated adjustments are unnecessary—and thus suppressed—during unperturbed self-initiated movements. The utility of this suppression is to prevent counterproductive responses that could act as internal perturbations. Our experimental design required participants to visually track their velocity during *Reaching* or maintain their neck posture during *Isometric Contraction*. Consequently, these tasks demanded active control of head and neck kinematics (active arm movement with head control). During GVS, the head and neck kinematics could be perturbed and have a negative impact on motor performance. To further test this interpretation, vestibular suppression can be examined in tasks where head position can be adjusted without compromising task execution, thereby avoiding conflicts between these GVS-driven responses and motor performance. By removing velocity constraints and visual tracking, shared neural drive could be compared in conditions where visual feedback does not affect motor performance (active arm movement without head control), for example when performing the task with and without visual input (eyes open vs. eyes closed). To further investigate the conditions under which vestibular suppression occurs, the resting task can be modified to

include the head and neck to be involved in a visual tracking activity, without upper extremity movement (active head control without arm movement). This could be tested by comparing vestibular responses when participants passively rest versus when they actively track a visual target using controlled head movements. If vestibular suppression extends to such conditions (both active arm movement without head control, and active head control without arm movement), this would suggest that suppression is not solely linked to voluntary limb movement but may also apply more broadly to tasks requiring precise head and neck control.

#### **4.2.2 Investigating ipsilateral cortico-vestibular downregulation**

The results from Chapter 3 showed decreased ipsilesional vestibular drive to neck muscles when GVS was applied. Although arm movement is not affected on the non-paretic side, there may be important consequences for balance control arising from decreased vestibular drive. These findings raise significant questions about the role of vestibular brainstem output in postural control in individuals who had a stroke.

To further investigate the functional impact of ipsilesional vestibular disruptions, we propose an experimental design aimed at testing changes in postural control following stroke. This can be achieved by manipulating postural demands and comparing balance performance between Control and Stroke participants. Specifically, tasks such as free versus constrained uni- and bipedal standing provide conditions with differing reliance on vestibular input: constrained standing (e.g., with trunk support) reduces vestibular demand, whereas free standing requires active postural adjustments driven by sensory feedback, including vestibular cues. We hypothesize that stroke survivors will show greater deficits in postural stability under free-standing conditions, where the vestibular system plays a more prominent role. This would provide evidence that impaired vestibular contributions after stroke directly affect balance strategies under unstable conditions.

Similarly, introducing external perturbations, such as changes in the base of support, could help reveal changes in motor strategies if vestibular function is compromised following stroke. These perturbations would also exacerbate postural instability, thereby providing insights into the extent to which decreased vestibular drive translates into postural control deficits. If postural control remains relatively unaffected across different stability conditions, this might indicate that other sensory inputs —such as visual or proprioceptive feedback— are compensating for the decreased vestibular drive. In such a case, the central nervous system may be re-weighting sensory information to maintain balance, which could have important implications for rehabilitation strategies. These interpretations not only have theoretical significance but also practical implications for rehabilitation. If increased postural instability is found in stroke survivors, then targeted therapies could be developed to improve vestibular function. Ultimately, these findings could inform more effective rehabilitation strategies aimed at improving balance control by directly addressing the vestibular deficits in the non-paretic —rather than the paretic— side of individuals with stroke.

#### **4.2.3 Neural Mechanisms Underlying Synergies**

The results from Chapter 3 showed decreased shared neural drive on the paretic side of stroke survivors during reaching with an abducted shoulder. We interpret this decreased drive as most likely arising from disrupted corticospinal pathways. Importantly, we did not observe an increase in shared neural drive to arm muscles at rest or during voluntary arm movement, which excludes a vestibular contribution to pathological synergies. However, attributing increased drive from RST as the only mechanism underlying pathological synergies is still debatable. Consequently, RST drive as well as other subcortical pathways such as those involved in reflex responses should be further investigated.

Pairing startling acoustic and visual stimuli can involuntarily elicit pre-planned movements —a phenomenon termed *startReact*— through presumed activation of subcortical circuits, including but not limited to the RST. Unlike the classic startle reflex, which generates a brief, generalized flexor response, *startReact*

responses replicate the kinematics of voluntarily planned movements and are typically faster, starting 30–40 ms after the acoustic stimulation. Honeycutt and Perreault showed that *startReact* elicits rapid elbow flexion with latencies and muscle activation patterns indistinguishable between stroke and unimpaired individuals. However, *startReact* responses were elicited less often during reaching with the abducted shoulder in stroke survivors [Lee et al., 2022]. These findings suggest that while voluntary execution may be compromised post-stroke, the motor plan remains intact and can be accessed through brainstem-mediated mechanisms [Honeycutt and Perreault, 2012, 2014, Honeycutt et al., 2014]. Consequently, pairing voluntary reaching movements while eliciting *startReact* and stretch reflex responses may provide insights about changes in subcortical and spinal drive contribute to motor output after during voluntary reaching. By assessing shared neural drive within a paradigm that includes both RST and stretch reflex stimulation, we can better understand how their interaction contributes to abnormal muscle coactivation and the emergence of pathological synergies. This integrated approach may help identify specific neural mechanisms that could be targeted in rehabilitation.

In summary, while our results exclude a vestibular contribution to pathological synergies, they underscore the need to explore the role of the RST and other reflex mechanisms. By integrating targeted stimulation of subcortical pathways, future studies can provide a more complete understanding of the neural mechanisms underlying pathological synergies in stroke survivors. This comprehensive approach is essential for developing effective rehabilitation strategies that aim to restore functional motor control by addressing both neural and maladaptive neural responses.

## **Appendix 1: Introducing the distinction between ‘*Fine synergies*’ vs. ‘*Coarse synergies*’ to better describe sensorimotor disruptions**

**‘*Fine synergies*’ describe motor adaptation in people with drop foot in a way that supplements traditional ‘*Coarse synergies*’ by Bartsch-Jiménez A, Blazkiewicz M, Azadjou H, Novotny R, Valero-Cuevas FJ. *Frontiers in sports and active living*, 2023.**

### **Abstract**

Synergy analysis via dimensionality reduction is a standard approach in biomechanics to capture the dominant features of limb kinematics or muscle activation signals, which can be called ‘coarse synergies’. Here we demonstrate that the less dominant features of these signals, which are often explicitly disregarded or considered noise, can nevertheless exhibit ‘fine synergies’ that reveal subtle, yet functionally important, adaptations. To find the coarse synergies, we applied non-negative matrix factorization (NMF) to unilateral EMG data from eight muscles of the involved leg in ten people with drop-foot (DF), and of the right leg of 16 unimpaired (control) participants. We then extracted the fine synergies for each group by removing the coarse synergies (i.e., first two factors explaining  $\geq 85\%$  of variance) from the data and applying Principal Component Analysis (PCA) to those residuals. Surprisingly, the time histories and structure of the coarse EMG synergies showed few differences between DF and controls – even though the kinematics of drop-foot

gait is evidently different from unimpaired gait. In contrast, the structure of the fine EMG synergies (as per their PCA loadings) showed significant differences between groups. In particular, loadings for *Tibialis Anterior*, *Peroneus Longus*, *Gastrocnemius Lateralis*, *Biceps* and *Rectus Femoris*, *Vastus Medialis* and *Lateralis* muscles differed between groups ( $p < 0.05$ ). We conclude that the multiple differences found in the structure of the fine synergies extracted from EMG in people with drop-foot vs. unimpaired controls—not visible in the coarse synergies—likely reflect differences in their motor strategies. Coarse synergies, in contrast, seem to mostly reflect the gross features of EMG in bipedal gait that must be met by all participants—and thus show few differences between groups. However, drawing insights into the clinical origin of these differences requires well-controlled clinical trials. We propose that fine synergies should not be disregarded in biomechanical analysis, as they may be more informative of the disruption and adaptation of muscle coordination strategies in participants due to drop-foot, age and/or other gait impairments.

### 4.3 Introduction

Applying dimensionality reduction techniques to kinematic or electromyographic (EMG) data is a form of unsupervised learning [Valero-Cuevas et al., 2009a, Clewley et al., 2008] to capture the lower-dimensional structure of the neural control of movement [d’Avella et al., 2003, Tresch and Jarc, 2009, Kutch and Valero-Cuevas, 2012, Rabbi et al., 2020, Ting and McKay, 2007, Valero-Cuevas, 2016, Clewley et al., 2008]. Independently on whether or not these ‘synergies’ are of neural origin [Tresch and Jarc, 2009, Kutch and Valero-Cuevas, 2012], they are ‘descriptive’ [Valero-Cuevas, 2016, Brock and Valero-Cuevas, 2016] (in a mathematical sense) of the basis functions that best explain a high percentage of the variance in the data \*. The investigator must first determine *a priori* if linear or nonlinear basis functions are most appropriate, and what is the discrete number of basis functions (i.e., synergies) that explain a ‘high enough’ percentage of the variance [Clewley et al., 2008]. In practice, methods that produce linear basis functions

---

\*That is, the original data can be approximated as a combination of the basis functions extracted from the original data.

are most popular such as Non-Negative Matrix Factorization (NMF) [Lee and Seung, 1999, Rabbi et al., 2020], Principal Component Analysis (PCA) [Ting and Macpherson, 2005], Independent Component Analysis (ICA) [Hyvärinen and Oja, 2000], and Factor Analysis (FA) [Saito et al., 2015].

In the fields of biomechanics and neuromechanics, the number of synergies that together explain 80- 90% of the variance are considered sufficient to explain the dominant characteristics of the data and, therefore, most informative [Turpin et al., 2021, d'Avella et al., 2003, Tresch and Jarc, 2009, Kutch and Valero-Cuevas, 2012, Rabbi et al., 2020, Ting and McKay, 2007, Valero-Cuevas, 2016, Ó'Reilly and Federolf, 2021]. We call these '*coarse synergies*'. The residuals from the coarse synergies (i.e., which represent the remaining 20–10% of the variance) are, by construction, data (i) in which the investigator is *a priori* not interested (because they explicitly set the cut-off for variance explained), (ii) which cannot be accounted for by the linear model (a by-product of the preferred method [Clewley et al., 2008]), or (iii) are considered noise (an assumption which must be proven) [Barradas et al., 2020, Valero-Cuevas et al., 2009b]. In either case, they are considered irrelevant or unimportant.

Here, we question this traditional interpretation of coarse synergies and the assumptions about their residuals to explore the subtle ways in which synergies can differ across populations. Our rationale is that there are coarse mechanical features of, in this case, locomotion that must be common to all participants – and are therefore not very informative of differences across populations. Therefore, we look to residuals as a more informative source of subtle differences.

In particular, here we focus on analysing the residuals after removing coarse synergies to establish whether or not they are irrelevant, and if they are informative of fine features of muscle coordination that are not captured by the coarse synergies. To do so, we apply dimensionality reduction to the residuals of the coarse synergies to extract '*fine synergies*'. As a first example of this approach, we use EMG from leg muscles during locomotion to compare coarse and fine synergies between people with drop foot (DF) vs. unimpaired control participants (C).

## **4.4 Materials and Methods**

### **Participants**

Two groups of people participated in this study. Ten individuals with clinically diagnosed unilateral drop foot without comorbidities that prevented locomotion formed the experimental group (DF). Their mean age was  $52.9 \pm 17.9$  years, height  $174.8 \pm 9.1$  cm, and body mass  $68.8 \pm 18.7$  kg. The following medical diagnosis were represented: peroneal nerve palsy secondary to lumbar disc herniation (n=2); post motor vehicle injury (n=1); progressive muscular dystrophy (n=3); surgical removal of a tumor at the level of the head of the fibula (n=2); ischemic disease of the lower limbs surgically fitted with stents (n=1); and, amyotrophic lateral sclerosis (n=1). In daily life, all participants were ambulatory and did not report dependence on a wheelchair. During test day, they verbally declared a good health and physical condition to participate in the study. Sixteen unimpaired participants with a mean age of  $25.3 \pm 7.1$  years, height of  $176.6 \pm 6.8$  cm and body mass of  $74.1 \pm 10.5$  kg constituted the control group (C). All participants gave their informed written consent to participate in this study. The procedures were approved by the Ethical Committee of the Medical Center of Postgraduate Education in Warsaw, Poland (84/PB/2016).

### **Instrumentation and data collection**

Unilateral surface EMG (sEMG) was collected from eight muscles using a Noraxon system (Noraxon USA. Inc., USA). Data were collected from the involved limb of persons from the DF group, and from the right limb from control participants. The activity was recorded from the following eight muscles: *Tensor Fasciae Latae* (TFL), *Biceps Femoris* (BF), *Peroneus Longus* (PL), *Gastrocnemius Lateralis* (GL), *Vastus Lateralis* (VL), *Tibialis Anterior* (TA), *Vastus Medialis* (VM) and *Rectus Femoris* (RF). For each participant, the bipolar Ag-AgCl EMG electrodes (10-mm diameter, 20-mm dipole distance) location was identified according to guidelines

for electrode placement developed by the Surface Electromyography for the Non-Invasive Assessment of Muscles (SENIAM) project and verified based on clinical muscle tests.

All participants walked barefoot and naturally at their self-selected speed along a 10m walkway. Trials with incidents were discarded from further analysis and the procedure was repeated. Two force plates (Kistler Holding AG, Switzerland) were used to determine ground reaction forces using Nexus 1.7.1 software, which afterwards was confirmed manually for each participant. Data was then exported to the Vicon Polygon system, which independently divided the gait into individual cycles and calculated the gait spatio-temporal parameters. EMG and Force plate systems were synchronized and had a sampling frequency of 1000Hz. After data collection from the Drop foot group, kinetic and kinematic data were visually inspected to determine the results' homogeneity (Figure 4.6).

## Data analysis and muscle synergy extraction

Surface EMG signals were high-pass filtered to remove movement artifacts, using a third-order Butterworth high-pass filter at 20 Hz. On-line sEMG signals were displayed for inspection of the signal quality during measurement. The sEMG signals were rectified and smoothed with a 2Hz second-order Butterworth low-pass filter to obtain the muscle contraction linear envelope. The third gait cycle from each participant was selected for analysis based on ground reaction forces data. The sEMG envelopes were processed into a time normalized sEMG profile (i.e., from 0 to 100% of gait cycle, starting at heel strike). Next, each muscle's sEMG time series for each participant was normalized by the maximal peak value demonstrated by that specific muscle across gait cycles. Therefore, the magnitude of muscle activity was not taken into consideration in this temporal analysis.

Extraction of coarse synergies: We used the NMF algorithm to extract muscle synergies and their corresponding activation coefficients (i.e., weights) [Lee and Seung, 1999]. This method calculates a set of synergy weights ( $W_{m \times n}$ ) and synergy activations ( $A_{x \times j}$ ), such that  $sEMG = W \times A + residuals$ ,

where  $n$  is the number of synergies,  $m$  is the number of muscles (eight in this study), and  $j$  is equal to the number of sEMG data points [Turpin et al., 2021]. The residuals are defined as the difference between the experimental sEMG envelopes and the sEMG envelopes reconstructed from the product of the synergy weights and activations. The procedure to select the number of coarse synergies was to include as many as necessary to have  $\geq 80\%$  of variance accounted for (VAF) [Turpin et al., 2021]. To compare the coarse features of muscle coordination between control (C) and drop foot (DF) groups, we applied Statistical Parametric Mapping (SPM) to the reconstructed activity profiles, and a mixed design robust ANOVA with trimmed means [Mair and Wilcox, 2020] to compare the muscle weights extracted from the two coarse synergies that accounted for  $\geq 80\%$  of variance. The *spm1d* package ([www.spm1d.org](http://www.spm1d.org)) was used to perform SPM analysis [Pataky, 2012]. SPM was used to compare the reconstructed muscles activity profiles between groups C and DF to detect whether the coarse synergies showed statistically significant differences over the gait cycle.

Extraction of fine synergies: To extract the residual sEMG signals, the above reconstructed signals were subtracted from the original experimental sEMG envelopes. PCA was applied to the residual components of EMG to extract the fine synergies for each participant in both groups. In contrast to the experimental sEMG envelopes that have a 0 floor and 1 ceiling—which NMF can accommodate best—the residuals are zero-mean time-series for which PCA is appropriate. For each participant, we extracted the principal components (PC's) and their loadings, which were then normalized based on the highest loading per participant for both groups [Valero-Cuevas et al., 2016].

To compare the fine features of muscle coordination between control (C) and drop foot (DF) groups, we also applied Statistical Parametric Mapping (SPM) to the reconstructed activity profiles, and a mixed design robust ANOVA with trimmed means to compare the normalized muscle loadings extracted from the fine synergies. Non parametric post-hoc analyses were used to compare individual muscle pairs when

Table 4.1: Spatiotemporal gait patterns mean ( $\pm$  standard deviation) in drop foot (DF) and Control (C) groups.

	DF group	C group	<i>p</i> -value
Cadence (steps/min)	$81.11 \pm 2.42$	$90.65 \pm 4.45$	0.0001
Step length (m)	$0.5 \pm 0.07$	$0.66 \pm 0.09$	0.0002
Step width (m)	$0.11 \pm 0.02$	$0.11 \pm 0.02$	-
Stride time (s)	$1.43 \pm 0.14$	$1.29 \pm 0.07$	0.0090
Walking speed (m/s)	$0.8 \pm 0.03$	$1.33 \pm 0.06$	0.0001

the results from the robust ANOVA revealed a main or interaction effect. All statistical procedures were performed with RStudio (RStudio Team, MA, USA).

## 4.5 Results

### Spatio-temporal parameters

The spatiotemporal parameters of both groups are listed in table 4.1, and were compared using t-tests for independent samples. Cadence for the DF group was  $81.1 \pm 2.42$  steps/min, while the Control group was  $90.6 \pm 4.45$  steps/min. Step length was  $0.5 \pm 0.07$ m for the DF group and  $0.66 \pm 0.09$ m for the Control group. Step width was  $0.11 \pm 0.02$  for both groups. Stride time was  $1.43 \pm 0.14$  (s) for DF and  $1.29 \pm 0.07$  (s) for the Control group. Finally, walking speed was  $0.8 \pm 0.03$  (m/s) for the DF group and  $1.33 \pm 0.06$  (m/s) for the Control group. All participants were significantly different between groups ( $p < 0.01$ ), except for Step Width (Table 4.1).

### Coarse synergies

As expected, only two NMF factors sufficed to explain the gross features of muscle coordination in both groups (Tables S4.2 and S4.3). In the control group two factors explained an average of  $88.1 \pm 3\%$  of variance accounted for (Table S4.2 and Figure 4.1). Whereas for the drop foot group, the first two factors explained,

on average,  $86.9 \pm 2.7\%$  of variance accounted for (Table S4.3 and Figure 4.1). We defined these first two factors that explain  $\geq 85\%$  to be the *coarse synergies* for the Control and Drop Foot groups.

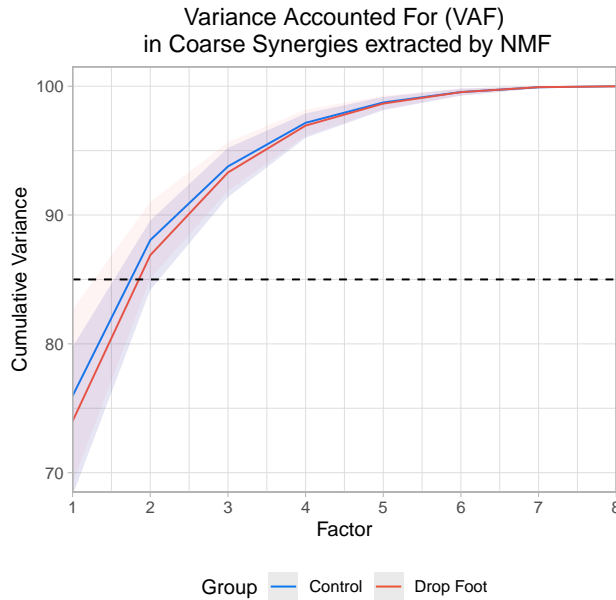


Figure 4.1: Cumulative variance accounted for each Factor extracted by NMF in drop foot (DF) and Control (C).

The time histories of the coarse EMG synergies in the DF group showed few differences compared to Controls. While there are visual differences between the DF and Control groups, the only statistically significant ones (as per SPM,  $p < 0.01$ ) occurred in the first *coarse synergy* from 10 to 18% of the gait cycle (Figure 4.2A). For the second *coarse synergy*, significant differences ( $p=0.015$ ) were only observed from 32% to 37% of the gait cycle (Figure 4.2B).

The structure of the coarse EMG synergies showed differences only for one muscle between the DF and Control groups. Muscle weights \* extracted from NMF (Figure 4.2C-D) were compared using a Robust mixed effects ANOVA model. In the *first coarse synergy*, the analysis revealed a main effect for Muscle ( $p < 0.01$ ), and Group ( $p=0.032$ ), with no interaction ( $Muscle \times Group$ ,  $p = 0.3$ ). Post-hoc analysis revealed significant

\*In NMF factors are described by their ‘weights,’ whereas in PCA the term ‘loadings’ is used.

differences between groups for muscle VL ( $p<0.01$ ) only. Comparison of muscles weights extracted from the second coarse synergy did not show main effects for Muscle ( $p=0.07$ ), Group ( $p=0.05$ ) nor interaction ( $Muscle \times Group$ ,  $p=0.53$ ).

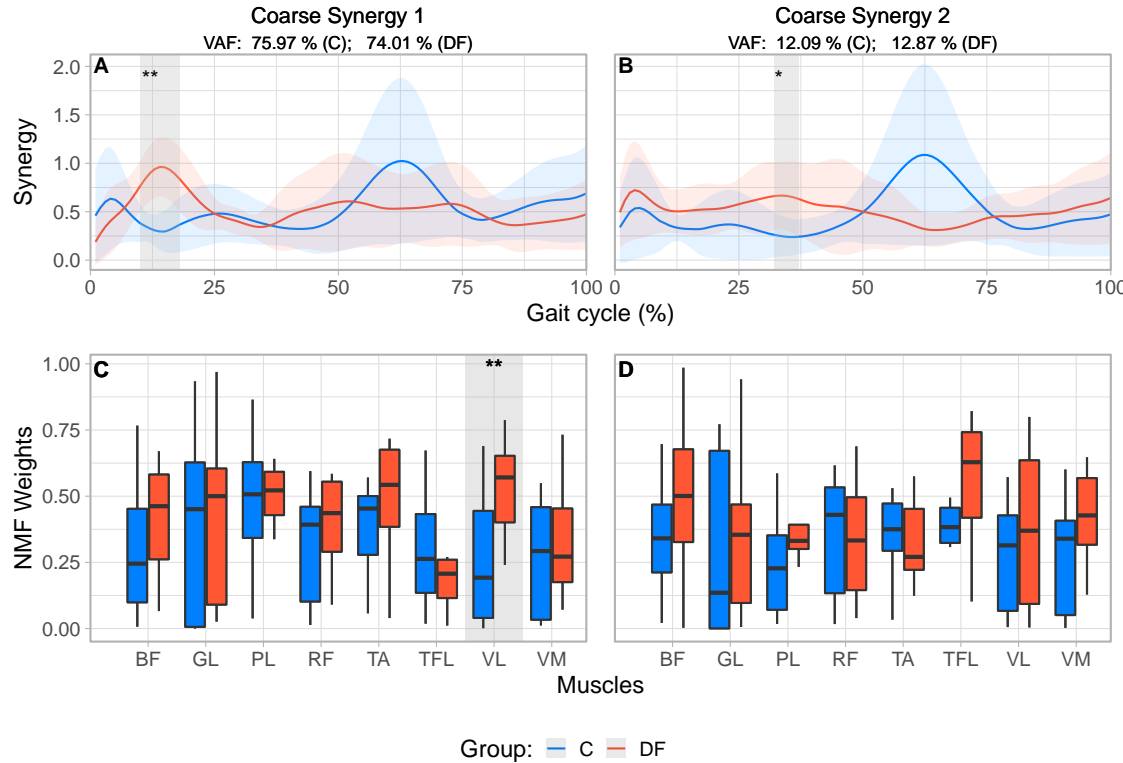


Figure 4.2: A-B: Reconstructed muscle activity profiles based on weights extracted from first two *coarse synergies* for each group, accounting for > 86% of variance in each group. Shaded areas identify differences between groups based on SPM{t} results and their corresponding levels of significance. C-D: Coarse synergies muscle weights extracted from NMF for unimpaired control participants (C) and persons with drop foot (DF).

\*Significant at 5%; \*\*Significant at 1%

## Fine synergies

Three *fine synergies* sufficed to explain  $\geq 85\%$  of variance in the residuals in both groups: 90.47% ( $\pm 3.79$  SD) and 90.46% ( $\pm 3.24$  SD) in the Control and DF groups, respectively (Figure 4.3).

SPM analysis did not reveal differences between groups at any level of significance in the histories of the three fine synergies (Figure 4.4A-C).

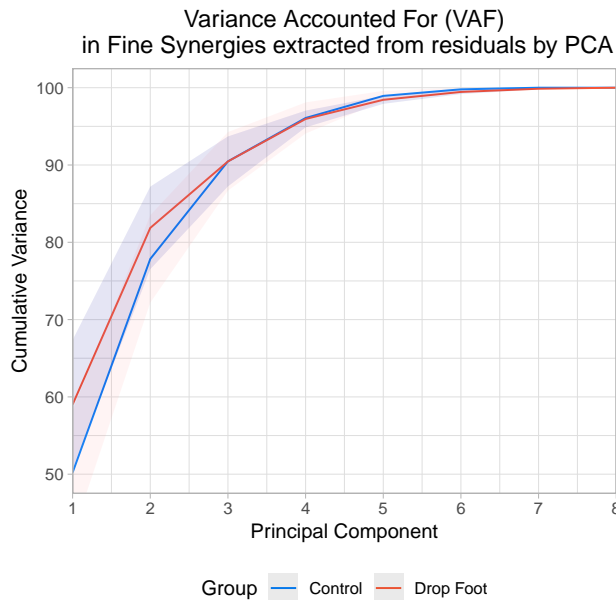


Figure 4.3: Cumulative variance accounted for each PC extracted from residuals by PCA in drop foot (DF) and control (C).

The structure of the first two fine synergies showed multiple statistically significant differences between the Control and DF groups, as per their loadings. Muscle loadings extracted from PCA (Figure 4.4D-F) were also compared using a Robust mixed effects ANOVA model, which revealed a main Group effect for the first and second *fine synergies* ( $p < 0.01$ , for both synergies), and a Muscle main effect ( $p < 0.01$ ) in the second ‘fine synergy’. Post-hoc analysis revealed statistical differences between both groups for muscles TA ( $p=0.016$ ), BF ( $p = 0.038$ ), RF ( $p=0.049$ ), GL ( $p=0.015$ ), VL ( $p = 0.01$ ) and VM ( $p=0.01$ ) in the first synergy, and PL ( $p=0.024$ ), RF ( $p=0.036$ ), TA ( $p=0.031$ ), and VM ( $p=0.036$ ), in the second *fine synergy*.

The third fine synergy did not show differences in its structure between Control and DF groups. The third synergy did not have a main Muscle ( $p=0.40$ ), Group ( $p=0.49$ ), nor interaction effect ( $Muscle \times Group$ ,

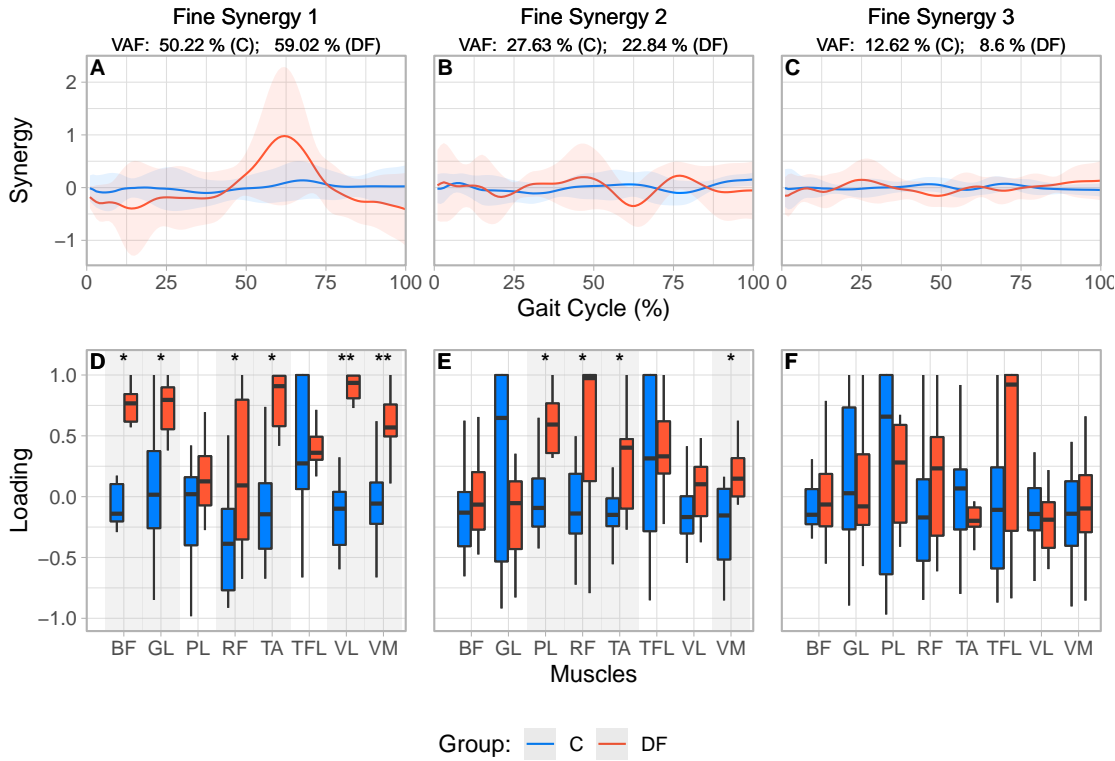


Figure 4.4: A-C: Reconstructed muscle activity profiles based on loadings extracted from first three ‘fine synergies’ for each group. D-F: Fine synergies loadings extracted from PCA for unimpaired control participants and persons with drop foot. Also note the loadings in DF are in general closer to +1 in the DF case, indicating greater synergistic correlation among muscle activations.

$p=0.52$ ). Moreover, all of their loadings tended to include or hover near zero. These results suggest the third fine synergy is likely unimportant to both groups (Figure 4.4F).

## 4.6 Discussion

Descriptive synergies which explain the majority of the variance in data (i.e., *coarse synergies*) are a common metric to compare performance across populations. We argue that coarse synergies, in the case of DF at least, can be uninformative about differences between groups as they mostly capture the dominant biomechanical features of locomotion common to all participants. We thus explored the notion that descriptive *fine*

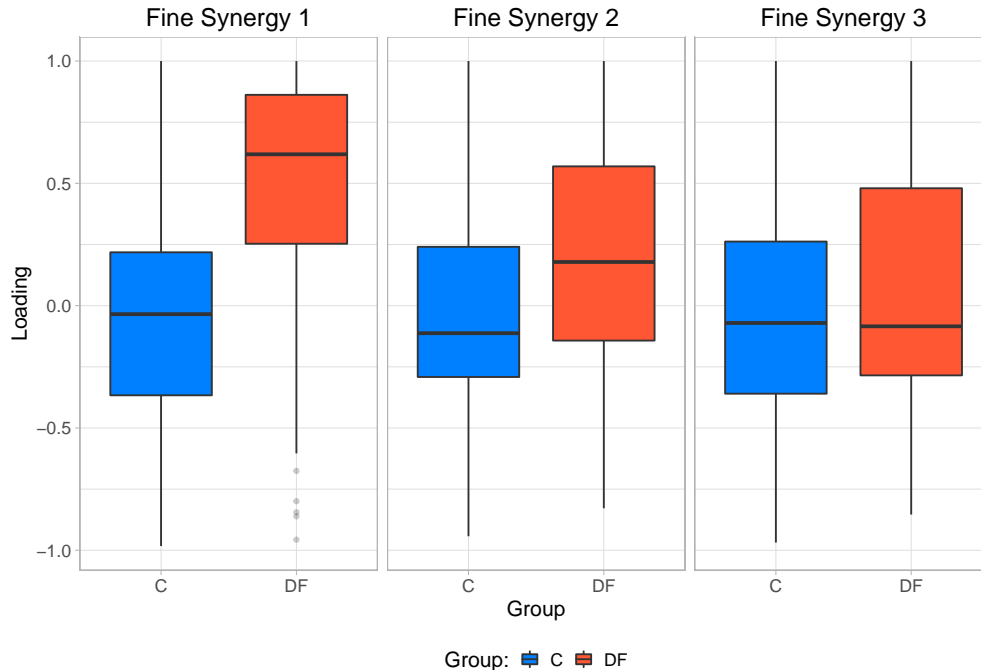


Figure 4.5: Mean Fine synergy loadings for each group extracted by PCA.

*synergies* extracted from the residuals to the *coarse synergies* may be—by virtue of containing subtler features—more informative of differences across populations.

Our results show this is the case when analyzing EMG signals from control and DF participants as the fine synergies showed the most differences across populations—potentially revealing subtle disruptions and adaptations of muscle coordination strategies in participants with DF.

An important methodological aspect of our approach is that we first used NMF on the EMG data, and then PCA on their residuals. Our rationale is twofold. NMF is a well-founded approach for analyzing rectified and normalized EMG signals that lie between values of 0 and 1 due to the non-negative input constraint to perform factorization. As such, it is better suited to extract coarse synergies ( $\geq 85\%$  VAF) from processed EMG signals [Lee and Seung, 1999, d’Avella and Tresch, 2001, Ting and Macpherson, 2005]. The residuals of the EMG signals after removal of the coarse synergies are zero-mean by construction, and therefore PCA is the more appropriate technique for extracting fine synergies [Clewley et al., 2008]. We then focused on analyzing these residual EMG signals first and foremost to establish whether or not they

had enough structure in their correlations to make them informative of fine features of muscle coordination that are not captured by the coarse synergies.

The nature of PCA loadings should be clarified before proceeding. PCA is a dimensionality reduction technique that approximates a high-dimensional signal with fewer basis vectors (PCs) that capture important features of correlations in the original signal. The values of PCA loadings have a range between -1 and 1, therefore, describe whether and how the elements of the original signal are correlated. Namely, loadings describe if there is structure to their correlations, or if their correlations hover near zero and therefore render the synergies informative. Importantly, PCA is obtained from the covariance matrix of the individual EMG signals, thus the correlations among EMG signals are what determine their loadings and not their overall level of activation. Therefore, a weakened muscle with a low level of activation—such as the TA in the DF group—can still have a loading close to 1 (or -1) in a PC if its activity is highly correlated (or anti-correlated) with the other muscles. On the other hand, a muscle could have a loading hovering near zero even if it is highly activated but uncorrelate with other muscles in that PC.

Given this preface, our results showed that the first two fine synergies in the DF participants were different from those in the controls. This is evidenced by the DF loadings being statistically different from controls in Figure 4.4 and 4.5. This is also valid for TA –even though we know it is weaker in the DF group—because its loadings are statistically different in the first and second fine synergies compared to controls. In contrast, all three fine synergies of the control participants, and the third fine synergy of the DF group, show little correlation structure as they loadings are hovering near zero. Therefore, those fine synergies are uninformative.

Dimensionality reduction techniques to extract coarse synergies have known limitations [Barradas et al., 2020, Brock and Valero-Cuevas, 2016, Kutch and Valero-Cuevas, 2012, Clewley et al., 2008]. For example, synergies are necessarily descriptive of the correlations among muscle activities; but do not necessarily speak to the actual neural control producing the task [Brock and Valero-Cuevas, 2016]. In addition, PCA

relies on signal normalization, which for EMG is performed via maximum voluntary contraction (MVC) of each muscle. However, this process is unreliable and true maximal force is difficult to attain in individuals with motor deficits [Cho et al., 2022]. Here, we normalized EMG signals based on the maximal activity of each muscle during the gait cycle. We did this to prove that weakness based on changes in the EMG signal is not the only change in muscle activity between groups, and is actually a change in the correlation structure among muscles that produces differences between groups. Since we already know that the activity levels will be different across groups, by normalizing to the maximal activity during the gait cycle we make the amplitudes of the signals comparable to reveal differences in the correlations among muscle activations. If scaling down the signals due to weakness is the only change during DF, we should not have found differences in the muscle loadings compared to controls. The presence of these differences in the fine synergies and not in the coarse synergies highlights the ability of fine synergies to reveal compensatory motor coordination strategies.

In order to test the usefulness of coarse vs. fine synergies to detect differences across groups, we compared the DF group to the so-called clinically neurotypical group. We consider young self-declared unimpaired people as such. On the other hand, if we had considered an age-matched group to those with DF, we would have the concern that they might exhibit some comorbidities of aging that would confound our results. Initially, 15 older subjects were screened for enrollment in our study; however, they did not meet our inclusion criteria due to comorbidities. Thus we kept younger individuals as controls to avoid potential confounds of aging.

We recognize that our study had a small sample size, compared populations of different ages, and the number of electrodes may not fully capture the muscle activation patterns of the leg. However, to the best of our knowledge, aging does not affect kinetic and kinematic parameters during gait [Rowe et al., 2021]. While age could partly explain our results (or an interaction between age and DF), this could only be confirmed using a larger sample and a more complex experimental design that is beyond the scope of

this work. Importantly, our goal was not to definitively declare DF from its various diagnoses, levels of impairment, clinical evolution (and/or age) as the main cause of differences between groups. We also do not claim that synergies of any kind can provide clinical insights unless and until they are used in the context of well-controlled clinical trials (which for DF is beyond the scope of this work). Rather, we used data from DF populations as a first example that allows us to question the traditional approach to, and interpretation of, descriptive ‘coarse synergies’ as biomarkers for changes in motor strategies. Our results show that changes due to DF (and/or aging) are not reflected in coarse synergies, further supporting the importance of analyzing “fine synergies” —which is the main topic and goal of our study.

To mitigate the limitations of our small sample size, we used robust inferential methods for hypothesis testing, which perform well with small sample sizes and when the assumptions of parametric statistics regarding normality and homoscedasticity are not met, and provide more accurate statistical results compared to classic parametric statistical techniques based on means comparisons [Mair and Wilcox, 2020].

From a technical perspective, our wired equipment limited the number of channels to record EMG signals from each participant to eight. We therefore chose to record the signals only from the affected side of each DF participant. Also, due to cable length, participants were only able to walk 10m, the reason for which we analyze only the third cycle once they reached a stable gait pattern before starting to decelerate and come to a full stop. Therefore, we could not record EMG during three full strides at a participant’s comfortable speed to assess recording’s reliability [Edelstein, 1986].

Notwithstanding these limitations, we find that coarse synergies are not as informative of differences across populations during gait, as compared to fine synergies. In particular, we saw an increase in the correlation of the weakened TA muscle activation with other muscles in the DF group (i.e., higher loading value), which was also seen in most of the recorded muscles in the first and second fine synergies, with only *Tensor Fasciae Latae* not being statistically different in any synergy (Figure 4.4). In the DF group, the increased loading for the *Biceps Femoris* may act as a compensatory mechanism to decrease hip flexion

during initial contact, potentially translating to a decreased step length. Additionally, the increased loading for the *Vastus Medialis* and *Lateralis* could represent a mechanism to decrease knee flexion during midstance. These changes have been previously reported in people with DF during ground clearance and foot-ground interaction [Błażkiewicz et al., 2017]. Previous findings have also shown that the presence of weakness during foot dorsiflexion in DF activates compensation strategies and influences muscle force and activation distribution [Błażkiewicz and Wit, 2019]. It was found that reduced forces of individual muscle groups of the ankle joint are compensated for by the increased strength of others acting on this joint (i.e. *Tibialis Posterior*, *Gastrocnemius Lateralis*), along with other muscles in neighboring joints (i.e. *Biceps Femoris*, *Rectus Femoris*, *Vastus Lateralis*, *Tensor Fasciae Latae*)[Błażkiewicz and Wit, 2019]. Considering that we found differences in PCA loadings within the same muscles (with the exception of *Tensor Fascia Latae*), our results from the fine synergies could reflect the same gait adaptations in the DF group as previously described.

Our results have allowed us to better characterize motor deficits and adaptations in persons with DF, based on differences in fine synergies as compared to control participants. This highlights the importance of considering not only the dominant features of a behavior (coarse synergies), but also the fine details revealed by fine synergies.

## Conflict of Interest Statement

The authors declare that the research was conducted in the absence of any commercial or financial relationships that could be construed as a potential conflict of interest.

## Author Contributions

MB and FVC contributed to conception and design of the study. AB, MB, MA and RN pre-processed the data, AB performed the statistical analysis. AB, MB, HA, RN and FVC interpreted the results. AB and FVC

wrote the first draft of the manuscript. AB, MB, HA and RN wrote sections of the manuscript and created the figures. All authors contributed to manuscript revision, read, and approved the submitted version.

## 4.7 Supplemental Data

### Kinetic and Kinematic data in Drop Foot Group

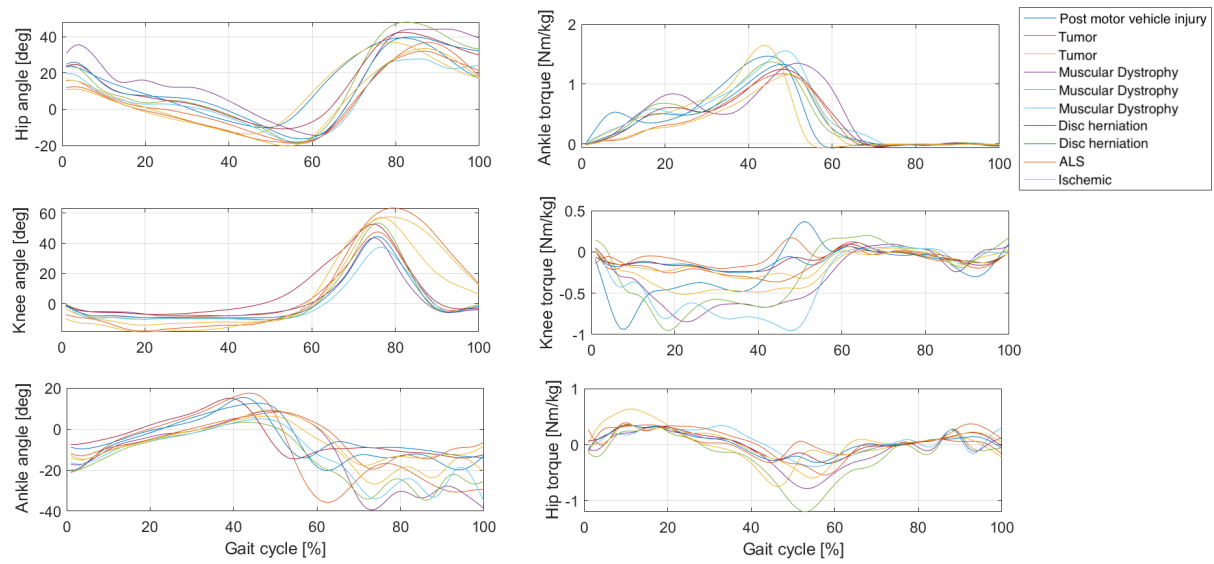


Figure 4.6: Kinematic and Kinetic data from lower extremity in the Drop Foot group.

## Tables

Table 4.2: Cumulative variance accounted for extracted from NMF for each subject in the Control group, with the respective Mean and Standard Deviation across factors.

	F1	F2	F3	F4	F5	F6	F7	F8
$S_1$	79.92	87.32	93.62	97.95	99.02	99.83	99.97	99.99
$S_2$	67.74	80.83	89.90	95.42	98.94	99.76	99.98	99.99
$S_3$	76.38	90.51	95.73	97.49	99.06	99.54	99.81	99.99
$S_4$	62.81	84.77	94.35	97.18	98.11	99.60	99.98	99.98
$S_5$	76.81	89.50	94.77	97.88	99.23	99.73	99.97	100.00
$S_6$	74.38	85.51	91.42	96.38	98.61	99.39	99.90	100.00
$S_7$	68.75	87.41	95.24	97.81	98.59	99.78	99.95	100.00
$S_8$	77.69	87.26	93.12	96.90	98.75	99.51	99.98	100.00
$S_9$	75.06	87.87	91.19	95.39	97.50	98.92	99.96	99.99
$S_{10}$	80.54	87.85	93.66	97.02	98.71	99.34	99.75	99.98
$S_{11}$	82.15	89.51	93.11	96.33	98.15	99.07	99.73	100.00
$S_{12}$	88.65	93.04	95.92	98.61	99.14	99.52	99.90	100.00
$S_{13}$	77.40	91.04	95.77	98.39	99.60	99.87	99.95	100.00
$S_{14}$	71.08	89.05	94.17	97.11	98.82	99.81	99.98	99.99
$S_{15}$	85.34	91.47	96.31	98.48	99.31	99.67	99.96	99.99
$S_{16}$	70.75	85.94	92.07	96.17	98.22	99.38	99.90	99.99
Mean	75.97	88.05	93.77	97.16	98.73	99.55	99.92	99.99
SD	6.72	2.97	1.89	1.02	0.54	0.27	0.08	0.01

Table 4.3: Cumulative variance accounted for extracted from NMF for each subject in the Drop Foot group, with the respective Mean and Standard Deviation across factors.

	F1	F2	F3	F4	F5	F6	F7	F8
$S_1$	79.92	87.32	93.62	97.95	99.02	99.83	99.97	99.99
$S_2$	67.74	80.83	89.90	95.42	98.94	99.76	99.98	99.99
$S_3$	76.38	90.51	95.73	97.49	99.06	99.54	99.81	99.99
$S_4$	62.81	84.77	94.35	97.18	98.11	99.60	99.98	99.98
$S_5$	76.81	89.50	94.77	97.88	99.23	99.73	99.97	100.00
$S_6$	74.38	85.51	91.42	96.38	98.61	99.39	99.90	100.00
$S_7$	68.75	87.41	95.24	97.81	98.59	99.78	99.95	100.00
$S_8$	77.69	87.26	93.12	96.90	98.75	99.51	99.98	100.00
$S_9$	75.06	87.87	91.19	95.39	97.50	98.92	99.96	99.99
$S_{10}$	80.54	87.85	93.66	97.02	98.71	99.34	99.75	99.98
Mean	74.01	86.88	93.30	96.94	98.65	99.54	99.92	99.99
SD	5.76	2.70	1.91	0.95	0.51	0.27	0.08	0.01

Table 4.4: Cumulative variance accounted for extracted from PCA for each subject in the Control group, with the respective Mean and Standard Deviation across Principal Components.

	PC1	PC2	PC3	PC4	PC5	PC6	PC7	PC8
$S_1$	56.88	83.98	92.77	98.60	99.49	99.80	100.00	100.00
$S_2$	46.83	76.98	95.14	98.40	99.61	99.93	100.00	100.00
$S_3$	55.41	75.20	89.96	95.19	97.64	99.36	100.00	100.00
$S_4$	64.43	84.15	91.77	97.11	99.53	99.92	100.00	100.00
$S_5$	55.29	81.82	93.94	97.67	99.62	99.90	100.00	100.00
$S_6$	42.97	75.39	90.19	95.55	99.02	99.84	100.00	100.00
$S_7$	63.96	84.76	94.12	98.37	99.66	99.90	100.00	100.00
$S_8$	43.38	75.29	89.79	95.10	98.89	99.88	100.00	100.00
$S_9$	37.63	64.70	81.28	92.23	99.09	99.86	100.00	100.00
$S_{10}$	49.60	79.79	91.38	95.45	98.23	99.86	100.00	100.00
$S_{11}$	40.43	69.33	84.59	92.72	98.03	99.68	100.00	100.00
$S_{12}$	41.73	81.34	89.03	93.96	98.16	99.17	100.00	100.00
$S_{13}$	54.60	84.10	95.69	98.24	99.23	99.94	100.00	100.00
$S_{14}$	48.93	75.25	89.77	97.56	99.28	99.93	100.00	100.00
$S_{15}$	52.81	78.91	90.90	95.28	98.44	99.70	100.00	100.00
$S_{16}$	48.57	74.60	87.25	95.89	99.19	99.97	100.00	100.00
Mean	50.22	77.85	90.47	96.08	98.94	99.79	100.00	100.00
SD	7.98	5.66	3.79	2.02	0.65	0.22	0.00	0.00

Table 4.5: Cumulative variance accounted for extracted from PCA for each subject in the Drop Foot, with the respective Mean and Standard Deviation across Principal Components.

	PC1	PC2	PC3	PC4	PC5	PC6	PC7	PC8
$S_1$	63.09	80.98	89.24	96.37	99.00	99.70	99.98	100.00
$S_2$	52.72	79.82	88.21	96.09	98.15	99.65	99.85	100.00
$S_3$	56.29	78.77	91.60	95.84	98.53	99.59	99.93	100.00
$S_4$	42.43	69.48	83.23	94.33	97.65	98.93	99.72	100.00
$S_5$	50.73	82.45	91.17	96.83	98.74	99.39	99.83	100.00
$S_6$	60.94	82.85	89.94	94.47	98.40	99.21	99.91	100.00
$S_7$	65.21	88.06	94.73	97.94	99.41	99.90	99.96	100.00
$S_8$	69.88	88.00	94.03	96.61	98.36	99.31	99.74	100.00
$S_9$	65.23	83.17	92.02	95.37	97.77	99.45	99.96	100.00
$S_{10}$	63.68	85.03	90.45	95.69	98.36	99.37	99.78	100.00
Mean	59.02	81.86	90.46	95.95	98.44	99.45	99.87	100.00
SD	8.35	5.34	3.24	1.09	0.53	0.28	0.10	0.00

## **Appendix 2: An open source package in R to help researchers estimate shared neural drive between physiological signals**

This appendix introduces an R-based package developed for the analysis of shared neural drive using physiological signals such as EMG. Developed using R, an open-source platform for statistical computing, the package provides an accessible and integrated workflow —from signal processing to statistical hypothesis testing— thus simplifying a comprehensive analysis within a single computational platform. By standardizing these procedures on a widely used, freely available platform, the package not only democratizes access to advanced analytical tools but also supports global research efforts, especially in settings with limited access to commercial software.

### **4.8 Signal Simulation and Magnitude-Squared Coherence Estimation**

In order to analyze the coherence between two signals, we developed a method based on the `gsignal` package in R.

```
devtools::install_github('angelobj/coherence', force=T) # Install package  
library(coherence) # Load library  
?coherence # See documentation for coherence function
```

All functions are thoroughly documented and examples are provided to test them in any environment. The methods included in the package allows us to generate two signals, compute their Fast Fourier Transform (FFT), and estimate their magnitude-squared coherence. The functions developed for this purpose include:

- `simulateSignals()`: Generates two signals sharing a specified frequency. Both signals have added noise, which can also be specified in the function.
- `coherence()`: Computes the magnitude-squared coherence between the two signals.

#### 4.8.1 Generating simulated signals

To simulate two signals sharing a single frequency, the following R function is used:

```
signals <- simulateSignals(samplingFreq = 1000,  
                           duration = 8, # Duration of each signal in seconds  
                           target_freq = 100, # Shared frequency between signals  
                           noise_level = 0.5, # Level of added noise to each signal  
                           plot = TRUE)
```

The function `simulateSignals()` generates two time series sharing a single main frequency. Then noise is added to each signal. The resulting signals can be plotted as in Figure 4.7.

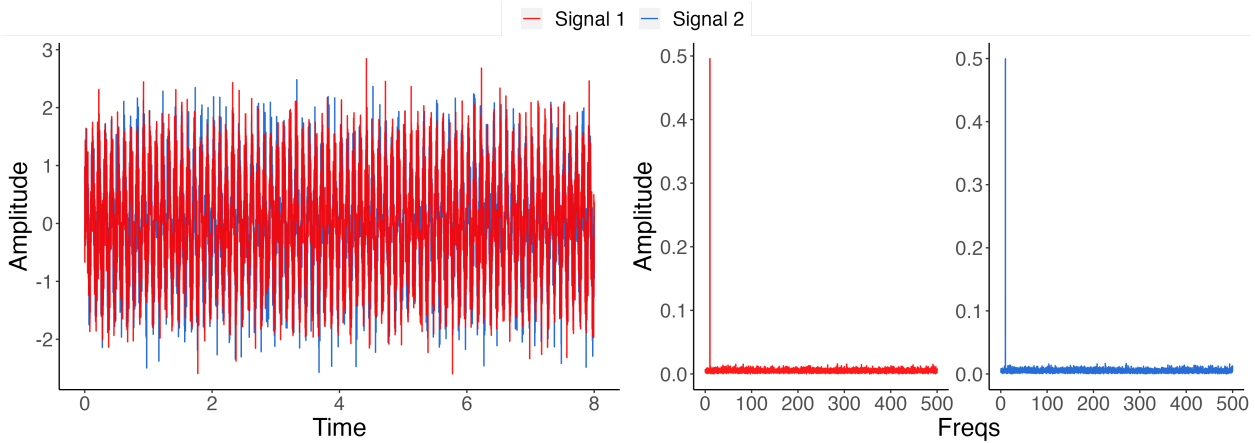


Figure 4.7: Simulated signals (left): Both signals share a single frequency (8 Hz), with a noise level set at 0.5 (arbitrary units). The signal duration is set in seconds. Both signals overlap due to the shared frequency between them. Fast Fourier Transform (right): An FFT analysis is performed to confirm a shared frequency (8Hz) plus added noise.

#### 4.8.2 Estimating Magnitude-Squared Coherence

Magnitude square coherence is estimated using the following function:

```
coh_result <- coherence(signals[, c("signal1", "signal2")], # Data frame with two signals
                         samplingFreq = 1000, # Signal's sampling frequency
                         out = "all",
                         plot = TRUE)
```

The coherence spectrum is displayed in Figure 4.8. The magnitude-square coherence provides insight into the degree of correlation between the two signals at each frequency.

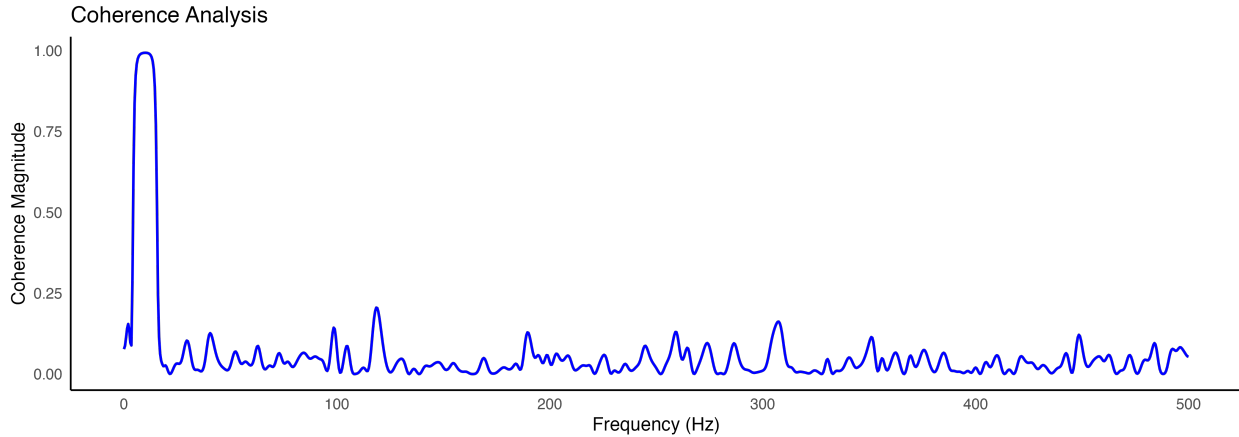


Figure 4.8: Magnitude-squared coherence spectrum of the simulated signals. The coherence is highest at the shared frequency of 10 Hz.

### 4.8.3 Transforming magnitude-squared coherence into *z*-scores

Given that coherence is a measure of correlation, directly applying statistical functions—such as computing group means—can lead to biased estimates due to the bounded nature of coherence values (ranging from 0 to 1). To address this issue, it is advisable to first normalize the magnitude-squared coherence values using the Fisher Z-transformation, which stabilizes variance and makes them more suitable for statistical analysis. This transformation converts coherence values into Z-scores, allowing for more accurate group comparisons and parametric statistical testing.

The Fisher Z-transformation used in the `DescTools` package is defined as:

$$Z = \frac{1}{2} \ln \left( \frac{1+r}{1-r} \right)$$

where  $r$  is the coherence value, and  $\ln$  is the natural logarithm. The code to transform coherence values into *z*-scores is:

```
fisherz(coh_result$coh$Cxy)
```

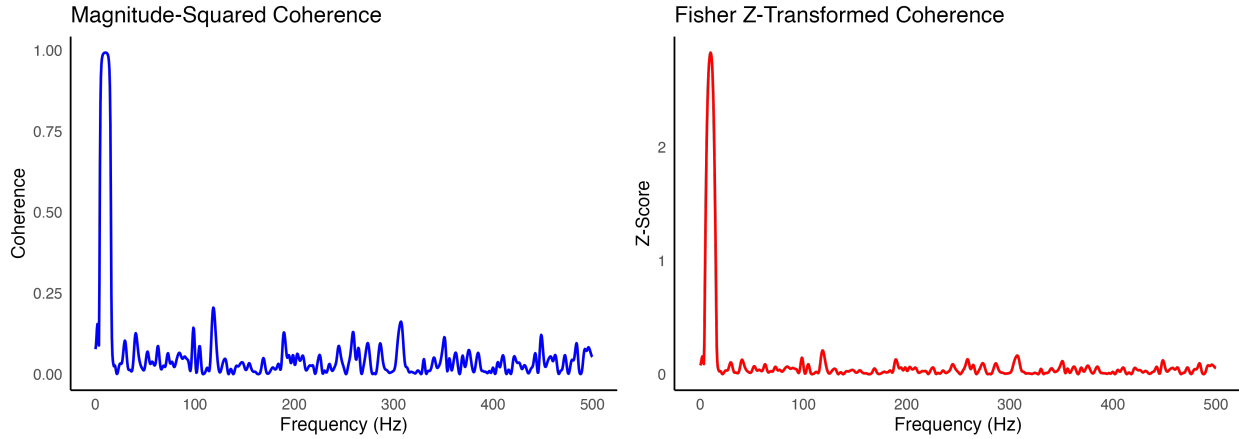


Figure 4.9: Magnitude-squared and z-transformed coherence for simulated signals. The coherence is highest at the shared frequency of 10 Hz

The developed package provides functions to estimate magnitude-squared coherence but does not include preprocessing functions such as filtering and rectification since there are other packages or base built in functions R. Proper preprocessing is essential for obtaining meaningful coherence estimates, as raw signals may contain artifacts, noise, or undesired frequency components that can bias coherence results.

As such, preprocessing plays a critical role in coherence analysis, as it helps to improve signal quality and remove confounding factors. Prior research has demonstrated that signal transformations, such as rectification and filtering, can significantly affect coherence estimates.

For example, studies by [Boonstra and Breakspear, 2012](#) have shown that full-wave rectification of electromyographic (EMG) signals provides a better representation of coherence by emphasizing common oscillatory activity across muscles. Rectification enhances signal periodicity and can increase the strength of coherence estimates at physiologically relevant frequencies [[Boonstra and Breakspear, 2012](#)].

Additionally, signal filtering is an important preprocessing step to remove unwanted frequency components. Electrical noise at 50-60 Hz (electrical noise) is a common issue in biomedical and electrophysiological recordings. If not removed, this noise can introduce artificial coherence peaks at these frequencies, leading to misleading results. A high-pass or notch filter can be applied to suppress these unwanted components before coherence computation.

# Bibliography

Sergei Adamovich, Philippe Archambault, Mohammad Ghafouri, Mindy Levin, Howard Poizner, and Anatol Feldman. Hand trajectory invariance in reaching movements involving the trunk. *Experimental Brain Research*, 138(3):288–303, May 2001. ISSN 00144819. doi: 10.1007/s002210100694. URL <http://link.springer.com/10.1007/s002210100694>.

Evangelos Anagnostou, Georgios P Paraskevas, Konstantinos Spengos, Sophia Vassilopoulou, Vasileios Zis, and Dimitrios Vassilopoulos. Same or opposite? association of head-movement weakness with limb paresis in stroke. *The neurologist*, 17(6):309–311, 2011.

Hesam Azadjou, Michalina Błażkiewicz, Andrew Erwin, and Francisco J Valero-Cuevas. Dynamical analyses show that professional archers exhibit tighter, finer and more fluid dynamical control than neophytes. *Entropy*, 25(10):1414, 2023.

Mark R Baker and Stuart N Baker. The effect of diazepam on motor cortical oscillations and corticomuscular coherence studied in man. *The Journal of physiology*, 546(3):931–942, 2003.

SN Baker, Etienne Olivier, and RN Lemon. Coherent oscillations in monkey motor cortex and hand muscle emg show task-dependent modulation. *The Journal of physiology*, 501(Pt 1):225, 1997. doi: 10.1111/j.1469-7793.1997.225bo.x.

Stuart N. Baker, Boubker Zaaimi, Karen M. Fisher, Steve A. Edgley, and Demetris S. Soteropoulos. Pathways mediating functional recovery. In *Progress in Brain Research*, volume 218, pages 389–412. Elsevier, 2015. ISBN 978-0-444-63565-5. doi: 10.1016/bs.pbr.2014.12.010. URL <https://linkinghub.elsevier.com/retrieve/pii/S0079612314000430>.

Saul Balagura and Russel G Katz. Undecussated innervation to the sternocleidomastoid muscle: a rein-statement. *Annals of Neurology: Official Journal of the American Neurological Association and the Child Neurology Society*, 7(1):84–85, 1980.

Victor R Barradas, Jason J Kutch, Toshihiro Kawase, Yasuharu Koike, and Nicolas Schweighofer. When 90% of the variance is not enough: residual emg from muscle synergy extraction influences task performance. *Journal of Neurophysiology*, 123(6):2180–2190, 2020.

Angelo Bartsch and Francisco Javier Valero-Cuevas. Vestibular contribution to motor output is also suppressed by voluntary action of the arm. *Journal of Physiology*, pages 1–18, 2025. doi: 10.1113/JP287077.

Angelo Bartsch-Jimenez, Michalina Błażkiewicz, Hesam Azadjou, Ryan Novotny, and Francisco J Valero-Cuevas. Fine synergies” describe motor adaptation in people with drop foot in a way that supplements traditional “coarse synergies. *Frontiers in sports and active living*, 5:1080170, 2023.

Randall F Beer, Michael D Ellis, Bradley G Holubar, and Julius PA Dewald. Impact of gravity loading on post-stroke reaching and its relationship to weakness. *Muscle & Nerve: Official Journal of the American Association of Electrodiagnostic Medicine*, 36(2):242–250, 2007.

Michalina Błażkiewicz and Andrzej Wit. Compensatory strategy for ankle dorsiflexion muscle weakness during gait in patients with drop-foot. *Gait & posture*, 68:88–94, 2019.

Michalina Błażkiewicz, Ida Wiszomirska, Katarzyna Kaczmarczyk, Grażyna Brzuszkiewicz-Kuźmicka, and Andrzej Wit. Mechanisms of compensation in the gait of patients with drop foot. *Clinical Biomechanics*, 42:14–19, 2017.

Jean-Sébastien Blouin, Christopher J. Dakin, Kees van den Doel, Romeo Chua, Bradford J. McFadyen, and John Timothy Inglis. Extracting phase-dependent human vestibular reflexes during locomotion using both time and frequency correlation approaches. *Journal of Applied Physiology*, 111(5):1484–1490, November 2011. ISSN 8750-7587, 1522-1601. doi: 10.1152/japplphysiol.00621.2011. URL <https://www.physiology.org/doi/10.1152/japplphysiol.00621.2011>.

Tjeerd W. Boonstra. The potential of corticomuscular and intermuscular coherence for research on human motor control. *Frontiers in Human Neuroscience*, 7, 2013. ISSN 1662-5161. doi: 10.3389/fnhum.2013.00855. URL <http://journal.frontiersin.org/article/10.3389/fnhum.2013.00855/abstract>.

Tjeerd W. Boonstra and Michael Breakspear. Neural mechanisms of intermuscular coherence: implications for the rectification of surface electromyography. *Journal of Neurophysiology*, 107(3):796–807, February 2012. ISSN 0022-3077, 1522-1598. doi: 10.1152/jn.00066.2011. URL <https://www.physiology.org/doi/10.1152/jn.00066.2011>.

Bruno Bordoni, Ryder R Reed, Prasanna Tadi, and Matthew Varacallo. Neuroanatomy, cranial nerve 11 (accessory). *StatPearls*, 2018.

Oliver Brock and Francisco Valero-Cuevas. Transferring synergies from neuroscience to robotics comment on “hand synergies: Integration of robotics and neuroscience for understanding the control of biological and artificial hands” by m. santello et al. *Physics of life reviews*, 17:27, 2016.

P Brown. Pathophysiology of spasticity. *Journal of neurology, neurosurgery, and psychiatry*, 57(7):773, 1994.

Robert M. Brownstone and Jeremy W. Chopek. Reticulospinal systems for tuning motor commands. *Frontiers in Neural Circuits*, 12:1–10, 4 2018. ISSN 16625110. doi: 10.3389/fncir.2018.00030.

Signe Brunnstrom. Movement therapy in hemiplegia. *A neurophysiological approach*, 1970.

J.A. Buford. Reticulospinal system. In Larry R. Squire, editor, *Encyclopedia of Neuroscience*, pages 151–158. Academic Press, Oxford, 2009. ISBN 978-0-08-045046-9. doi: <https://doi.org/10.1016/B978-008045046-9.01337-1>. URL <https://www.sciencedirect.com/science/article/pii/B9780080450469013371>.

J. Carriot, M. Jamali, M. J. Chacron, and K. E. Cullen. Statistics of the Vestibular Input Experienced during Natural Self-Motion: Implications for Neural Processing. *Journal of Neuroscience*, 34(24):8347–8357, June 2014. ISSN 0270-6474, 1529-2401. doi: 10.1523/JNEUROSCI.0692-14.2014. URL <https://www.jneurosci.org/lookup/doi/10.1523/JNEUROSCI.0692-14.2014>.

Marcello Cherchi, Nicholas P Bellinaso, Katrena Card, Ashley Covington, Amber Krumpe, Michael S Pfeifer, Angela Truitt, Hyun Jin Yoo, Heather E Rudisill, and Timothy C Hain. Sound evoked triceps myogenic potentials. *Otology & Neurotology*, 30(4):545–550, 2009.

Woorim Cho, Victor R Barradas, Nicolas Schweighofer, and Yasuharu Koike. Design of an isometric endpoint force control task for electromyography normalization and muscle synergy extraction from the upper limb without maximum voluntary contraction. *Frontiers in Human Neuroscience*, 16, 2022.

Supriyo Choudhury, A. Shobhana, Ravi Singh, Dwaipayan Sen, Sidharth Shankar Anand, Shantanu Shubham, Mark R. Baker, Hrishikesh Kumar, and Stuart N. Baker. The Relationship Between Enhanced Reticulospinal Outflow and Upper Limb Function in Chronic Stroke Patients. *Neurorehabilitation and Neural Repair*, 33(5):375–383, May 2019. ISSN 1545-9683, 1552-6844. doi: 10.1177/1545968319836233. URL <http://journals.sagepub.com/doi/10.1177/1545968319836233>.

Constantinos N Christakos, Nikos A Papadimitriou, and Sophia Erimaki. Parallel neuronal mechanisms underlying physiological force tremor in steady muscle contractions of humans. *Journal of neurophysiology*, 95(1):53–66, 2006.

Robert H Clewley, John M Guckenheimer, and Francisco J Valero-Cuevas. Estimating effective degrees of freedom in motor systems. *IEEE Transactions on Biomedical Engineering*, 55(2):430–442, 2008.

Kathleen E. Cullen. Internal models of self-motion: neural computations by the vestibular cerebellum. *Trends in Neurosciences*, 46(11):986–1002, November 2023a. ISSN 01662236. doi: 10.1016/j.tins.2023.08.009. URL <https://linkinghub.elsevier.com/retrieve/pii/S0166223623002072>.

Kathleen E. Cullen. Vestibular motor control. In *Handbook of Clinical Neurology*, volume 195, pages 31–54. Elsevier, 2023b. ISBN 978-0-323-98818-6. doi: 10.1016/B978-0-323-98818-6.00022-4. URL <https://linkinghub.elsevier.com/retrieve/pii/B9780323988186000224>.

Kathleen E Cullen and Omid A Zobeiri. Proprioception and the predictive sensing of active self-motion. *Current Opinion in Physiology*, 20:29–38, April 2021. ISSN 24688673. doi: 10.1016/j.cophys.2020.12.001. URL <https://linkinghub.elsevier.com/retrieve/pii/S2468867320301668>.

Christopher J. Dakin, John Timothy Inglis, Romeo Chua, and Jean-Sébastien Blouin. Muscle-specific modulation of vestibular reflexes with increased locomotor velocity and cadence. *Journal of Neurophysiology*, 110(1):86–94, July 2013. ISSN 0022-3077, 1522-1598. doi: 10.1152/jn.00843.2012. URL <https://www.physiology.org/doi/10.1152/jn.00843.2012>.

Andrea d’Avella and MMCM Tresch. Modularity in the motor system: decomposition of muscle patterns as combinations of time-varying synergies. *Advances in neural information processing systems*, 14, 2001.

Andrea d’Avella, Philippe Saltiel, and Emilio Bizzi. Combinations of muscle synergies in the construction of a natural motor behavior. *Nature neuroscience*, 6(3):300–308, 2003.

John C DeToledo and Noble J David. Innervation of the sternocleidomastoid and trapezius muscles by the accessory nucleus. *Journal of neuro-ophthalmology*, 21(3):214–216, 2001.

Julius P A Dewald, Patrick S Pope, Joseph D Given, Thomas S Buchanan, and W Zev Rymer. Abnormal muscle coactivation patterns during isometric torque generation at the elbow and shoulder in hemiparetic subjects. *Brain*, 118:495–510, 1995. URL <https://academic.oup.com/brain/article/118/2/495/468285>.

Wesley Ebisuzaki. A method to estimate the statistical significance of a correlation when the data are serially correlated. *Journal of climate*, 10(9):2147–2153, 1997.

Joan E Edelstein. H3c 3j7). how many strides are required for the analysis of electromyographic data in gait? *Scand J Rehabil Med*, 18:133–135, 1986.

Michael D. Ellis, Theresa Sukal, Tobey DeMott, and Julius P. A. Dewald. Augmenting Clinical Evaluation of Hemiparetic Arm Movement With a Laboratory-Based Quantitative Measurement of Kinematics as a Function of Limb Loading. *Neurorehabilitation and Neural Repair*, 22(4):321–329, July 2008. ISSN 1545-9683, 1552-6844. doi: 10.1177/1545968307313509. URL <http://journals.sagepub.com/doi/10.1177/1545968307313509>.

Michael D. Ellis, Yiyun Lan, Jun Yao, and Julius P. A. Dewald. Robotic quantification of upper extremity loss of independent joint control or flexion synergy in individuals with hemiparetic stroke: a review of paradigms addressing the effects of shoulder abduction loading. *Journal of NeuroEngineering and Rehabilitation*, 13(1):95, December 2016. ISSN 1743-0003. doi: 10.1186/s12984-016-0203-0. URL <https://jneuroengrehab.biomedcentral.com/articles/10.1186/s12984-016-0203-0>.

Michael D. Ellis, Carolina Carmona, Justin Drogos, and Julius P. A. Dewald. Progressive Abduction Loading Therapy with Horizontal-Plane Viscous Resistance Targeting Weakness and Flexion Synergy to Treat Upper Limb Function in Chronic Hemiparetic Stroke: A Randomized Clinical Trial. *Frontiers in Neurology*, 9:71, February 2018. ISSN 1664-2295. doi: 10.3389/fneur.2018.00071. URL <http://journal.frontiersin.org/article/10.3389/fneur.2018.00071/full>.

Marc Christopher Emos and Julie Rosner. Neuroanatomy, upper motor nerve signs. In *StatPearls [Internet]*. StatPearls Publishing, 2023.

Roger M. Enoka, Ioannis G. Amiridis, and Jacques Duchateau. Electrical Stimulation of Muscle: Electrophysiology and Rehabilitation. *Physiology*, 35(1):40–56, January 2020. ISSN 1548-9213, 1548-9221. doi: 10.1152/physiol.00015.2019. URL <https://www.physiology.org/doi/10.1152/physiol.00015.2019>.

Yin Fang, Janis J Daly, Jiayang Sun, Ken Hvorat, Eric Fredrickson, Svetlana Pundik, Vinod Sahgal, and Guang H Yue. Functional corticomuscular connection during reaching is weakened following stroke. *Clinical neurophysiology*, 120(5):994–1002, 2009.

Dario Farina, Francesco Negro, and Jakob Lund Dideriksen. The effective neural drive to muscles is the common synaptic input to motor neurons. *The Journal of physiology*, 592(16):3427–3441, 2014.

K. M. Fisher, B. Zaaimi, T. L. Williams, S. N. Baker, and M. R. Baker. Beta-band intermuscular coherence: a novel biomarker of upper motor neuron dysfunction in motor neuron disease. *Brain*, 135(9):2849–2864, September 2012. ISSN 0006-8950, 1460-2156. doi: 10.1093/brain/aws150. URL <https://academic.oup.com/brain/article-lookup/doi/10.1093/brain/aws150>.

Patrick A. Forbes, Gunter P. Siegmund, Alfred C. Schouten, and Jean-Sbastien Blouin. Task, muscle and frequency dependent vestibular control of posture. *Frontiers in Integrative Neuroscience*, 8, January 2015. ISSN 1662-5145. doi: 10.3389/fnint.2014.00094. URL <http://journal.frontiersin.org/article/10.3389/fnint.2014.00094/abstract>.

AR Fugel-Meyer, L Jaasko, I Leyman, S Ollson, and S Steglind. The post-stroke hemiplegic patient1, a method for evaluation of physical performance. *Scand. J. Rehabil. Med*, 7:13–31, 1975.

Kikuro Fukushima. Corticovestibular interactions: anatomy, electrophysiology, and functional considerations. *Experimental Brain Research*, 117(1):1–16, October 1997. ISSN 0014-4819. doi: 10.1007/PL00005786. URL <http://link.springer.com/10.1007/PL00005786>.

Joachim Groß, Lars Timmermann, Jan Kujala, Martin Dirks, Frank Schmitz, R Salmelin, and Alfons Schnitzler. The neural basis of intermittent motor control in humans. *Proceedings of the National Academy of Sciences*, 99(4):2299–2302, 2002.

P Grosse and P Brown. Corticomuscular and intermuscular frequency analysis: physiological principles and applications in disorders of the motor system. *Suppl Clin Neurophysiol*, 2005.

Pascal Grosse and Peter Brown. Acoustic startle evokes bilaterally synchronous oscillatory emg activity in the healthy human. *Journal of Neurophysiology*, 90:1654–1661, 9 2003. ISSN 00223077. doi: 10.1152/jn.00125.2003.

Alkis. M. Hadjiosif, Meret Branscheidt, Manuel A. Anaya, Keith D. Runnalls, Jennifer Keller, Amy J. Bastian, Pablo A. Celnik, and John W. Krakauer. Positive and negative stroke signs revisited: dissociations between synergies, weakness, and impaired reaching dexterity, July 2021. URL <http://medrxiv.org/lookup/doi/10.1101/2021.07.21.21260448>.

Alkis M Hadjiosif, Meret Branscheidt, Manuel A Anaya, Keith D Runnalls, Jennifer Keller, Amy J Bastian, Pablo A Celnik, and John W Krakauer. Dissociation between abnormal motor synergies and impaired reaching dexterity after stroke. *Journal of neurophysiology*, 127(4):856–868, 2022.

Shenghong He, Alceste Deli, Petra Fischer, Christoph Wiest, Yongzhi Huang, Sean Martin, Saed Khawaldeh, Tipu Z. Aziz, Alexander L. Green, Peter Brown, and Huiling Tan. Gait-Phase Modulates Alpha and Beta Oscillations in the Pedunculopontine Nucleus. *The Journal of Neuroscience*, 41(40):8390–8402, October 2021. ISSN 0270-6474, 1529-2401. doi: 10.1523/JNEUROSCI.0770-21.2021. URL <https://www.jneurosci.org/lookup/doi/10.1523/JNEUROSCI.0770-21.2021>.

Claire F. Honeycutt, Ursina A. Tresch, and Eric J. Perreault. Startling Acoustic Stimuli Elicit Rapid Hand Extension Following Stroke. In Winnie Jensen, Ole Kæseler Andersen, and Metin Akay, editors, *Replace, Repair, Restore, Relieve – Bridging Clinical and Engineering Solutions in Neurorehabilitation*, volume 7, pages 431–435. Springer International Publishing, Cham, 2014. ISBN 978-3-319-08071-0 978-3-319-08072-7. doi: 10.1007/978-3-319-08072-7\_65. URL [https://link.springer.com/10.1007/978-3-319-08072-7\\_65](https://link.springer.com/10.1007/978-3-319-08072-7_65). Series Title: Biosystems & Biorobotics.

Claire Fletcher Honeycutt and Eric Jon Perreault. Planning of Ballistic Movement following Stroke: Insights from the Startle Reflex. *PLoS ONE*, 7(8):e43097, August 2012. ISSN 1932-6203. doi: 10.1371/journal.pone.0043097. URL <https://dx.plos.org/10.1371/journal.pone.0043097>.

Claire Fletcher Honeycutt and Eric Jon Perreault. Deficits in startle-evoked arm movements increase with impairment following stroke. *Clinical Neurophysiology*, 125(8):1682–1688, August 2014. ISSN 13882457. doi: 10.1016/j.clinph.2013.12.102. URL <https://linkinghub.elsevier.com/retrieve/pii/S138824571301359X>.

Aapo Hyvärinen and Erkki Oja. Independent component analysis: algorithms and applications. *Neural networks*, 13(4-5):411–430, 2000.

Iole Indovina, Gianfranco Bosco, Roberta Riccelli, Vincenzo Maffei, Francesco Lacquaniti, Luca Passamonti, and Nicola Toschi. Structural connectome and connectivity lateralization of the multimodal vestibular cortical network. *NeuroImage*, 222:117247, November 2020. ISSN 10538119. doi: 10.1016/j.neuroimage.2020.117247. URL <https://linkinghub.elsevier.com/retrieve/pii/S1053811920307333>.

Derek G Kamper, Heidi C Fischer, Erik G Cruz, and William Z Rymer. Weakness is the primary contributor to finger impairment in chronic stroke. *Archives of physical medicine and rehabilitation*, 87(9):1262–1269, 2006.

François Klam and Werner Graf. Discrimination between active and passive head movements by macaque ventral and medial intraparietal cortex neurons. *The Journal of Physiology*, 574(2):367–386, July 2006. ISSN 0022-3751, 1469-7793. doi: 10.1113/jphysiol.2005.103697. URL <https://physoc.onlinelibrary.wiley.com/doi/10.1113/jphysiol.2005.103697>.

Na-hyeon Ko, Christopher M Laine, and Francisco J Valero-Cuevas. Task-dependent alteration of beta-band intermuscular coherence is associated with ipsilateral corticospinal tract excitability. *Frontiers in Sports and Active Living*, 5, 2023.

John W Krakauer. Arm function after stroke: from physiology to recovery. In *Seminars in neurology*, volume 25, pages 384–395. Copyright© 2005 by Thieme Medical Publishers, Inc., 333 Seventh Avenue, New ..., 2005.

Jason J Kutch and Francisco J Valero-Cuevas. Challenges and new approaches to proving the existence of muscle synergies of neural origin. *PLoS computational biology*, 8(5):e1002434, 2012.

Annie Kwan, Patrick A. Forbes, Diana E. Mitchell, Jean-Sébastien Blouin, and Kathleen E. Cullen. Neural substrates, dynamics and thresholds of galvanic vestibular stimulation in the behaving primate. *Nature Communications*, 10(1):1904, April 2019. ISSN 2041-1723. doi: 10.1038/s41467-019-09738-1. URL <https://www.nature.com/articles/s41467-019-09738-1>.

Christopher M Laine and Francisco J Valero-Cuevas. Intermuscular coherence reflects functional coordination. *Journal of neurophysiology*, 118(3):1775–1783, 2017.

Christopher M Laine, Brian A Cohn, and Francisco J Valero-Cuevas. Temporal control of muscle synergies is linked with alpha-band neural drive. *The Journal of Physiology*, 599(13):3385–3402, 2021.

Yiyun Lan, Jun Yao, and Julius P. A. Dewald. The Impact of Shoulder Abduction Loading on Volitional Hand Opening and Grasping in Chronic Hemiparetic Stroke. *Neurorehabilitation and Neural Repair*, 31(6):521–529, June 2017. ISSN 1545-9683, 1552-6844. doi: 10.1177/1545968317697033. URL <http://journals.sagepub.com/doi/10.1177/1545968317697033>.

James W. Lance and James G. McLeod. Muscle tone and movement. In *A Physiological Approach to Clinical Neurology*, pages 101–127. Elsevier, 1981. ISBN 978-0-407-00196-1. doi: 10.1016/B978-0-407-00196-1.50011-5. URL <https://linkinghub.elsevier.com/retrieve/pii/B9780407001961500115>.

Lisbeth Hoejkjaer Larsen, Ivan Chrilles Zibrandtsen, Troels Wienecke, Troels Wesenberg Kjaer, Mark Schram Christensen, Jens Bo Nielsen, and Henning Langberg. Corticomuscular coherence in the acute and subacute phase after stroke. *Clinical Neurophysiology*, 128(11):2217–2226, 2017.

Brian Lau, Marie-Laure Welter, Hayat Belaid, Sara Fernandez Vidal, Eric Bardinet, David Grabli, and Carine Karachi. The integrative role of the pedunculopontine nucleus in human gait. *Brain*, 138(5):1284–1296, May 2015. ISSN 0006-8950, 1460-2156. doi: 10.1093/brain/awv047. URL <https://academic.oup.com/brain/article-lookup/doi/10.1093/brain/awv047>.

Donald G Lawrence and Henricus GJM Kuypers. The functional organization of the motor system in the monkey: I. the effects of bilateral pyramidal lesions. *Brain*, 91(1):1–14, 1968a.

Donald G Lawrence and Henricus GJM Kuypers. The functional organization of the motor system in the monkey: II. the effects of lesions of the descending brain-stem pathways. *Brain*, 91(1):15–36, 1968b.

Daniel D Lee and H Sebastian Seung. Learning the parts of objects by non-negative matrix factorization. *Nature*, 401(6755):788–791, 1999.

Hyunglae Lee, Claire Honeycutt, and Eric Perreault. Influence of task complexity on movement planning and release after stroke: insights from startreact. *Experimental Brain Research*, 240(6):1765–1774, 2022.

Sheng Li, Yen-Ting Chen, Gerard E Francisco, Ping Zhou, and William Zev Rymer. A unifying pathophysiological account for post-stroke spasticity and disordered motor control. *Frontiers in neurology*, 10:468, 2019.

Jinbiao Liu, Yixuan Sheng, and Honghai Liu. Corticomuscular coherence and its applications: A review. *Frontiers in human neuroscience*, 13:100, 2019. doi: <https://doi.org/10.3389/fnhum.2019.00100>.

C. Lopez, O. Blanke, and F.W. Mast. The human vestibular cortex revealed by coordinate-based activation likelihood estimation meta-analysis. *Neuroscience*, 212:159–179, June 2012. ISSN 03064522. doi: 10.1016/j.neuroscience.2012.03.028. URL <https://linkinghub.elsevier.com/retrieve/pii/S0306452212002898>.

Christophe Lopez and Kathleen E. Cullen. Electrical stimulation of the peripheral and central vestibular system. *Current Opinion in Neurology*, 37(1):40–51, February 2024. ISSN 1350-7540, 1473-6551. doi: 10.1097/WCO.0000000000001228. URL <https://journals.lww.com/10.1097/WCO.0000000000001228>.

Patrick Mair and Rand Wilcox. Robust statistical methods in r using the wrs2 package. *Behavior research methods*, 52(2):464–488, 2020.

Ramon Manon-Espaillet and Robert L Ruff. Dissociated weakness of sternocleidomastoid and trapezius muscles with lesions in the cns. *Neurology*, 38(5):796–796, 1988.

L Mazzini and M Schieppati. Activation of the neck muscles from the ipsi-or contralateral hemisphere during voluntary head movements in humans. a reaction-time study. *Electroencephalography and Clinical Neurophysiology/Evoked Potentials Section*, 85(3):183–189, 1992.

Angus J. C. McMorland, Keith D. Runnalls, and Winston D. Byblow. A Neuroanatomical Framework for Upper Limb Synergies after Stroke. *Frontiers in Human Neuroscience*, 9, February 2015. ISSN 1662-5161. doi: 10.3389/fnhum.2015.00082. URL <http://journal.frontiersin.org/Article/10.3389/fnhum.2015.00082/abstract>.

Jacob G McPherson, Albert Chen, Michael D Ellis, Jun Yao, CJ Heckman, and Julius PA Dewald. Progressive recruitment of contralesional cortico-reticulospinal pathways drives motor impairment post stroke. *The Journal of physiology*, 596(7):1211–1225, 2018.

Derek M. Miller and William Z. Rymer. Sound-Evoked Biceps Myogenic Potentials Reflect Asymmetric Vestibular Drive to Spastic Muscles in Chronic Hemiparetic Stroke Survivors. *Frontiers in Human Neuroscience*, 11:535, November 2017. ISSN 1662-5161. doi: 10.3389/fnhum.2017.00535. URL <http://journal.frontiersin.org/article/10.3389/fnhum.2017.00535/full>.

Derek M. Miller, Cliff S. Klein, Nina L. Suresh, and William Z. Rymer. Asymmetries in vestibular evoked myogenic potentials in chronic stroke survivors with spastic hypertonia: Evidence for a vestibulospinal role. *Clinical Neurophysiology*, 125(10):2070–2078, October 2014. ISSN 13882457. doi: 10.1016/j.clinph.2014.01.035. URL <https://linkinghub.elsevier.com/retrieve/pii/S1388245714001242>.

Derek M Miller, James F Baker, and W Zev Rymer. Ascending vestibular drive is asymmetrically distributed to the inferior oblique motoneuron pools in a subset of hemispheric stroke survivors. *Clinical Neurophysiology*, 127(4):2022–2030, 2016.

Tatsuya Mima, Keiichiro Toma, Benjamin Koshy, and Mark Hallett. Coherence between cortical and muscular activities after subcortical stroke. *Stroke*, 32(11):2597–2601, 2001.

P Molina-Negro, RA Bertrand, E Martin And, and Y Gioani. The role of the vestibular system in relation to muscle tone and postural reflexes in man. *Acta oto-laryngologica*, 89(3-6):524–533, 1980.

Angshuman Mukherjee and Ambar Chakravarty. Spasticity mechanisms—for the clinician. *Frontiers in neurology*, 1:149, 2010.

Venkatesh N Murthy and Eberhard E Fetz. Coherent 25-to 35-hz oscillations in the sensorimotor cortex of awake behaving monkeys. *Proceedings of the National Academy of Sciences*, 89(12):5670–5674, 1992. doi: 10.1073/pnas.89.12.5670.

Adriana L Natali, Vamsi Reddy, and Bruno Bordoni. Neuroanatomy, corticospinal cord tract. 2018.

P. W. Nathan and Marion C. Smith. THE RUBROSPINAL AND CENTRAL TEGMENTAL TRACTS IN MAN. *Brain*, 105(2):223–269, 1982. ISSN 0006-8950, 1460-2156. doi: 10.1093/brain/105.2.223. URL <https://academic.oup.com/brain/article-lookup/doi/10.1093/brain/105.2.223>.

PW Nathan and Marion C Smith. Long descending tracts in man: I. review of present knowledge. *Brain*, 78(2):248–303, 1955.

Ludwig Niehaus, Malek Bajbouj, and Bernd-Ulrich Meyer. Impact of interhemispheric inhibition on excitability of the non-lesioned motor cortex after acute stroke. In *Supplements to Clinical neurophysiology*, volume 56, pages 181–186. Elsevier, 2003.

Grace Niyo, Lama I Almofeed, Andrew Erwin, and Francisco J Valero-Cuevas. A computational study of how an  $\alpha$ -to  $\gamma$ -motoneurone collateral can mitigate velocity-dependent stretch reflexes during voluntary movement. *Proceedings of the National Academy of Sciences*, 121(34):e2321659121, December 2024. doi: 10.1101/2023.12.08.570843. URL <http://biorxiv.org/lookup/doi/10.1101/2023.12.08.570843>.

Teryn E Nogles and Michael A Galuska. Middle cerebral artery stroke. In *StatPearls [Internet]*. StatPearls Publishing, 2023.

David Ó'Reilly and Peter Federolf. Identifying differences in gait adaptability across various speeds using movement synergy analysis. *PloS one*, 16(1):e0244582, 2021.

ES Papathanasiou, C Iosif, and SS Papacostas. Vestibular evoked myogenic potentials (vemps) from upper limb muscles. *Journal of the Neurological Sciences*, 333:e593, 2013.

Todd C Pataky. One-dimensional statistical parametric mapping in python. *Computer methods in biomechanics and biomedical engineering*, 15(3):295–301, 2012.

S. Pinto and M. De Carvalho. Accessory nerve stimulation: Motor response of the sternocleidomastoid muscle. *Neurophysiologie Clinique/Clinical Neurophysiology*, 38(2):133–136, April 2008. ISSN 09877053. doi: 10.1016/j.neucli.2007.12.004. URL <https://linkinghub.elsevier.com/retrieve/pii/S0987705308000154>.

Robert Porter and Roger Lemon. *Corticospinal Function and Voluntary Movement*. Oxford University Press, September 1995. ISBN 978-0-19-852375-8. doi: 10.1093/acprof:oso/9780198523758.001.0001. URL <http://www.oxfordscholarship.com/view/10.1093/acprof:oso/9780198523758.001.0001/acprof-9780198523758>.

R Core Team. *R: A Language and Environment for Statistical Computing*. R Foundation for Statistical Computing, Vienna, Austria, 2021. URL <https://www.R-project.org/>.

Mohammad Fazle Rabbi, Claudio Pizzolato, David G Lloyd, Chris P Carty, Daniel Devaprakash, and Laura E Diamond. Non-negative matrix factorisation is the most appropriate method for extraction of muscle synergies in walking and running. *Scientific reports*, 10(1):1–11, 2020.

H. A. Raptis, E. Dannenbaum, N. Paquet, and A. G. Feldman. Vestibular System May Provide Equivalent Motor Actions Regardless of the Number of Body Segments Involved in the Task. *Journal of Neurophysiology*, 97(6):4069–4078, June 2007. ISSN 0022-3077, 1522-1598. doi: 10.1152/jn.00909.2006. URL <https://www.physiology.org/doi/10.1152/jn.00909.2006>.

C. Nicholas Riddle and Stuart N. Baker. Convergence of Pyramidal and Medial Brain Stem Descending Pathways Onto Macaque Cervical Spinal Interneurons. *Journal of Neurophysiology*, 103(5):2821–2832, May 2010. ISSN 0022-3077, 1522-1598. doi: 10.1152/jn.00491.2009. URL <https://www.physiology.org/doi/10.1152/jn.00491.2009>.

Erynne Rowe, Marla K Beauchamp, and Janie Astephen Wilson. Age and sex differences in normative gait patterns. *Gait & Posture*, 88:109–115, 2021.

Akira Saito, Kohei Watanabe, and Hiroshi Akima. Coordination among thigh muscles including the vastus intermedius and adductor magnus at different cycling intensities. *Human Movement Science*, 40:14–23, 2015.

Anja Schlack, Klaus-Peter Hoffmann, and Frank Bremmer. Interaction of linear vestibular and visual stimulation in the macaque ventral intraparietal area (VIP). *European Journal of Neuroscience*, 16(10): 1877–1886, November 2002. ISSN 0953-816X, 1460-9568. doi: 10.1046/j.1460-9568.2002.02251.x. URL <https://onlinelibrary.wiley.com/doi/10.1046/j.1460-9568.2002.02251.x>.

P. Schindlein, M. Mueller, T. Bauermann, T. Brandt, P. Stoeter, and M. Dieterich. Cortical representation of saccular vestibular stimulation: VEMPs in fMRI. *NeuroImage*, 39(1):19–31, January 2008. ISSN 10538119. doi: 10.1016/j.neuroimage.2007.08.016. URL <https://linkinghub.elsevier.com/retrieve/pii/S1053811907007483>.

Toshio Shimizu, Akiko Hosaki, Taro Hino, Masaru Sato, Tetsuo Komori, Shunsaku Hirai, and Paolo M Rossini. Motor cortical disinhibition in the unaffected hemisphere after unilateral cortical stroke. *Brain*, 125(8):1896–1907, 2002.

Theresa M Sukal, Michael D Ellis, and Julius PA Dewald. Shoulder abduction-induced reductions in reaching work area following hemiparetic stroke: neuroscientific implications. *Experimental brain research*, 183: 215–223, 2007.

Myriam Taga, Charalambos C. Charalambous, Sharmila Raju, Jing Lin, Yian Zhang, Elisa Stern, and Heidi M. Schambra. Corticoreticulospinal tract neurophysiology in an arm and hand muscle in healthy and stroke subjects. *The Journal of Physiology*, 599(16):3955–3971, August 2021. ISSN 0022-3751, 1469-7793. doi: 10.1113/JP281681. URL <https://onlinelibrary.wiley.com/doi/10.1113/JP281681>.

Timothy L Tattersall, Peter G Stratton, Terry J Coyne, Raymond Cook, Paul Silberstein, Peter A Silburn, François Windels, and Pankaj Sah. Imagined gait modulates neuronal network dynamics in the human pedunculopontine nucleus. *Nature Neuroscience*, 17(3):449–454, March 2014. ISSN 1097-6256, 1546-1726. doi: 10.1038/nn.3642. URL <https://www.nature.com/articles/nn.3642>.

Wesley Thevathasan, Alek Pogosyan, Jonathan A. Hyam, Ned Jenkinson, Tom Foltynie, Patricia Limousin, Marko Bogdanovic, Ludvic Zrinzo, Alexander L. Green, Tipu Z. Aziz, and Peter Brown. Alpha oscillations in the pedunculopontine nucleus correlate with gait performance in parkinsonism. *Brain*, 135(1):148–160, January 2012. ISSN 1460-2156, 0006-8950. doi: 10.1093/brain/awr315. URL <https://academic.oup.com/brain/article-lookup/doi/10.1093/brain/awr315>.

Lena H Ting and Jane M Macpherson. A limited set of muscle synergies for force control during a postural task. *Journal of neurophysiology*, 93(1):609–613, 2005.

Lena H Ting and J Lucas McKay. Neuromechanics of muscle synergies for posture and movement. *Current opinion in neurobiology*, 17(6):622–628, 2007.

Matthew C Tresch and Anthony Jarc. The case for and against muscle synergies. *Current opinion in neurobiology*, 19(6):601–607, 2009.

Connie W Tsao, Aaron W Aday, Zaid I Almarzooq, Alvaro Alonso, Andrea Z Beaton, Marcio S Bittencourt, Amelia K Boehme, Alfred E Buxton, April P Carson, Yvonne Commodore-Mensah, et al. Heart disease and stroke statistics—2022 update: a report from the american heart association. *Circulation*, 145(8):e153–e639, 2022.

Nicolas A Turpin, Stéphane Uriac, and Georges Dalleau. How to improve the muscle synergy analysis methodology? *European Journal of Applied Physiology*, 121(4):1009–1025, 2021.

Thomas E Twitchell. The restoration of motor function following hemiplegia in man. *Brain*, 74(4):443–480, 1951.

Maria Clara Motta Barbosa Valente, Aline Tenório Lins Carnaúba, Janise Dal Pai, Kelly Cristina Lira de Andrade, and Pedro de Lemos Menezes. Vestibular evoked myogenic potentials (vemp) captured in the forearm flexor muscles: a study of its feasibility and reference ranges. *Clinics*, 75:e2020, 2020.

Francisco J Valero-Cuevas. *Fundamentals of neuromechanics*, volume 8. Springer, 2016.

Francisco J Valero-Cuevas, Heiko Hoffmann, Manish U Kurse, Jason J Kutch, and Evangelos A Theodorou. Computational models for neuromuscular function. *IEEE reviews in biomedical engineering*, 2:110–135, 2009a.

Francisco J Valero-Cuevas, Madhusudhan Venkadesan, and Emanuel Todorov. Structured variability of muscle activations supports the minimal intervention principle of motor control. *Journal of neurophysiology*, 102(1):59–68, 2009b.

Francisco J Valero-Cuevas, Verena Klamroth-Marganska, Carolee J Winstein, and Robert Riener. Robot-assisted and conventional therapies produce distinct rehabilitative trends in stroke survivors. *Journal of neuroengineering and rehabilitation*, 13(1):1–10, 2016.

Jing Xu, Firas Mawase, and Marc H Schieber. Evolution, biomechanics, and neurobiology converge to explain selective finger motor control. *Physiological Reviews*, 104(3):983–1020, 2024.